GEOTECHNICAL ENGINEERING

MECHANICAL ENGINEERING

MATERIALS STUDIES RELATED TO LUNAR SURFACE EXPLORATION

by

J. K. MITCHELL
I. S. E. CARMICHAEL
R. E. GOODMAN
J. FRISCH
P. A. WITHERSPOON
F. E. HEUZÉ

FINAL REPORT: VOLUME III OF IV

PREPARED FOR MARSHALL SPACE FLIGHT CENTER
HUNTSVILLE, ALABAMA UNDER NASA CONTRACT
NSR 05-003-189

MARCH, 1969

SPACE SCIENCES LABORATORY

UNIVERSITY OF CALIFORNIA · BERKELEY

G E O T E C H N I C A L E N G I N E E R I N G

MATERIAL STUDIES RELATED TO LUNAR SURFACE EXPLORATION

By

James K. Mitchell
Ian C. Carmichael
Joseph Frisch
Richard E. Goodman
Paul A. Witherspoon
Francois E. Heuzé

FINAL REPORT: VOLUME III OF IV

Prepared for Marshall Space Flight Center
Huntsville, Alabama, under NASA Contract
NSR 05-003-189

March 1969

Space Sciences Laboratory

University of California, Berkeley 94720

TABLE OF CONTENTS

LIST OF ILLUSTRATIONS

CHAPTER 1

CHAPTER 2

CHAPTER 3

LIST OF TABLES

PREFACE

This report presents in its four volumes the results of studies conducted during the period March 6, 1967 — June 30, 1968, under NASA research contract NSR 05-003-189, "Materials Studies Related to Lunar Surface Exploration." This study was sponsored by the Advanced Lunar Missions Directorate, NASA Headquarters, and was under the technical cognizance of Dr. N. C. Costes, Space Sciences Laboratory, George C. Marshall Space Flight Center.

This report reflects the combined effort of five faculty investigators and a full time project manager/engineer assisted by six graduate research assistants, representing several engineering and scientific disciplines pertinent to study of lunar surface material properties. James K. Mitchell, Professor of Civil Engineering, served as Principal Investigator and was responsible for those phases of the work concerned with problems relating to lunar soil mechanics and the engineering properties of lunar soils. Co-investigators were Ian C. Carmichael, Professor of Geology, in charge of geological studies; Joseph Frisch, Professor of Mechanical Engineering, who was responsible for analysis of friction and adhesion problems and the testing of materials under high-vacuum conditions; Richard E. Goodman, Associate Professor of Geological Engineering, who was concerned with the engineering geology and rock mechanics aspects of the lunar surface; and Paul A. Witherspoon, Professor of Geological Engineering, who conducted studies related to thermal and permeability measurements on the lunar surface. Francois E. Heuzé, Assistant Specialist, served as project manager and contributed to studies in the areas of rock mechanics and engineering geology.

INTRODUCTION

I. OBJECTIVES

It is axiomatic that, among the myriad of technical and scientific factors that must be considered in the lunar exploration program, the nature of lunar soil and rock surface materials is of prime importance in the design of spacecraft landing systems, the design of surface mobility systems, the design of experiments to be conducted on the lunar surface, mission planning, and, ultimately, to mission success. Without specific knowledge of the mechanical properties of lunar soils, designers and mission planners have no choice but to adopt ultraconservative designs and procedures in an effort to insure astronaut safety. Thus it is of paramount importance that as much specific information as possible about lunar surface material properties be obtained prior to the first manned lunar mission, and that planning and design options for further missions remain open thereafter in order to accommodate changes as more and more specific data become available.

The study described in this report was initiated in an effort to better define both the surface material related engineering problems and the relevant properties of the materials themselves. Information developed as a result of this effort was then utilized in specific studies of problems considered to be of critical importance and for the development of analysis and testing methods that appear particularly promising for the study of lunar surface properties by both remote and tactile means.

Specific objectives that were set at the onset of the study were:

1. To define geological and engineering problems associated with on-site lunar exploartion dependent on knowledge of soil and rock properties for solution.

2. To critically evaluate current knowledge concerning lunar surface materials, their properties, and their relationships to problems associated with on-site lunar exploration, and to select reasonable models for lunar surface conditions.

3. To make preliminary formulations of desirable on-site soil and rock mechanics studies for extended lunar exploration and to make recommendations as to appropriate apparatus and required astronaut skills for performance of such investigations.

4. To undertake preliminary studies for development of rock testing devices for use in a borehole on the lunar surface for the determination of the stress-strain characteristics of rocks.

5. To review friction and adhesion problems and to make recommendations for improved design of existing apparatus for determination of frictional and adhesive characteristics of different metallic and nonmetallic materials under high vacuum and at high and low temperatures.

6. To make recommendations and cost estimates for the design of apparatus for measuring silicate mineral solubility and viscosity at high temperatures and pressures and for determining the distribution of silicates between gas and liquid phases.

7. To review critically theories for the origin of the moon and to consider logical sequences for investigations to be carried out on the lunar surface for most efficient determination of composition, structure and history of the moon.

The results of studies of this type are intended to aid in attainment of the following longer range goals:

1. Development of capability for predicting, at least in a semi-quantitative manner, soil conditions at any point on the moon on the basis of remote measurements.

2. Development of capability for detailed quantitative determination of soil and rock properties at any chosen site where scientific or engineering work is contemplated.

3. Development of methods of analysis suitable for solution of soil and rock mechanics problems on the moon.

4. Utilization of the information obtained, both as an aid in the interpretation of geologic processes on the moon and as a means for developing improved understanding of soil and rock behavior on the earth.

II. SCOPE OF WORK AND OUTLINE OF FINAL REPORT

As work proceeded on each of these objectives several specific topics emerged as particularly needing more detailed study, and, consequently, during the later phases of the study efforts were intensively directed at these topics. Thus the trend has been from studies of a braod and general nature within a particular area to the isolation of specific problems and more detailed studies of these problems. This is reflected in the general outline of the 4 volumes constituting this report, as shown below:

VOLUME I

LUNAR SOIL MECHANICS AND SOIL PROPERTIES

Chapter 1. Lunar Soil and Rock Problems and Considerations in Their Solution
(James K. Mitchell)

Chapter 2. Engineering Properties of Lunar Soils
(James K. Mitchell and Scott S. Smith)

Chapter 3. Materials Properties Evaluations from Boulder Tracks on the Lunar Surface
(James K. Mitchell and Scott S. Smith)

Chapter 4. Impact Records as a Source of Lunar Surface Material Property Data
(James K. Mitchell, Donald W. Quigley, and Scott S. Smith)

Chapter 5. Lunar Stratigraphy as Revealed by Crater Morphology
(Francois E. Heuzé and Richard E. Goodman)

Chapter 6. Geochemical Studies
(I. S. E. Carmichael and J. Nicholls)

Appendix. Library of Lunar Surface Exploration Materials
(Francois E. Heuzé)

VOLUME II

APPLICATION OF GEOPHYSICAL AND GEOTECHNICAL METHODS TO LUNAR SITES EXPLORATION

—

VOLUME III

PRELIMINARY STUDIES ON SOIL/ROCK ENGINEERING PROBLEMS RELATED TO LUNAR EXPLORATION

VOLUME III (Con't.)

—

VOLUME IV

PRELIMINARY STUDIES FOR THE DESIGN OF ENGINEERING PROBES

C H A P T E R 1

TRAFFICABILITY

By

James K. Mitchell, Scott S. Smith, and Donald W. Quigley

CHAPTER 1

TRAFFICABILITY

(James K. Mitchell, Scott S. Smith, and Donald W. Quigley)

I. INTRODUCTION

Extended lunar exploration may include surface traverses ranging beyond the capability of astronauts on foot. Consequently consideration has been given to the design and development of both manned and unmanned roving vehicles for mobility purposes. Because of the severe constraints on weight, power supply, and time that will be associated with any lunar mission, as well as the need to insure safety to as great an extent as possible, a precision of vehicle design and of estimation of relevant mobility factors will be needed that exceeds by far any requirements imposed on the design and performance prediction of terrestrial vehicles. Furthermore, terrestrial vehicle design and mobility prediction are both capable of trial and error development because of the opportunity for continued testing and redesign under the appropriate environmental and soil conditions. In the case of lunar vehicles the designs and predictions must be correct the first time.

The design of a vehicle to negotiate a given terrain depends on both the topographic characteristics of the terrain and the physical properties of the surface materials with which the vehicle interacts. Factors of particular importance are the following:

A. Topography Related Factors

1. Mean terrain slope on a scale compatible with the length of a contemplated traverse or part of traverse.

2. Distribution of lunar-surface roughness characteristics on a scale compatible with the dynamic response characteristics of the vehicle.

B. Surface Material Related Factors

1. Lateral homogeneity of surface conditions.

2. Relative stiffnesses of vehicle wheel and suspension

system and the ground.

3. The bearing capacity and the pressure-sinkage relationship of the supporting ground; i.e., the surface yielding characteristics.

4. Resistance to wheel motion due to sinkage and "bulldozing" action.

5. Tractive force that can be developed at the vehicle-ground interface. This will be strongly dependent on the friction-adhesion characteristics between the wheel and the surface, and the strength characteristics of the supporting soil mass.

Not all factors in either group or between groups are independent of each other; nonetheless, such separation is convenient. Emphasis during the present project has been on the consideration of methods for handling group B factors. It is pertinent to note, however, that the Astrogeology Branch of the U. S. Geological Survey at the suggestion of the Marshall Space Flight Center has studies in progress of the topographic characteristics in a data format that can be used for the design and testing of lunar roving vehicles. Additional work on this problem is being done by MSFC, Jet Propulsion Laboratory, Manned Spacecraft Center, General Motors, Chrysler, Bendix, Bellcom, ACIC, and others. The "power spectral density" function provides one useful form for presentation of terrain data for use in vehicle design. Rozema (1967) has recently summarized the method for determination of the power spectral density function and illustrated its interpretation as a quantitative terrain roughness indicator.

Unfortunately the data available for lunar terrain characterization on a scale needed for mobility analyses are severely limited. Lunar Orbiter photographs, while providing complete coverage of the near side of the moon do not, in general, provide high enough resolution for terrain characterization on a scale compatible with vehicle dimensions. In addition, strong photogrammetric analysis is not possible because of (1) limited stereo coverage of the moon, (2) a very small base-height ratio, and (3) distortion between adjacent Orbiter framelets. Some profiles are becoming available through application of photoclinometry; however this technique suffers from the lack of the needed photographic resolution

and the necessity for assuming an average photometric function. Thus the most reliable topographic analysis of small terrain features is limited to the areas in the vicinity of the five successful Surveyor landing sites and those areas covered by the final pre-impact photos in the Ranger VII, VIII, and IX series.

Industry, e.g., Bendix Corporation, AC Electronics, Chrysler Corporation, Grumman Aircraft, Hayes International, TRW, Northrup, and others, has made extensive study of vehicles suitable for operation on the lunar surface (both manned and unmanned). Several model and prototype designs have been investigated, and rather extensive test programs have been conducted. Wheel designs have been used which have been based on anticipation of soft soil conditions on the moon.

Effort during the present project was concentrated on the wheel-surface interaction part of the trafficability problem. The objectives of the studies were (1) to review methods for solution of mobility problems, (2) to present recommendations for a method to be used for integration of soil data into vehicle design and mission planning, and (3) to consider methods for determination of the needed soil data.

This chapter is organized as follows. First the two most widely used methods for solution of off-road mobility are summarized and their potential applicability to the lunar trafficability problem is examined. Next the general approach to lunar mobility studies as developed by NASA and expressed in terms of the ELMS (Engineering Lunar Model Surface) model is examined in terms of current knowledge of the lunar surface. A similitude approach to the solution of the soil-vehicle interaction problem is then discussed, followed by the presentation of recommendations for further theoretical and experimental study of the trafficability problem. A number of recent references pertinent to lunar trafficability are summarized in Appendix A to this chapter and comment is made where appropriate.

II. METHODS FOR TRAFFICABILITY ANALYSIS

Two main approaches have been developed for solution of off-the-road mobility problems; i.e., that developed by the U. S. Army Ordnance Tank-

Automotive Command Land Locomotion Research Laboratory and that of the Army Mobility Branch, Corps of Engineers, Waterways Experiment Station.

A. U. S. Army Ordnance Tank-Automotive Command Land Locomotion Research Laboratory Method (Soil Value System)

The U. S. Army Ordnance Tank-Automotive Command Land Locomotion Research Laboratory in the 1950's, under the direction of Dr. M. G. Bekker, developed a quasi-theoretical method of trafficability analysis (Bekker, 1956, 1960; Reece, 1964, 1966; Liston, 1964; Roth, 1960).

In this method a semi-rational analysis is used from which equations for tractive effort and resistance to motion can be derived. The difference between these quantities gives the force available for acceleration or climbing slopes. The pressure-sinkage relation is given by the following power law.

$$p = \left(\frac{k_c}{b} + k_\phi\right) z^n \qquad (1\text{-}1)$$

It should be noted that this relationship is independent of applied tractive effort. If it is assumed that the shearing resistance of the soil increases continuously with strain, the shear stress in the soil is computed using

$$s = (c + p \tan \phi)(1 - e^{-j/K}) \qquad (1\text{-}2)$$

The terms in equations (1) and (2) are defined as follows

p = pressure applied to the soil
b = width of loaded area
z = depth of penetration of applied load (sinkage)
s = soil shear stress
j = soil shear deformation
K = stress-strain constant
n, k_c, k_ϕ, c, ϕ = soil constants

The soil deformation constants n, k_c, and k_ϕ are obtained from the results of loading tests performed on two plates of different sizes. The soil

strength constants c and ϕ and the stress-strain constant, K,* are obtained by rotating an annular ring fitted with grousers on the soil surface (Bevameter). The pattern of soil deformation developed in this test is dissimilar to that developed under wheels. Values of the various soil constants are given in Table 1-1 for several soils. Unfortunately unique relationships between the soil deformation constants and the commonly used soil mechanics strength and density parameters (c, ϕ, ρ) do not appear to exist.

Using these relationships for soil response, equations can be derived theoretically which are intended to describe vehicle performance and soil trafficability. The general form of these relationships is shown below (Bekker, 1962):

Total Thrust (H):

$$H = b \int_0^{\ell} s\,d\ell \qquad (1\text{-}3)$$

where

b = width of loaded area

ℓ = length of loaded area

Motion Resistance due to Soil Compaction (R):

$$R = b \int_0^{z_m} p\,dz \qquad (1\text{-}4)$$

where

z_m = maximum depth of sinkage of loaded area

*For soils which exhibit a peak in the stress vs strain curve with stress falling off to an ultimate value less than the peak value, two stress-strain constants, K_1 and K_2 are needed.

TABLE 1-1

VALUES OF CONSTANTS FOR SOIL VALUE SYSTEM OF TRAFFICABILITY ANALYSIS FOR SOME SOILS

Soil Description	c(psi)	$\phi°$	k_c $\left(\frac{lb}{in^{n+1}}\right)$	k_ϕ $\left(\frac{lb}{in^{n+2}}\right)$	n	K_1	K_2	K	Reference
Dry Sand			0.	7.0	0.8				Janosi (1958)
Dry Mason Sand	0.165	30°	0.11	3.56	1.13			1.75	Pavlics (1961)
Dry Sand			0.	7.0	0.8				Bekker (1960)
Dry Sand	0.	29°	0.	6.0	0.95				A.C. Electronics (1967)
Dry Sand	0.03	31°	0.	6.0	1.0				A.C. Electronics (1967)
Dry Yuma Sand γ = 96 - 106 pcf	0.	36°-39°	0.-10.	4.-16.	0.6-1.0				W.E.S. (1964)
Dry Yuma Sand γ = 96 pcf	0.	37°	0.-4.	5.-11.	0.6-0.9				W.E.S. (1964)
Firmly Settled Silt	6.5	10°				1.	1.1		Bekker (1960)
Perlite - Soft Fluffy Material	0.	31°	0.	0.7	1.05				A.C. Electronics (1967)
Michigan Farm Soil			5.7	6.8	0.66				Janosi (1958)
Loam	0.43	36°	2.22	16.3	0.65			0.9	Pavlics (1961)
Sandy Loam (W.C. = 19%)	0.6	36°	20.	9.	0.16				Bekker (1960)
Sandy Loam (W.C. = 20%)	0.53	38°	16.	7.	0.17				Bekker (1960)
Sandy Loam (W.C. = 22%)	0.25	36°	2.5	2.2	0.18				Bekker (1960)
Sandy Loam	0.2	35°				0.3	2.		Bekker (1960)
Cohesive Soil			21.	4.	0.43				Bekker (1960)
Buckshot Clay	3.89	11.8°	1.8	20.	0.2				W.E.S. (1962)
Compact Clay γ = .0575 lb/in^3	0.1							1.5	Onafeko & Reece (1967)
Loose Sand γ = .048 lb/in^3	0.12							1.5	Onafeko & Reece (1967)

Vehicle Drawbar-Pull (DP):

$$DP = H - R \tag{1-5}$$

Drawbar-Pull-to-Weight Ratio (λ):

$$\lambda = \frac{DP}{W} \tag{1-6}$$

where

W = total vehicle weight

Maximum Negotiable Slope (α):

$$\alpha = (100\lambda)\% \tag{1-7}$$

Power Required to Drive the Vehicle with a Velocity,v(HP):

$$HP = \frac{Rv}{\eta_1} \tag{1-8}$$

where

η_1 = mechanical efficiency of running gear and transmission

Range of Action in a Homogeneous Terrain (L):

$$L_i = \frac{e\ \eta_1\ \eta_2}{R} \tag{1-9}$$

where

e = energy reservoir available

η_2 = power conversion efficiency of the engine

Fuel Consumed in a Non-Homogeneous Terrain (F):

$$F = \left(\frac{\chi}{\eta_1}\right)(R_1L_1 + R_2L_2 + \ldots + R_kL_k) \qquad (1\text{-}10)$$

where

χ = specific fuel consumption of vehicle

Specific equations representing the above relationships for various types of vehicle running gear can be found in many references, including Bekker (1956, 1960, 1962) and Willis (1966).

The Land Locomotion Laboratory or Bekker method of trafficability analysis has come under criticism in recent years because of simplifying assumptions and questionable predictive capability. The pressure-sinkage equation has been criticized (Willis, 1966); the assumed pressure distribution on the rolling wheel has been shown to be incorrect (Onafeko and Reece, 1967); "slip-sinkage" has been neglected (Reece, 1964); and horizontal soil deformation has been neglected, (Reece, 1964). In essence, the method does not adequately describe the complex soil-vehicle interaction, and thus critics of the method contend that it usually results in an overestimation of a vehicle's performance in a given soil. A further serious limitation is that the method was derived and evaluated only for vehicle performance on level ground.

On the other hand, the proponents of the method can also show evidence that tends to support its validity. Thus, it is not at all clear at the present time just how much value the method really has. Onafeko and Reece (1967) conclude that this method is the only existing method which provides a basis for the development of a more complex and realistic analysis. They note also that for conditions of zero slip

and small sinkage the predictions of rolling resistance and sinkage are quite close to the measured values. The method can perhaps best be considered as a first step towards the goal of an analytical system of soil-vehicle mechanics that may be used in the design of vehicles and the prediction and evaluation of their performance. This method has been used for most lunar roving vehicle design and testing studies conducted thus far. It appears that most individuals involved in these designs are cognizant of many of its limitations; however, there is no other method which is now available that will provide a basis for quantitative analysis.

B. Army Mobility Branch, Corps of Engineers, Waterways Experiment Station Method

The basis of this method is that vehicle support by the soil and traction are dependent on the shearing resistance of the soil and that this resistance can be measured by a simple penetration test (Reece, 1965-1966; Roth, 1960; Waterways Experiment Station, 1954). It is a purely empirical method developed over a period of about 20 years for the purpose of quickly determining in the field whether or not an area of natural ground is negotiable by a given vehicle. The method is based upon a measure of soil strength provided by a cone penetrometer.

The cone index is defined by the pounds force that must be applied to the handle of the cone penetrometer, per square inch of cone base area, in order to force it into the ground. A cone with a 30° apex angle and one-half square inch base area is used for the measurement. As the cone penetrometer is forced into the ground, the variation of cone index with depth is determined.

To estimate the cone index that will prevail under the moving vehicle for multicoverage operations, a remolding test is necessary. This test consists of measuring the cone index of a sample of soil confined in a small cylinder before and after pounding it with 100 blows of a 2-1/2 pound hammer falling 12 inches. A remolding index is obtained by dividing the cone index of the soil after it has been pounded by its cone index before the blows were applied. A rating cone index (RCI), the final measure of a soil's trafficability, is obtained by multiplying the in-situ

cone index by the remolding index. Multicoverage operations are not likely to be of great importance during lunar exploration.

Whether or not a vehicle will be able to pass over a given soil can be predicted by comparing the rating cone index of the soil with the vehicle's vehicle cone index (VCI). The (VCI) is equal to the (RCI) of a soil over which the vehicle can pass either 50 times in the same ruts without becoming immobilized (50-pass criterion) or a single time (one pass criterion). The (VCI) has been related to vehicle characteristics using the vehicle mobility index (MI). Empirical relationships between (MI) and (VCI) have been established for different vehicles. The nature of these relationships and the procedure for computing the mobility index are outlined in Appendix B. Roth (1960) indicates that the maximum slope negotiable by a vehicle can be related to the difference between the rating cone index and the vehicle cone index.

This method, commonly referred to as the WES cone index method, has been found to predict the mobility ("go" or "no-go") of different vehicles very well for wet clay soils and less well but still satisfactorily for granular soils. The method in its present form cannot be used for determination of design parameters for new vehicles or for prediction of all parameters needed for detailed mission planning.

III. APPLICATION OF METHODS TO LUNAR TRAFFICABILITY PROBLEMS

Of the two methods discussed thus far, the Bekker soil value system would appear at first glance to provide the most useful information for solution of roving vehicle trafficability problems since this system yields quantitative vehicle design and performance data. The cone index, on the other hand, is limited to "go" and"no-go" predictions.

Consideration must also be given, however, to the soil testing required for obtaining the needed soil data for use in each method.

The soil testing device used in the Bekker method is the Bevameter (Bekker, 1956, 1960, 1965; Thorman, 1963). This instrument is used to perform loading tests on two plates of unequal area and an annular ring shear test. All test data are automatically recorded in graph form. There are disadvantages to the test, however, and they are formidable.

Although the tests are not difficult to perform, they are time consuming. A lunarized version as presently designed has to be mounted either on a spacecraft or lunar roving vehicle. Because it cannot be hand carried and quickly deployed, it will be difficult to perform many tests in a number of different areas.

A major difficulty is that the annular shear test does not give accurate values of ϕ, the apparent angle of internal friction for granular materials. Comparisons with shear tests have invariably shown that Bevameter values of ϕ are too low (Reece, 1964; Bailey, 1965). Reece was unable to find any consistent correlation between values of c and ϕ determined using the Bevameter and those determined using triaxial and plane strain tests and concluded that a better understanding of the Bevameter ring shear test is needed. Finally, the Bevameter can only perform tests at the surface of a soil deposit and cannot be used to determine the variation of strength to a depth of one or two wheel widths; i.e., to a depth significant in terms of induced stresses.

The WES cone index method uses a cone penetrometer test to obtain an index of the pertinent soil strength properties. The device is hand held and easily transported. In its present form, the U. S. Army cone penetrometer is not self recording, but the Israeli Corps of Engineers has developed such a device (Bailey, 1965). The main advantages of the cone penetrometer are its simplicity and transportability. It can be hand carried and used many times over a wide area without consuming a great deal of time. It can also probe below the surface of the soil to obtain strength values at depths down to 1-1/2 to 2 feet. Its main disadvantage is that proper interpretation of test data requires considerable experience and this could be a serious limitation for lunar operations. The instrument does not provide explicit values of c and ϕ. Therefore, while the device is easy to use, data it provides may be difficult to interpret.

In a sense the two methods of trafficability analysis are complementary rather than conflicting. The Bekker method is used mainly for the design of vehicles, while the WES method is used primarily for the determination of vehicle mobility in a given area. Vehicle design can be more adequately performed by use of the Bekker method because it enables

quantitative estimates to be made of drawbar-pull capacities and power requirements. Whether or not a given vehicle can traverse a given soil is most easily determined by use of the cone penetrometer and the WES method of mobility analysis. Power requirements for vehicle traverses in a given area of the lunar surface can only be estimated (at the present time) by use of the Bekker method.

It appears, therefore, that both methods in their present form are unsuitable for direct application to the lunar soil mobility problem. Most studies thus far have made use of the Bekker approach. It should be noted, however, that wheel designs proposed thus far for lunar roving vehicles are such that performance is relatively unaffected by the soil conditions. This is illustrated more specifically later.

IV. ENGINEERING LUNAR MODEL SURFACE (ELMS MODEL)

The Engineering Lunar Model Surface (ELMS) was developed because of a need for a standard representative lunar surface profile to serve as a reference for determination of lunar roving vehicle performance requirements and for evaluation of performance capabilities of proposed designs (Mason, McCombs and Cramblit, 1964).

Twenty 100-kilometer traverses were selected from Maria and Uplands regions of the moon (ten from each). Profiles for each of these traverses were determined using lunar surface maps, charts and photographs. Ranger, Orbiter, and Surveyor missions had not been flown at the time this was done. Because of the very small scale of the data available, the profiles reflect slopes on a regional scale; i.e., tens of kilometers horizontally and hundreds of meters vertically. From these profiles charts were prepared to show percent of total distance and frequency of occurrence versus slope angle for both Maria and Upland Regions.

Assumptions were made for the soil properties associated with the Maria and Upland profiles. It was assumed that the lunar surface consists of dry, powdery, dust or fine sand-like particles. It was further assumed that the steeper the slope the more compact and strong the soil cover. Cohesion was assumed to be zero and the friction angle was taken as 32°. On this basis k_ϕ and n, respectively, were assumed to increase

from 0.5 and 0.5 for slopes up to 4° to values of 6.0 and 1.25 for slopes between 20° and 25°. Slopes greater than 30° were assumed to have a hard surface. It was further assumed that slippage factors K_1 and K_2 (Bekker, 1956) should be 0.2 and 1.25, respectively.

At the time the ELMS model was developed, specific mechanical property data for the lunar surface and detailed terrain profiles were virtually non-existent and assumptions were required in order that roving vehicle studies could proceed. With the availability of Ranger, Orbiter, and Surveyor data it became possible to make more accurate analyses of slope distributions on the lunar surface and to re-examine the soil property assumptions. Vaughan (1967) has made such a reanalysis for the Mare areas of the moon.

Vaughan's updated ELMS model differs from the original ELMS model primarily in terms of the subdivision of lunar terrain into baseline models and the distribution of slopes within the subdivisions. Essentially the same soil constants are assumed as for the original ELMS model. These properties are independent of the baseline model and depend only on slope angle as indicated in Table 2.

Table 2

Soil Constants for Updated ELMS Model
(After Vaughan, 1967)

Slope Angle (degrees)	k_ϕ	n	Soil Type
<6	0.5	0.5	Very fine grained material
6-10	1.0	0.75	Medium grained fragmental material
10-20	3.0	1.0	Loose type fragmental material
20-30	6.0	1.25	Bonded, fragmental material similar to hard sand
35	6.0	1.25	

For all slopes: $c = 0$, $k_c = 0$, $k_1 = 0.2$, $k_2 = 1.25$; $\tan \phi$ (for drawbar-pull calculations) = 0.4 to 0.7. Coefficient of friction for metallic materials in contact with lunar surface = 0.6

The four baseline models assumed by Vaughan and their characteristics may be summarized as follows:

(1) Dark Mare Model

a. Dark in texture (albedo = 0.068) with low median slopes ($\sim 7°$). Pockmarked with craters ranging from a few centimeters to five meters in diameter.

b. Larger craters (20-30 m) are assumed to have blocky ejecta (1 meter or less) within a radius of 2 crater diameters from crater center.

c. Power spectral density function* to characterize terrain for mobility purposes:

$$P(\Omega) = k\Omega^N \quad m^2/\text{cycles/m}$$
$$k = 2.4 \times 10^{-4}$$
$$\Omega = 0.05 - 0.5 \text{ cycle/meter}$$
$$N = -2$$

(2) Regional Mare Model

a. Albedo = 0.075 to 0.090, moderate slopes with pronounced heterogeneity; ridges, crater fields, irregular depressions, subdued craters, domes, rilles, etc. are superimposed on the basic mare material.

b. Crater distribution is random and the craters in the 20-30 m range are considered to have blocky ejecta (1 m or less) within a radius of 2 crater diameters from the crater center.

c. Power spectral density function parameters:

$$k = 4.3 \times 10^{-4}$$
$$\Omega = 0.05 - 0.5 \text{ cycles/meter}$$
$$N = -2$$

---

*See Appendix A, 7. and 8., and Rozema (1967)

(3) Smooth-Rayed Mare Model

a. Albedo = 0.088 to 0.096, areas of the dark regional mare upon which a mixture of blocky rubble and fine grained materials have been deposited. Small craters and their ejecta are subdued by fine-grained material. Some areas littered with boulders 1 m or larger.

b. Craters are randomly distributed and craters in the 20-30 meter range have blocky ejecta (1 m or less) within a radius of 2 crater diameters from the crater center.

c. Power spectral density function parameters:

$$k = 3.6 \times 10^{-4}$$
$$\Omega = 0.05 - 0.5 \text{ cycles/meter}$$
$$N = -2$$

(4) Rough-Rayed Mare Model

a. Albedo = 0.096 to 0.114, rough ejecta blankets and many slope reversals due to secondary craters not yet filled in by fine-grained material.

b. Craters are randomly distributed and craters in the 20-30 meter range have blocky ejecta (1 m or less) within a radius of 2 crater diameters from the crater center.

c. Power spectral density function parameters:

$$k = 5.8 \times 10^{-4}$$
$$\Omega = 0.05 - 0.5 \text{ cycles/meter}$$
$$N = -2$$

The distribution of slopes assumed for each of these models is shown in Fig. 1-1. Also shown is the slope distribution in the vicinity of the Ranger 7, 8, and 9 impact areas as developed by Choate (1966). It may be seen from Fig. 1-1 that for slope angles in the range of about 2 to 6° the Smooth-Rayed Mare Model gives the closest approximation to the

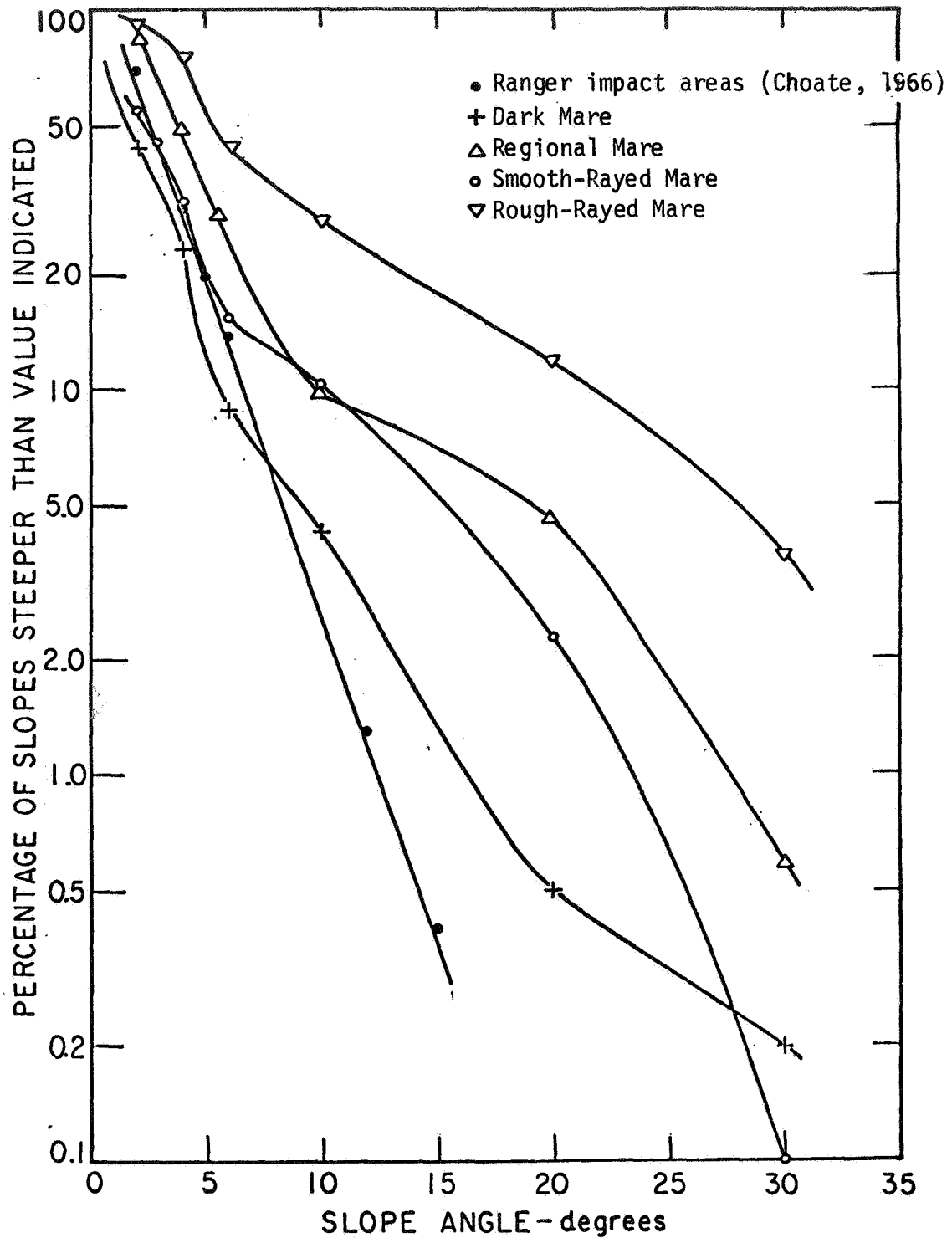

FIG. 1-1. LUNAR SLOPE DISTRIBUTIONS ACCORDING TO VAUGHAN (1967).

actual distribution found by Choate. For all models proposed by Vaughan the proportion of slopes greater than 6 to 8° is higher than for areas studied by Choate.

Subsequent to the work of Choate (1966) and Vaughan (1967) more detailed analyses of the terrain revealed by Orbiter and Surveyor photography have been made by the Astrogeology Branch of the U. S. Geological Survey.* The results of this work suggest that a more realistic representation of lunar slope distributions can be made through characterization of the surface topography by four terrain types: smooth mare, rough mare, hummocky upland, and rough upland. Work by the U.S.G.S. is continuing on this basis.

Fig. 1-2 shows the approximate crater distribution to be expected in a 50 km^2 area in the vicinity of a certified LM landing site for each of the baseline terrains for the updated ELMS model.

As more information has become available concerning the actual topographic characteristics of the lunar surface and the mechanical properties of the surface material, it has become apparent that rigorous adherence to the conditions assumed by the original and updated ELMS models is not appropriate. As noted above, the recent studies by the U.S.G.S. show that more reasonable characteristics of terrain types are possible. Power spectral density methods are now being used to represent the surface roughness characteristics, and the appropriate values of the parameters k, and N can be determined by photoclinometric studies of different regions (provided suitable Orbiter photographs are available).

Since the Surveyor results have shown there to be little difference between mechanical properties at each of the five landing sites, there is no evidence to support the assumption of the ELMS model that soil strength increases with increase in slope angle as indicated in Table 1-2. Furthermore, the Bekker trafficability system is not directly applicable to locomotion on slopes. Thus the significance of any predictions made using the ELMS model properties would remain in question, even if the k_ϕ

---

*Pike, R. (1968) Unpublished.

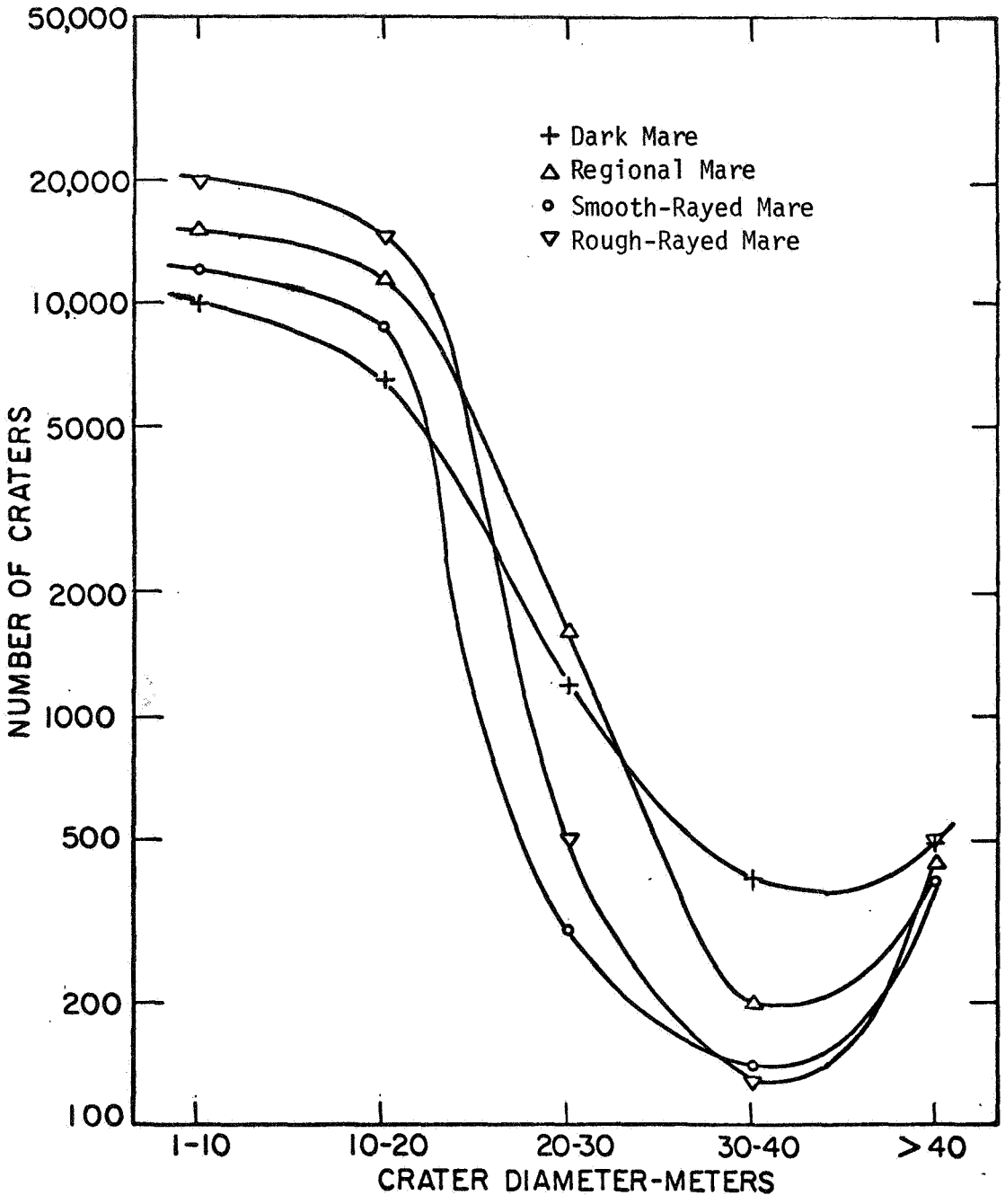

FIG. 1-2. CRATER DISTRIBUTION ACCORDING TO THE UPDATED ELMS MODEL (VAUGHAN, 1966).

and n values were correct.

It is instructive, however, to consider the values for the soil constants that might be appropriate for trafficability analysis by the Bekker method should estimates of behavior be desired using this approach. According to the updated ELMS model, Table 2, k_ϕ increases from 0.5 to 6.0 as the slope angle increases from less than 6° to 20°; whereas n increases from 0.5 to 1.25 over the same range. k_c is taken as zero. The coefficient of friction for metallic materials in contact with the lunar surface is assumed to be 0.6.* Analysis by Scott (1968)** has led him to the conclusion that appropriate values of k_ϕ and n for the lunar soil are 5.0 and 1.0, respectively.

Since it has been clearly established that the lunar soil is slightly cohesive (0.05 - 0.1 psi), the k_c term in equation (1-1) should also have a value. Its importance relative to k_ϕ cannot be stated at present, however. The data in Table 1 are of little help in this regard as there appears to be little correlation between c and k_c for different soils. Even in the case of dry sand there appears to be some question concerning the value of k_c. Tests by the Waterways Experiment Station (1964) on dry Yuma Sand gave values as high as 10 depending on the density of the material. This same study yielded values of k_ϕ in the range of 4 to 16, increasing with density (96 - 106 lb/ft^3). It is of interest to note also that for the Yuma sand at a density of 96 lb per cu ft, the friction angle was 37°, k_ϕ was about 8 ± 3, k_c was in the range of 0 to 4, and n was 0.67 with scatter from 0.6 to 0.9. Thus for the lunar soil with $\phi = 37°$ assumptions of $k_\phi = 5$ and $c = 0$ may be reasonably conservative; whereas, a value of $n = 1.0$ may be slightly high.

In spite of the fact that performance factors computed using the Bekker equations may be in considerable error, it would be instructive at this stage to make a parameter study of the influence of variations of properties on the performance of different types of wheels.

---

*This coefficient should have a controlling influence on the slip between wheel and soil, which in turn will influence performance. Existing theories do not account adequately for friction and/or adhesion between wheel and soil. Actual values for the interaction between metals and the lunar soil are not known.

**Scott, R. F., personal communication, May 1968.

V. MOBILITY AND TRAFFICABILITY ANALYSIS BY SIMILITUDE

Both the soil value system and the WES cone index method for trafficability and vehicle mobility analysis have advantages and disadvantages when applied to the lunar mobility problem as stated in an earlier section. These are (1) the soil value system yields quantitative information that can be used for the design and performance analysis of vehicles, but it rests on uncertain theory and requires soil tests for determination of parameters that are not conveniently adapted to lunar operations, and (2) the cone index method provides only "go-no go" information which cannot be used in design or for quantitative performance predictions, but the needed soil data can be obtained using a simple penetration test which could be easily adapted for use on the moon. While the land locomotion soil values can be converted to cone index values in accordance with equation (A-6), it is not possible at the present time to convert in the reverse direction. Thus the results of cone index measurements on the moon could not be used by themselves as a basis for performance evaluation using the soil value system. The method under development by Van Deusen (Appendix A, Abstract G) for analysis of the dynamic interaction of vehicles and the lunar surface may be useful, provided reliable values for the needed soil parameters can be obtained.

Attention was directed at an approach under development by the Waterways Experiment Station which may ultimately provide practical solutions to a range of mobility problems (WES, 1965; Freitag, 1965, 1966a, 1966b). This approach is based on the results of a dimensional analysis of the significant soil-vehicle parameters. Relationships are defined which give a dimensionless measure of vehicle performance and a set of dimensionless numbers which describe the soil-vehicle system. The cone index is used as a measure of the soil properties. For a saturated clay soil the cone index, C_{WES}, is constant with depth and its value (units: $ML^{-1}T^{-2}$) is used directly. In the case of ideal cohesionless soils the cone index increases linearly with depth, for a homogeneous deposit, and the gradient, G (units: $ML^{-2}T^{-2}$), of the cone index versus depth curve is used. The method has apparently not yet been developed

sufficiently to take soils exhibiting both cohesion and friction into account.

The dimensionless measures of vehicle performance are:

$$\text{Pull number} = DP/W \tag{1-12}$$

$$\text{Sinkage number} = z/d \tag{1-13}$$

$$\text{Torque number} = Q/dW \tag{1-14}$$

$$\text{Towed force number} = P_T/W \tag{1-15}$$

where

DP = pull of wheel (MLT^{-2})
W = load on wheel (MLT^{-2})
Z = wheel sinkage (L)
d = wheel diameter (L)
Q = torque on powered wheel (ML^2T^{-2})
P_T = force required to tow the wheel (MLT^{-2})

The dimensionless numbers used to describe the soil-vehicle system are:

$$\text{Clay mobility number} = \frac{C_{WES}\, bd}{W}\left(\frac{\delta}{h}\right)^{1/2} \tag{1-16}$$

$$\text{Sand mobility number} = \frac{G(bd)^{3/2}}{W}\left(\frac{\delta}{h}\right) \tag{1-17}$$

where

b = tire width (L)

δ = tire deflection (L)

h = tire section height (L)

The WES has had good success in the development of graphs, from the results of model tests, which relate the performance parameters to the sand and clay mobility numbers. These correlations are then used to predict the performance characteristics of prototype vehicles. Were these already established relationships suitable for description of lunar roving vehicle wheel performance, then the approach would be very attractive for solution of lunar mobility problems, since not only could the simple cone index test be used for measurement of the soil properties but also meaningful model tests could be conducted on earth for analysis of the soil-vehicle interaction.*

Unfortunately the WES method does not allow for a soil possessing both frictional and cohesive strength components. The cohesion of lunar soils is sufficiently small, however, that the material could probably be considered as cohesionless without great loss of accuracy. Of more significance, however, is the fact that the dimensionless correlations have been developed for pneumatic tires. The metal-elastic and wire wheels proposed for lunar roving vehicles probably do not behave in a similar manner to pneumatic tires.

Nonetheless an effort was made to determine whether the WES correlations gave an approximate prediction of the correct performance of the metal-elastic wheel, since some actual performance data were available (in the report described in Abstract I, Appendix A) for two soils; a coarse, dry sand and very soft, fluffy perlite. The wheel performance data could be used directly; however, cone index gradient values had to be estimated from k_ϕ which was given in the report for each soil. This conversion was based on a k_ϕ vs G curve

---

*The AC Electronics-Defense Research Laboratory has worked out the similitude requirements for modelling of lunar vehicles on earth so that vehicle dynamics may be simulated.

published by the WES (Green, 1967). The same values are obtained using equation (A-6) and the appropriate values of k_ϕ and n for the soils tested. Predicted and measured values of the pull number, DP/W, are shown in Fig. (1-3) for the metal elastic wheel on both sand and perlite. Fig. (1-4) compares predicted and measured values of the towed force number (motion resistance).

It may be seen that the performance values for the metal-elastic wheel are not in agreement with the values predicted on the basis of the WES correlation curve in the case of the pull number. One or more of several possible factors may be responsible for this discrepancy. In the development of the sand mobility number, three "pi" terms were neglected in the dimensional analysis because they were considered of minor importance in a pneumatic tire-sand system. These terms include the wheel slip (S), the soil friction angle (ϕ), and the coefficient of friction between tire and soil (μ). All pneumatic tires studied by WES developed maximum drawbar pull at about 20% slip. Both the metal-elastic and wire wheels proposed for lunar roving vehicles develop maximum drawbar pull at about 60% slip.

Yuma sand, used by WES, had a friction angle of 35° - 37°; whereas, the dry sand and perlite used for the metal-elastic wheel tests had friction angles of 29° and 31°, respectively. It would be expected that the value of μ between pneumatic tire and soil would differ from that between metal wheel and soil.

In addition to these factors, the pressure distribution under the wire and metal-elastic wheels is likely to differ considerably from that under a pneumatic tire as a consequence of the much different load distributing characteristics of the two wheel types. Thus the metal-elastic wheel and the pneumatic tire represent geometrically dissimilar systems and it is not surprising that different correlations should exist between the dimensionless performance and soil-vehicle interaction factors. Furthermore the wheel loads and contact pressures that are likely for lunar roving vehicles are of considerably smaller magnitude than for usual terrestrial vehicles.

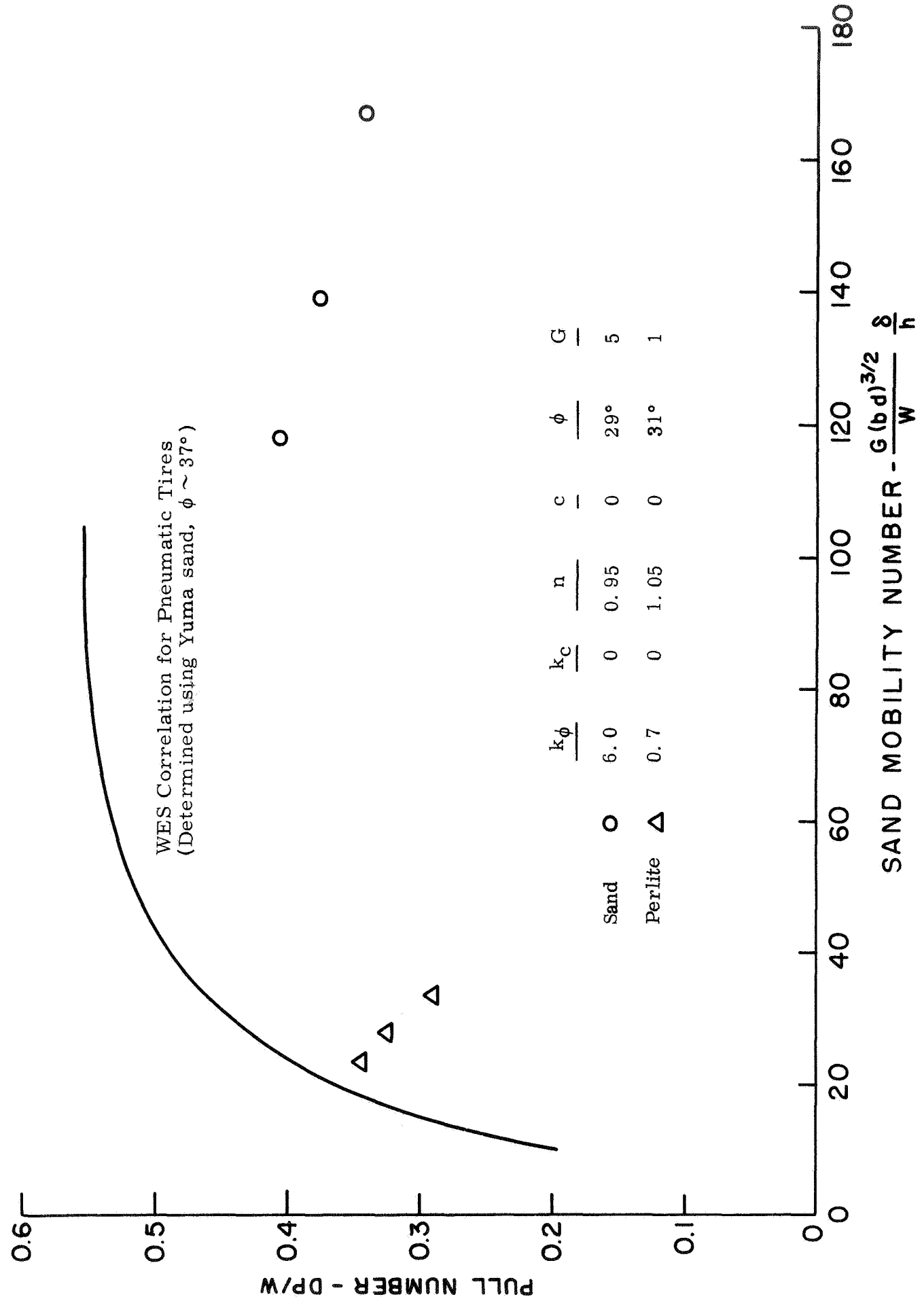

FIG. 1-3. Predicted and Observed Performance Data for the Metal-Elastic Wheel (Pull Number)

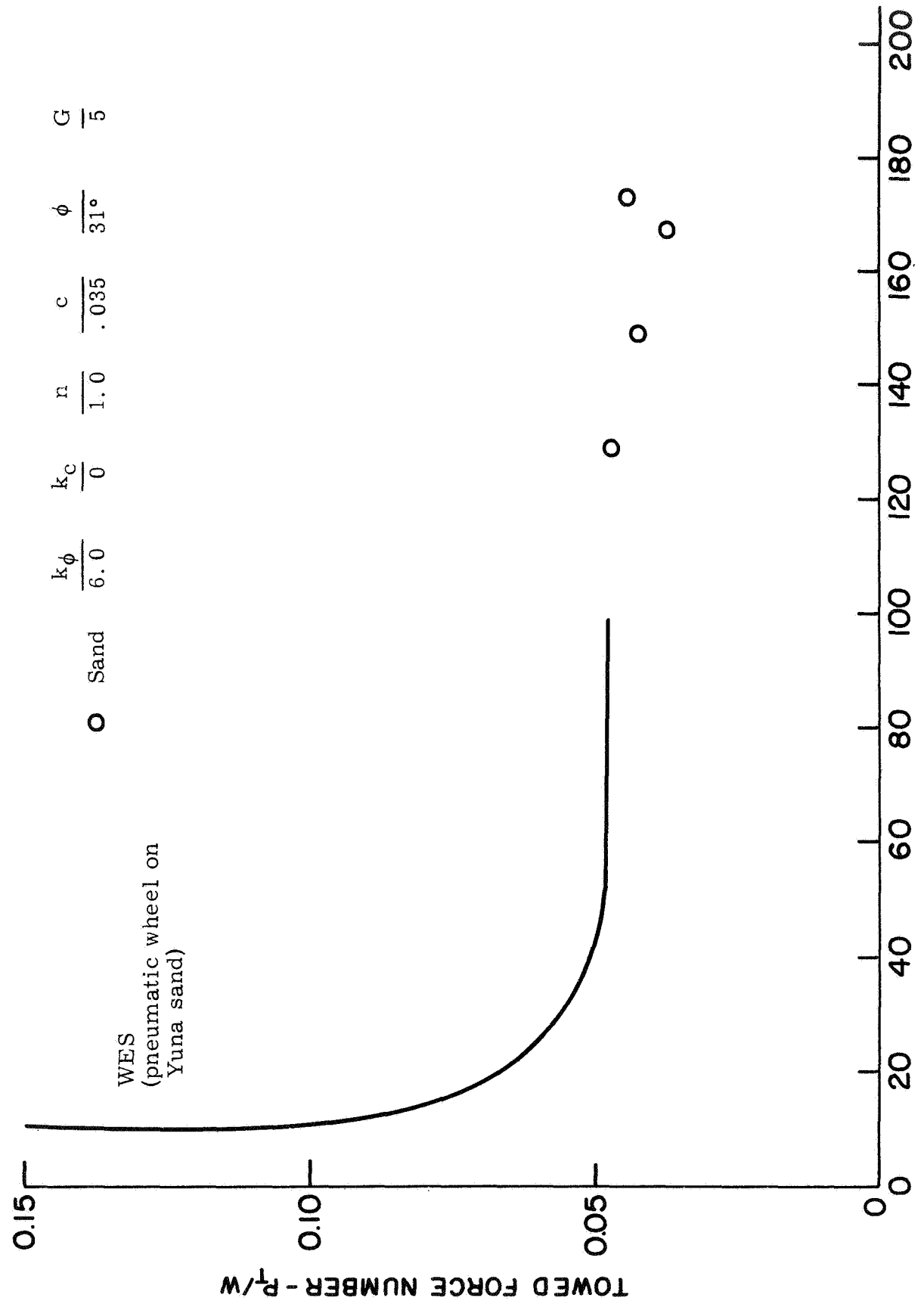

FIG. 1-4. Predicted and Observed Performance Data for the Metal-Elastic Wheel (Towed Force Number)

On the other hand Fig. 1-4 shows good agreement between the extrapolated WES correlation curve for the towed force number and the observed towed force relationship for the metal elastic wheel. This number measures the rolling resistance of the wheel and it may be seen therefore, that from this standpoint the metal-elastic wheel behavior is as efficient as would be anticipated for a pneumatic tire.

From this analysis it appears reasonable to conclude that the correlations already developed for pneumatic tires, which permit the application of model test results to the prediction of prototype vehicle performance and make possible also the determination of performance values from a knowledge of the cone index, cannot be extended directly to the case of wheel types proposed for lunar roving vehicles. For these types of wheels it would be necessary to conduct an extensive test program for determination of the appropriate correlation factors between mobility number and each performance parameter. It is recommended that such a program be carried out, since the cone index method for soil property evaluation would be so easily adaptable to the lunar surface. Time is short, however, and vehicle designs are now well along. In the majority of instances the soil value system has been used for handling soil-vehicle interaction. Thus it is desirable also that the soil value approach be studied further to better determine its overall reliability. Effort should be made to develop simple methods for determining the soil value system parameters.

Some additional comment on the pull number (P/W) data contained in Fig. 1-3 is in order. It may be seen that the values for the metal elastic wheel were only slightly greater for the sand than for the perlite in spite of the fact that the perlite was a very soft and compressible material compared with the sand. The pull that could be exerted by the wheel was considerably less than that which could be developed by a pneumatic tire. Similar behavior was observed for the wire wheel. In addition the results show that as the sand mobility numbers increased the pull number decreased, which is opposite to the behavior shown by the pneumatic tire.

The metal-elastic wheel behavior is consistent with a design objective which would produce a wheel which is intended for operation

over a wide range of soil types from very soft to hard. In effect a wheel has been developed whose performance is relatively insensitive to soil type. The penalty paid for this is that the wheel is less efficient in terms of pull to weight ratio than is the more conventional pneumatic tired wheel.

Further evidence of the insensitivity of metal-elastic wheel performance to soil characteristics in cohesionless soil is provided by the following analysis. Bekker (1960) has given the following equation for maximum drawbar pull for a rectangular loaded area of width, b, and length, ℓ.

$$DP = b\ell c + W \tan \phi - \frac{\left(\frac{W}{\ell}\right)^{(n+1)/n}}{(n+1)(k_c + bk_\phi)^{1/n}} \qquad (1\text{-}18)$$

For the metal-elastic wheel under a 100 lb load, b was 10.0 inches and ℓ was 20.4 inches. For a cohesionless soil, c and $k_c = 0$. Thus equation (1-18) becomes:

$$DP = W \tan \phi - \frac{\left(\frac{W}{\ell}\right)^{(n+1)/n}}{(n+1)(bk_\phi)^{1/n}} \qquad (1\text{-}19)$$

$$\frac{DP}{W} = \tan \phi - \frac{W^{1/n}}{(n+1)(bk_\phi)^{1/n}(\ell)^{(n+1)/n}} \qquad (1\text{-}20)$$

Evaluation of the second term on the right shows it to be only about 0.01 using the appropriate values for b, ℓ, and W, and k_ϕ for perlite. For the dry sand the value would be even less. Thus for this type of wheel the optimum pull number could be given simply by:

$$\frac{DP}{W} = \tan \phi \qquad (1\text{-}21)$$

Although the perlite was highly compressible and the dry sand was essentially incompressible they had similar values of ϕ (31° and 29°) and thus according to equation (1-21) optimum values of $\frac{DP}{W}$ should be comparable. Fig. 1-3 shows that in fact they were.

Now that it has been established that the lunar surface is in fact not covered by a thick layer of highly compressible dust and that the soil properties are similar to those of a "damp sand" terrestrial soil, some reconsideration of lunar roving vehicle design may be in order. The rather high degree of conservatism embodied by the wire and metal-elastic wheels may not be needed. Problems of vehicle dynamics, slope negotiability, and maneuverability may be more important than the problem of soil-wheel interaction on the lunar surface as regards the design of a vehicle that will permit travel on the lunar surface. A greatly improved understanding of wheel-soil interaction will be needed, however, if designs are to be optimized.

VI. NEEDED TRAFFICABILITY RESEARCH

As a result of studies thus far it would appear, at least in the vicinity of the Surveyor sites, that our knowledge of the mechanical properties of surface soils on the moon exceeds our present ability to use that knowledge in a quantitative manner for the design of lunar roving vehicles and prediction of their performance. This is not to say, however, that we now know all we need to know concerning the soil properties. Quite the contrary, it is still imperative that the tentative conclusion from Surveyor results that surface soils are reasonably similar in properties at different points on the moon must be confirmed. Density estimates are still open to question, and reliable values of the coefficient of friction between lunar soils and metals are needed.

Perhaps the most important but least known aspect of lunar soil behavior needed for trafficability analyses is the stress-strain relationship associated with lunar soil deformation. Some pressure-sinkage data were obtained using the Soil Mechanics Surface Sampler on Surveyor VII. Hopefully these data will provide some better insight into the problem. Visual observations during the Surveyor program as well as

the known behavior of terrestrial soils having similar ultimate strength properties (c and ϕ) indicate that the lunar soil deforms as an almost incompressible material. Thus the general form of the stress-strain relationship can be estimated. Meaningful quantitative analysis of wheel-soil interaction will probably require specific quantitative knowledge of this relationship.

Earth-based simulations may provide one possible source for this needed information. Simulated lunar soils having the proper gradation, density, cohesion, and angle of internal friction can be prepared and tested under confining pressures representative of those on the moon. The results of such tests would provide insight into the deformation behavior of actual lunar soils. Simple tests; e.g., penetrometers, analysis of spacecraft-soil and astronaut-soil interactions during early Apollo missions, will provide invaluable data concerning lunar soil variability and, to some extent, the stress-strain behavior. Studies of lunar rolling stones (see Volume I, Chapter 3) are a further source of useful information relating to wheel-soil interaction. A simple test could easily be devised to provide useful data on the behavior of rolling wheels during early Apollo missions. For example, an instrumented "wheel-on-a-stick" could be fabricated, or spheres of different size and density could be rolled down crater walls and their tracks photographed.

More complex tests and apparatus could be devised for use on the lunar surface that would detail more exactly the deformation behavior under the particular test conditions selected. There would, at this stage, be little to be gained by doing this, however. The reason for this is contained in the opening sentence of this section. Without a valid theory or reliable empirical basis for making performance predictions it is impossible to know exactly what form of soil data are needed and how they should be obtained.

It is recommended, therefore, that research be intensified on the problem of wheel-soil interaction with studies proceeding on two fronts. For the short range it may be possible to extend the WES similitude method to performance predictions for lunar roving vehicle wheels. Tests should be conducted using appropriate wheel types and loadings and

simulated lunar soils. Investigations should made of the influence of wheel load, wheel size, wheel slip, soil conditions, terrain inclination as related to wheel performance parameters (sinkage, motion resistance, drawbar pull, torque). Empirical correlations thus established would probably provide as reasonable a basis as any at present for prediction of performance. If possible, soil properties should be introduced into these correlations by means of cone penetrometer test results. The test is simple, the apparatus is simple, and cone penetrometer measurements could easily be made in early Apollo Missions.

For the long range, intensified efforts should begin now to develop an improved understanding of the mechanics of wheel-soil interaction with the ultimate objective of the formulation of a rational theory for performance prediction. Such a theory should relate wheel characteristics, loading conditions, soil properties and performance in a consistent manner. The task is formidable and the result may be in a form so complex that it cannot be applied in a practical manner. Nonetheless the results would still serve to focus attention on (1) the relative importance of various vehicle system factors and (2) the soil properties pertinent to solution of the problem. Such a study should begin with an analysis of the interdependent character of the stresses and deformations in the wheel and soil. Modern computation methods often make such analyses possible using numerical techniques.

VII. CONCLUSIONS

The following conclusions and recommendations have emerged from this preliminary study of the soil-vehicle interaction part of the lunar roving vehicle trafficability problem.

(1) While complete monoscopic photographic coverage of the moon has been provided by Orbiter, the small scale and limited quality and quantity of stereo coverage makes topographic analysis on the scale needed for trafficability studies difficult.

(2) Both the soil value (U. S. Army Ordnance Tank-Automotive Command Land Locomotion Research Laboratory Method) and the cone index (Army Mobility Branch, Corps of Engineers, Waterways

Experiment Station) systems of trafficability analysis have been reviewed. These two systems are used most extensively for off-the-road locomotion studies at the present time. The major advantage of the soil value system is that it yields quantitative values of performance parameters, e.g. total thrust, drawbar pull, power requirements, fuel consumption, which can be used for vehicle design and mission planning. Its major disadvantages are that parts of the theoretical basis of the method are questionable, the testing required for determination of the needed soil data is complex and not readily adaptable to lunar surface operations, and it is directly applicable only to level ground conditions.

The cone index method, on the other hand, involves very simple penetration testing which could be easily adapted for lunar operations. The disadvantage of this method, however, is that the information obtained is only suitable for determination of whether a given vehicle will or will not satisfactorily negotiate a given terrain. This may possibly be overcome in the future through further development of similitude analysis techniques.

(3) A review of recent trafficability and mobility literature has indicated the following (See Appendix):

a. The soil value system appears to be widely used as a basis for lunar roving vehicle analyses.

b. It would be desirable to continue studies for development of methods of converting c, ϕ, and ρ to k_c, k_ϕ, and n.

c. A means for conversion of cone index data to soil value system parameters would be very useful.

d. Further analysis of bearing capacity approaches to vehicle mobility would appear desirable.

e. The analogue computer technique for modeling the dynamics of soil-vehicle interaction appears promising (Abstract G Appendix A) and is deserving of further study.

f. A number of reports were reviewed which are concerned mainly with the design and testing of proposed lunar roving vehicles of various types. Many of these studies were done on simulated lunar-surface materials that were prepared without the detailed knowledge of soil conditions that has been provided by Surveyor. Some reanalysis and further testing using "Surveyor Soil" would appear in order.

(4) The Engineering Lunar Model Surface (ELMS) has been reviewed and found inappropriate for quantitative representation of lunar surface properties for trafficability analyses. Terrain characterization techniques now being developed by the U.S.G.S. are promising. Further work is needed before realistic and reliable analysis of soil vehicle interaction can be made.

(5) A similitude approach to the solution of lunar trafficability problems is very appealing, since quantitative measures of vehicle performance could conceivably be obtained using model tests and the results of simple soil tests; e.g. cone index. Unfortunately the similitude correlations developed by the Waterways Experiment Station for pneumatic tires do not appear suitable for description of the behavior of proposed lunar vehicle wheels; e.g. metal-elastic wheel, wire wheel. It is desirable that accelerated test programs be initiated with the objectives of (1) possible extension of the method for use with proposed lunar vehicle wheel types and (2) evaluation of key trafficability factors such as the influence of slopes and light wheel loads and contact pressures.

(6) A limited study of available data on the performance characteristics of the metal-elastic and wire wheels suggests that these designs may be overly conservative for application to the lunar surface. Some reconsideration of these designs appears in order.

(7) Needed trafficability research has been considered and specific recommendations are made in Section VI for (1) terrestrial

testing of simulated soils, (2) testing on the lunar surface during early Apollo missions, (3) further development of the similitude method for trafficability analysis, and (4) intensified studies for better theoretical description of wheel-soil interaction.

REFERENCES

1. AC Electronics-Defense Research Laboratories (1967), "Lunar Wheel and Drive Experiment Test Program", 2 Vols., Contract NASB-20267, June.

2. Bailey, W. (1965), "Comparison of Methods of Measuring Soil Shear Strength Using Artificial Soils", American Society of Agricultural Engineers Paper No. 64-113, Transactions of the ASAE, Vol. 8.

3. Bekker, M. G. (1956), "Theory of Land Locomotion", University of Michigan Press, Ann Arbor.

4. Bekker, M. G. (1960), "Off-The-Road Locomotion", University of Michigan Press, Ann Arbor.

5. Bekker, M. G. (1962), "Land Locomotion on the Surface of Planets", American Rocket Society Journal, Vol. 32, No. 11, November.

6. Bekker, M. G. (1962), "Mechanics of Off-The-Road Locomotion", James Clayton Lecture, Institute of Mechanical Engineers, November 13.

7. Bekker, M. G. (1965), "Mechanics of Locomotion and Lunar Surface Vehicle Concepts", SAE Automotive Engineering Congress, Detroit, Michigan, January 14-18.

8. Choate, R. (1966), "Lunar Slope Angles and Surface Roughness from Ranger Photographs", Jet Propulsion Laboratory Report 32-994.

9. Firth, B. W. (1967), "Resistance of Soils to Sinkage and Translation of Rigid Bodies: A Study by Means of Dimensional Analysis", Paper 670172, Automotive Engineering Congress, Society of Automotive Engineers, Detroit, Michigan, January.

10. Freitag, D. R. (1965), "A Dimensional Analysis of the Performance of Pneumatic Tires on Soft Soils", Tech. Rept. No. 3-688, U. S. Army Engineer Waterways Experiment Station, Vicksburg, Miss., August.

11. Freitag, D. R. (1966a), "A Dimensional Analysis of the Performance of Pneumatic Tires on Sand", Paper No. 66-128, 59th Annual Meeting of American Society of Agricultural Engineers, Amherst, Massachusetts, June.

12. Freitag, D. R. (1966b), "A Dimensional Analysis of the Performance of Pneumatic Tires on Clay", Journal of Terramechanics, Vol. 3, No. 3, pp. 51-68.

13. Hegedus, E. (1965), "Plate Sinkage Study by Means of Dimensional Analysis", Journal of Terramechanics, Vol. 2, No. 2.

14. Janosi, Z. (1958), "Prediction of WES Cone Index by Means of Land Locomotion Soil Values", OTAC Report No. 5, December.

15. Liston, R. D. (1964), "Methods and Goals of the Mechanics of Off-The-Road Locomotion", Society of Automotive Engineers, Paper No. 782A, January.

16. Mason, R. L., McCombs, W. M., and Cramblit, D. C. (1964), "Engineering Lunar Model Surface (ELMS), TR-83-D, Future Studies Branch, Launch Support Equipment Engineering Division, John F. Kennedy Space Center, September 4.

17. Onafeko, O. and Reece, A. R. (1967), "Soil Stresses and Deformations Beneath Rigid Wheels",Journal of Terramechanics, Vol. 4, No. 1, pp. 59-80.

18. Pavlics, F. (1961), "Bevameter 100. A New Type of Field Apparatus for Measuring Locomotive Stress-Strain Relationships in Soils", Proceedings of the First International Conference on the Mechanics of Soil-Vehicle Systems, June.

19. Reece, A. R. (1964), "Problems of Soil-Vehicle Mechanics", U. S. Army Land Locomotion Laboratory, March.

20. Reece, A. R. (1965-1966), "Principles of Soil-Vehicle Mechanics", Proc. Institution of Mechanical Engineers, Vol. 180, Part 2A.

21. Roth, B. J. (1960), "Aspects of Soil Trafficability", M. S. Thesis, Ohio State University.

22. Rozema, Wesley (1967), "The Power Spectral Density Function as a Surface Roughness Quantifier", Memorandum, U. S. Geological Survey, Branch of Astrogeology, Flagstaff, Arizona.

23. Thorman, H. C. (1963), "Review of Techniques for Measuring Rock and Soil Strength Properties at the Surface of the Moon", SAE Automotive Engineering Congress, Detroit, Michigan, January 14-18.

24. Trafficability Research Team, Corps of Engineers Israel Defense Army (1961), "A Proposed Recording Penetrometer", Proc. 1st International Conference on the Mechanics of Soil-Vehicle Systems, Turin and Saint Vincent, Italy, June 12-16.

25. U. S. Army Engineer Waterways Experiment Station (1962), "Report of Mobility Consultants Conference", June 13-15.

26. U. S. Army Engineer Waterways Experiment Station (1954), "Tests on Natural Soils with Self-Propelled Vehicles, 1951-53", Tech. Memo No. 3-240, 12th Suppl., November.

27. U. S. Army Engineer Waterways Experiment Station, CE (1965-), "Performance of Soils Under Tire Loads", Technical Report No. 3-666, a continuing series of reports beginning January 1965.

28. U. S. Army Engineer Waterways Experiment Station (1964), "Measuring Soil Properties in Vehicle Mobility Research", Technical Report No. 3-652, Report 1, August.

29. Vaughan, O. H. (1967), "Lunar Environment: Design Criteria Models for Use in Lunar Surface Mobility Studies", NASA TMX-53661, Sept. 28.

30. Willis, B. M. D. (1966), "The Load Sinkage Equation in Theory and Practice", Proc. Second International Conference of the International Society for Terrain-Vehicle Systems.

LIST OF SYMBOLS

a	distribution exponent
a_i	constants representing the elastic properties of the wheel
A	penetration area
b	width of loaded area
B_0	characteristic width of loading plate
c	soil cohesion
C	surface roughness coefficient
C_s	soil coefficient of viscous damping
C_{WES}	WES cone index
d	wheel diameter
DP	drawbar pull
e	energy reservoir
E	Young's modulus
f	radial penetration of obstacle into the circle of the undeformed wheel
F	fuel consumption
F_r	radial force
G	cone index gradient
h	tire section height
H	total thrust
HP	horsepower
j	soil shear deformation
k	constant for any given spectral estimate
k_c, k_ϕ	soil sinkage constants
K, or K_1, K_2	soil stress-strain constant(s)

K_i	soil constant
K_s	coefficient of subgrade reaction
L	length dimension
L_i	range of vehicle action
M	mass
MI	vehicle mobility index
n	soil sinkage constant
N	constant for any given spectral estimate
N_D	composite bearing capacity factor
N_q	Terzaghi bearing capacity factor
p	normal pressure
p_m	pressure required for fluidization
P_T	wheel towing force
$P(\Omega)$	power spectral density function
Q	torque on powered wheel
r	distance between contact element and axle
R	motion resistance due to soil compaction
RCI	rating cone index
RN	random number
$R(\tau)$	correlation function
s	soil shear stress
T	time
v	vehicle velocity
VCI	vehicle cone index
w	wheel deformation
W	vehicle weight
Y	obstacle height

Y_{max}	maximum obstacle height
Y_0	random surface profile
z	depth of penetration of applied load (sinkage)
z_m	maximum sinkage possible or sinkage at which collapse occurs
α	maximum negotiable slope
γ	soil unit weight
Δ	finite length
δ	tire deflection
θ	angle from the vertical to a point on the wheel circumference
ℓ	length of loaded area
η_1	mechanical efficiency of running gear and transmission
η_2	power conversion efficiency of the engine
ν	Poisson's ratio
λ	drawbar pull to weight ratio
λ_L, λ_p	constants for a particular wheel
ρ	soil density
τ	distance between points
ϕ	soil angle of internal friction
χ	specific fuel consumption of vehicle
Ω	spatial frequency

APPENDIX 1-A

RECENT TRAFFICABILITY AND MOBILITY LITERATURE

A review of recent literature on trafficability and mobility, particularly as related to lunar roving vehicles has been made. A number of these papers and reports are summarized here and comment is made where appropriate to aid in assessment of the state-of-the-art.

A. "An Analysis of New Techniques for the Estimation of Footing Sinkage in Soils", by L. Karafiath, Land Locomotion Research Branch, OTAC Report No. 18, October 1957

Theoretical evaluation is made of new techniques introduced by the Land Locomotion Research Laboratory for the purpose of determining the sinkage of various loaded areas in terms of k_c, k_ϕ and n values. New relationships were established between the friction angle, ϕ, and k_ϕ, k_c and n values as follows:

For a strip load:

$$\left(\frac{k_c}{b} + k_\phi\right) = \gamma \frac{N_D}{\ell} + \gamma N_q \qquad (1\text{-A-}1)$$

$$n = \frac{1}{\frac{\ell N_q}{2N_D} + 1} + 1 \qquad (1\text{-A-}2)$$

where

N_q = $f(\phi)$ = 21 for ϕ = 30° and 58 for ϕ = 36°

N_D = $g(\phi)$ = 4.6 for ϕ = 30° and 10.6 for ϕ = 36°

ℓ = width of the loaded strip

γ = soil unit weight

Comment: Since the Bekker method as crude as it may be, provides about the only presently available basis for quantitative vehicle performance estimates, a method for converting measured c, ϕ, and γ data to values of k_c, k_ϕ and n would be useful. This approach based on the assumption of incompressible soil deformation is an attempt at such a method. When put in a form suitable for analysis of circular footings, a bearing area geometry probably more suitable for analysis of lunar vehicles than a strip, the soil constant n is very sensitive to roughness of the loading plate through its influence on the length of the failure surface.

For the case of strip loading n is very insensitive to variations in the internal friction angle of the soil, ϕ, having a value only slightly greater than 1.0. The equations show $\left(\frac{k_c}{b} + k_\phi\right)$ to be sensitive to variations in ϕ however. In addition calculated $\left(\frac{k_c}{b} + k_\phi\right)$ values indicate a discrepancy in the method. For example, assuming that $\phi = 35°$, $\gamma = 0.01$ lb/in^3, $\ell = 10"$, equation (1-A-1) gives a value of 0.4 for $\left(\frac{k_c}{b} + k_\phi\right)$. If $\frac{k_c}{b}$ is assumed to be small, than $k_\phi = 0.4$. Therefore, equation (1-A-1) yields a value for k_ϕ which is approximately one-tenth the value estimated by Scott (1968) from the results of the Surveyor experiments.

B. "Locomotion Over Soft Soil and Snow", by A. Assur, SAE Publication No. 782F, January 1964

A relationship between load and sinkage is derived for 3 different types of soil behavior under load.

1. Fluidization - progressive increase in compressibility of soil under increasing load (progressive failure).
2. Compaction - progressive decrease in compressibility of soil under increasing load.
3. Collapse - progressive increase in compressibility of soil followed by collapse at maximum load. (Analogous to a crust over a soft foundation soil).

Case 1
Fluidization

$$z = \frac{p}{K_i(1 + B_0/b)(1 - p^2/p_m^2)} \qquad (1\text{-A-3})$$

Case 2
Compaction

$$p = \frac{K_i(1 + B_0/b)z}{1 - z^2/z_m^2} \qquad (1\text{-A-4})$$

Case 3
Collapse

$$p = \frac{K_i(1 + B_0/b)z}{1 + z^2/z_m^2} \qquad (1\text{-A-5})$$

In these equations:

- p = pressure
- z = sinkage
- b = width of loaded area
- B_0 = characteristic width of loading plate
- p_m = pressure required for final fluidization
- z_m = maximum sinkage possible in Case 2 or sinkage at which collapse occurs in Case 3

The constants K_i, B_0, p_m, and z_m can be determined by performing two load-sinkage tests on a soil using two loading plates of different width, b. They also may be determined from Bekker's soil constants k_ϕ, k_c, and n. According to Assur, these relationships apply directly to the behavior of sands, clays, and snow.

Comment: The relationships between sinkage and load for soil have been derived using assumed simple relationships between the soil stiffness and pressure or sinkage depending on the case. Therefore, the validity of these expressions is directly determined by the validity of these assumptions. The applicability of these equations can be easily determined by plotting two curves from the test data, $\frac{p}{z}$ versus p^2 and $\frac{z}{p}$ versus z^2. If the first plot is a straight line Case 1 is applicable and if the later plot is a straight line Case 2 or Case 3 can be used. Because of the complexity of the problem it is not likely that Assur's relationships will be all inclusive.

C. "Prediction of WES CONE INDEX by Means of Land Locomotion Soil Values", by Z. Janosi, OTAC Report No. 5, December 1958

The purpose of this paper was to present the results of an investigation which indicated that the "cone index" could be predicted from the soil value system parameters, k_ϕ, k_c and n. The reverse procedure of predicting the physical soil values from the cone index alone is not possible. The cone index in terms of k_c, k_ϕ, and n is given by:

$$C_{WES} = 1.625 \left[\frac{k_c}{n+1} \left((z + 1.5)^{n+1} - z^{n+1} \right) + 0.516 k_\phi \left(\frac{(z + 1.5)^{n+2}}{(n+1)(n+2)} + \frac{z^{n+2}}{n+2} - \frac{(z + 1.5) z^{n+1}}{n+1} \right) \right] \quad (1\text{-A-6})$$

The computed cone index was very close to the measured C_{WES} in the case of sand, but in the case of clay the values were in error by as much as 40%.

Comment: Development of relationships that would enable determination of k_c, k_ϕ and n from cone index and cone index gradient would be of considerable value since cone index measurements on the moon would be much easier than Bevameter tests.

D. "Bevameter 100. A New Type of Field Apparatus for Measuring Locomotive Stress-Strain Relationships in Soils", by F. Pavlics, Proceedings of the First International Conference on the Mechanics of Soil-Vehicle Systems, June 1961

The objective of this paper was to develop a test method utilizing rigid wheels for measuring physical soil parameters used in land locomotion mechanics (n, k_c, k_ϕ, c, ϕ, K). Theoretical analysis was made as the load-sinkage and traction-slip relations for a rigid wheel. Tests were performed in two different kinds of soil. This new approach was proposed to provide a quick and

continuous method for soil testing in the field.

Comparison of test results obtained from wheel tests with those obtained with the conventional bevameter showed that the sinkage soil parameters (n, k_c, k_ϕ) were in very close agreement. Shear soil parameters (c and ϕ) were slightly higher in the wheel tests. There is a significant difference between the values of the deformation modulus K, but it was felt that the K from wheel tests was more accurate than the K from the conventional test.

Comment: A simple "wheel-on-a-stick" measurement for the lunar surface has been suggested by us and U. S. Geological Survey Personnel. If ever given further consideration, then this reference must be studied in detail.

E. "Engineering Lunar Model Obstacles (ELMO)", by J. R. Olivier and R. E. Valentine, NASA TR-145-D, March 1965

It was recommended in the ELMS* model that a 20 percent allowance be included to cover the energy required to negotiate small objects. Since no analytical method could be found for defining the microporfile of the lunar surface and for computing energy required for traversing such a profile, the method in this paper was developed to fill the need. The procedure uses two parameters, terrain definition spacing and terrain elevation, to describe surface roughness. Terrain definition spacing is used as a specified constant value. Elevations are chosen randomly according to the distribution function.

$$Y = Y_{max} (RN)^a \qquad (1\text{-A-}7)$$

where

RN = random number

a = distribution exponent

Y_{max} = maximum obstacle height

*The Engineering Lunar Model Surface (ELMS) was discussed in more detail in a previous section.

A surface profile from such a system yields a series of discrete points. The general roughness of the terrain can be adjusted by varying the parameters.

Assumptions used were:

1. The reference plane is horizontal
2. The vehicle mass acts at the wheel center
3. The vehicle moves in only two directions
4. The wheels are rigid
5. Energy values are ideal energies
6. Constant wheel spacing
7. Inertia effects can be neglected

Comment: It is our understanding that ELMO has been abandoned in favor of power spectral density methods for description of surface roughness. A major limitation of ELMO is that natural relationships between heights at any two given points are ignored; i.e., the height at any given point is assumed to be unaffected by the height at any adjacent point. Consideration of natural terrains shows that it is unrealistic to assume that a maximum height is as likely to be followed by one near the minimum as by another near the maximum.

F. "A Technical Discussion on Terrain Characterization and Simulation Using Spectral Methods", by GM's Defense Research Laboratories, September 1965

A method which avoids the pitfalls inherent in the ELMO and ELMS models, is time series or spectral, analysis. It allows simple and quick reconstruction of models of sample terrains having desired statistical properties. With the assumption that a terrain area of moderate size is homogeneous with respect to surface roughness, the statistical properties of a single terrain profile are examined in order to characterize the entire terrain area. When analyzing random processes, the correlation function defines the degree of relationship as a function of the horizontal distance between two elevation points. The correlation function, $R(\tau)$, is equal to the average of the products of the elevation of points spaced at a distance τ.

$$R(\tau) = \text{Average } [g(t) \cdot g(t + \tau)] \qquad (1\text{-A-8})$$

τ = distance between points.

Under the assumption of homogeneity

$$R(\tau) \simeq \frac{1}{\Delta} \int_0^{\Delta} g(t)\ g(t + \tau) dt \qquad (1\text{-A-9})$$

This equation is approximate because of finite length Δ.

By applying a Fourier transform and considering the function to be periodic, but with infinite fundamental period the following relationship is formed:

$$R(\tau) = \frac{1}{\pi} \int_0^{\infty} P(\Omega) \cos \Omega\tau \, d\Omega \qquad (1\text{-A-10})$$

$$P(\Omega) = 2 \int_0^{\infty} R(\tau) \cos \Omega\tau \, d\tau \qquad (1\text{-A-11})$$

where $P(\Omega)$ is the power spectral density function (the power in a band of frequencies).

The power spectral density function can be applied to the analysis of the dynamic response of a vehicle to a terrain of given characteristics. A range of spatial frequencies significant to evaluation of dynamic response of 0.01 to 1.5 cycles/meter is suggested by the plots given by Van Deusen (1966). Vaughan (1967) recommends a range of 0.05 to 0.5 cycles/meter as likely to influence vehicle mobility. If the vehicle cannot be considered a linear system as is likely, power spectral density analysis of terrain can still be used for dynamic response evaluation by employing analog computer simulation in the following type of system.

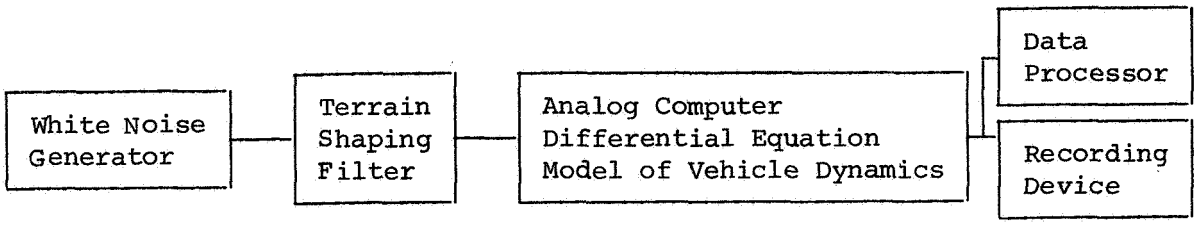

The responses of various portions of the vehicle (center of gravity, wheel structure etc.) are recorded as functions of time on a device such as a strip chart recorder. Energy consumption brought about by rough terrain can be studied in this manner under any desired set of assumptions. For example, in the ELMO analysis, energy consumption is considered to be the net potential energy imported to the vehicle by raising part, or all, of its mass, with provision for transfer of this energy from one axle to another.

G. "A Statistical Technique for the Dynamic Analysis of Vehicles Traversing Rough Yielding and Non-Yielding Surfaces", by B. D. Van Deusen, Chrysler Corporation, Contract NASW-1287, May 1966

A statistical analysis technique has been developed for the classification of virgin terrestrial and extraterrestrial surfaces. It has been demonstrated from available data that the power spectral density of profile height for a traverse across the lunar surface is equal to $C\Omega^{-2}$ where C is the surface roughness coefficient and Ω is spatial frequency. The single parameter C completely specifies the surface roughness in a statistical sense. Van Deusen considers that the exponent of 2 is appropriate as natural surfaces have not been shown to favor a predominant frequency. Artificial surfaces may have different values, however.

A dynamic non-linear yielding surface model was developed from existing information on soil mechanics. The model includes the hysteresis due to initial soil compaction and effects of vehicle speed and loading area.

Analog computer techniques were used to simulate lumped parameter models of typical lunar vehicles. An analog computer network,

capable of accurately predicting the dynamic response of vehicles traversing yielding and non-yielding surfaces was developed and implemented. A technique was included which allows a random surface profile, Y_0, to be introduced between the vehicle model and the yielding surface model and allows vehicle-surface separation. The model used for the analysis is shown in Fig. 1-A-1.

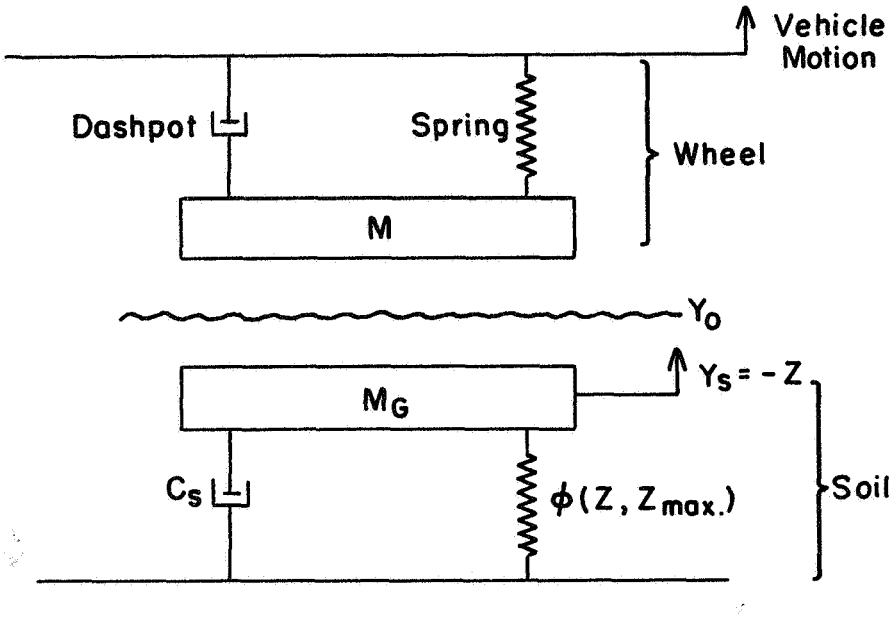

FIG. 1-A-1. Model for Analysis of Dynamic Interaction of Wheel and Yielding Soil Surface (after Van Deusen, 1966)

The following soil properties are needed for use in this model:

E = Young's modulus

ν = Poisson's ratio

ρ = density

K_s = coefficient of subgrade reaction

C_s = coefficient of viscous damping

Z_m = sinkage at maximum bearing strength, or

P_m = maximum bearing strength

Comment: The approach is appealing theoretically; however, few field data are available to support the theoretical predictions at this time. Reasonable estimates can probably be made for most of the needed soil parameters, at least for soil typical of that at the Surveyor sites. A major exception would be the value of the viscous damping coefficient, although perhaps a rough estimate might be possible using Surveyor landing dynamics data.

H. "Scale Model Testing of Land Vehicles in a Simulated Low Gravity Field", by D. Schuring, SAE Publication No. 660148, January 1966

The performance of lunar vehicles is best simulated here on earth by a freely maneuvering model (as opposed to a mathematical model or suspended vehicle). This can be either an exactly similar model whose important elements, like masses, springs, and dampers are scaled down to 1/6 in size, or an approximately similar model with springs, masses, and dampers scaled down to any size.

An approximate similar model is flexible (the size, springs, dampers, and masses can be adapted readily for almost any desired simulation. A major disadvantage results from the high velocity required; it must be higher than the velocity of the original vehicle. Therefore, high power and, in turn heavy motors are needed which limit the desirable mass reduction. Another disadvantage is restriction to linear springs and dampers.

These limitations can be avoided by using the 1/6-scale exactly similar model. Meeting its power requirements should be easy because velocities must be equal. Also, the springs and dampers can have any nonlinear characteristics.

I. "Lunar Wheel and Drive Experiment Test Program", 2 Volumes, by AC Electronics-Defense Research Laboratories, Contract NASB-20267, June 1967

This report outlines the activities concerning the study, analyses, design, manufacture, and test of wheels and mechanical drive systems for lunar vehicle application performed for the National Aeronautics and Space Administration by AC Electronics-

Defense Research Laboratories, General Motors Corporation.

A starting point for test planning was the review of vehicle concepts seriously considered for lunar surface vehicle applications which identified wheel and wheel drive designs under consideration. Although the survey included many wheel and drive concepts proposed previously, emphasis was on specified designs proposed by the Bendix Corporation and the Boeing Company — GM Team for Lunar Mobile Laboratory (MOLAB) and Local Scientific Survey Module (LSSM). The Metal-Elastic Wheel (Fig. 1-A-2) and Wire Frame Wheel (Fig. 1-A-3) concepts were selected as well as the Nutating and Harmonic Drive Mechanisms.

The testing and analysis program included the following:

1. Existing wheel and drive concepts were updated to reflect state-of-the-art technology.
2. Designs were established to reflect common design criteria.
3. Design analyses were made.
4. Critical components were tested to determine:
   a. load-deflection and dynamic characteristics
   b. drawbar-pull and wheel towing capability.
5. Designs were updated based on analyses and the results of the tests.
6. Final test articles and test equipment were fabricated.
7. A test program was conducted on final test articles, which included determination of:
   a. load-deflection characteristics
   b. drawbar-pull and wheel towing characteristics
8. Recommendations were given.

Common design criteria were established for the candidate wheel and drive concepts to allow a direct comparative evaluation. The following LSSM mission requirements and restraints were used.

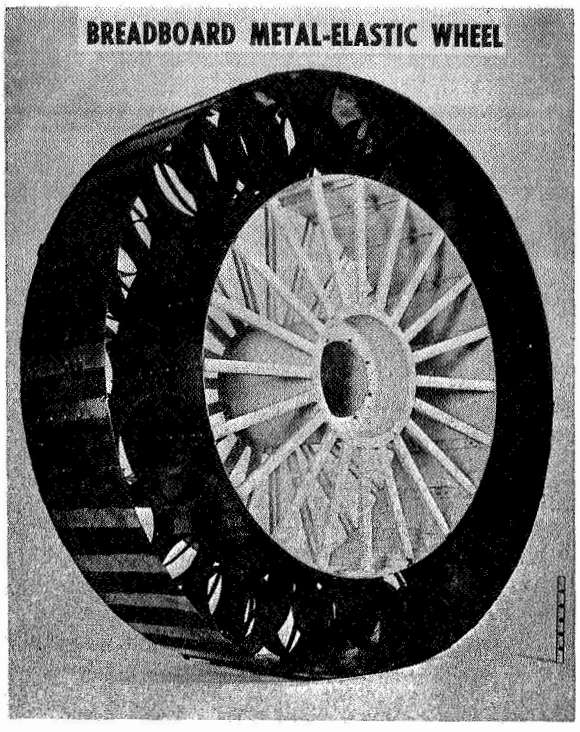

FIG. 1-A-2. Breadboard Metal-Elastic Wheel

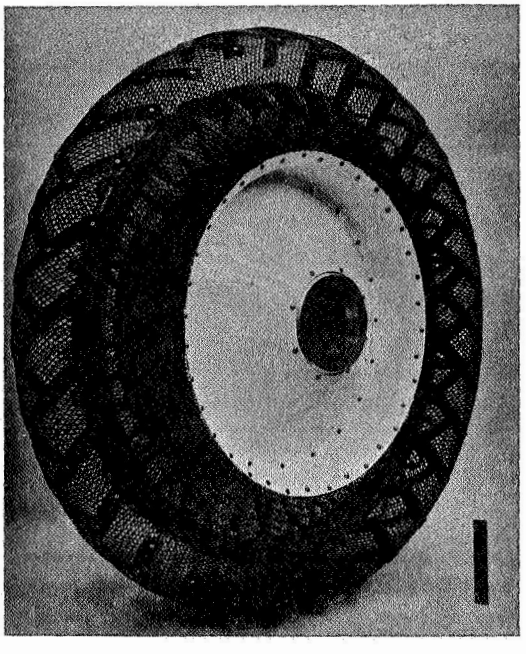

FIG. 1-A-3. Breadboard Wire Frame Wheel
(AC Electronics-Defense Research Laboratories, 1967)

Total travel	=	200 km
Travel time	=	40 hrs
Max. velocity	=	16 km/hr
Stand by duration	=	6 months
Terrain profile	=	ELMS

Test results indicated that both the metal-elastic and wire frame wheel concepts are technically feasible and can be successfully developed for a lunar surface vehicle application. It was also shown that the fatigue life of the wheels was adequate for smooth surface operation. Dynamic model testing, however, indicated that neither of the two wheel types could survive operation over a severe obstacle course for the full length of an LSSM mission. In the case of very soft and loose surface conditions (bearing strength < 1 psi) the metal-elastic wheel would have definite advantages due to low ground pressure. For harder conditions, however, the superior stability and inherent damping characteristics of the wire frame wheel make it more desirable, according to GM. It was recommended that the final designs be fabricated and further testing be conducted.

Based on test results and supporting analyses, it was concluded that although both drive mechanisms are technically feasible concepts, the development status of the harmonic drive is substantially ahead of that of the nutating drive. Neither test results nor analyses have shown any advantage for the nutating drive design.

Comment: The data for rolling resistance as a function of wheel load showed considerable scatter, which was attributed to inaccuracy in measurement.

The test results showed that in a soil with some cohesion the metal-elastic wheel performs better than the wire wheel. This was attributed to the longer length of failure plane in the case of the metal-elastic wheel. Other factors may also influence the results.

J. "Hypothetical Terrain Profile Energy Calculations", Special Study Report, BSR-2039, March 1967

Detailed energy calculations are presented for the SP-LSSM vehicle traversing a hypothetical terrain profile. Two speed conditions were used. One was specified by MSFC, and the second was recommended for minimal energy consumption by the contractor. It was concluded that the energy allocated for negotiating obstacles and small surface roughness in the SP-LSSM study is conservative if the expected lunar traverses are no worse than the hypothetical profile.

An attempt was made to obtain the average vehicle speed which would give minimum energy consumption. For all hypothetical soils used the soil parameter k_c was assumed equal to zero.

Comment: The terrain profiles assumed in this study were arbitrary in terms of obstacle heights, breadths, and spacings. Power spectral density methods applied to actual lunar terrain would probably be better. Bekker's soil value system was used for analysis of energy transmitted to the soil. Soil properties similar to those of the ELMS model were assumed, with the exception that for 0° slopes the soil was assumed incompressible. Thus the relevance of the results to actual lunar conditions may be questioned.

K. "A Contour-Adapting Wheel Model", by Dieter Schuring and Max Howell,Jr., A. C. Electronics, General Motors Corporation

A mathematical wheel model is presented that adapts its shape to any obstacle shape or terrain contour. An empirical equation of radial ground pressure that takes the shape of the obstacle or terrain and the wheel's elastic properties into account is the basis of the model.

Pressure-Radial Penetration Equation:

$$p(\theta) = \lambda_p \left(\frac{df}{d\theta}\right) + \lambda_L f \qquad (1\text{-A-}12)$$

$p(\theta)$ = pressure distribution

f = radial penetration of the obstacle into the circle of the undeformed wheel

λ_p & λ_L = constants for a particular wheel

Load-Deflection Equation:

$$F_r = b\lambda_p \int_{-\pi}^{+\pi} r \left(\frac{df}{d\theta}\right) d\theta + \lambda_L A \qquad (1\text{-A-}13)$$

F_r = radial force

b = width

r = distance between contact element and axle

A = penetration area = $b \int_{-\pi}^{\pi} r f d\theta$

Wheel Deformation-Pressure Equation:

$$w(\theta) = p_0 \frac{a_0}{2} + a_1(\bar{p}_1 \cos\theta + p_1 \sin\theta) + a_n(\bar{p}_n \cos\theta + p_n \sin n\theta) \qquad (1\text{-A-}14)$$

$w(\theta)$ = wheel deformation

a_i = constants representing the elastic properties of the wheel

The remainder of the expression on the right side of the equation is obtained by approximating the pressure, $p(\theta)$, through a Fourier series.

The approach was tested by comparing mathematical results with experimental response of the Metal Elastic Wheel being considered

for use on lunar vehicles. The measured load-deflection was compared to the analytical curve for two obstacles. The results showed good agreement between measured and analytical values. The wheel deformation for the Metal Elastic Wheel on a flat surface was computed by equation (1-A-14) above and compared to the measured deformation. Again the results showed good agreement.

APPENDIX 1-B

DETERMINATION OF VEHICLE MOBILITY INDEX FOR USE IN ARMY MOBILITY BRANCH (WES) METHOD OF TRAFFICABILITY ANALYSIS

Empirical relationships between the vehicle mobility index (MI), which reflects the vehicle characteristics, and the vehicle cone index (VCI) are of the form shown in Fig. 1-B-1. The MI of a vehicle is computed using the following empirical equations (Waterways Experiment Station, 1954):

Tracked Vehicles

$$MI = \frac{\text{contact pressure}}{\text{track factor}} \times \frac{\text{weight factor}}{\text{grouser factor}} + \text{bogie factor} - \text{clearance factor} \times \text{engine factor} \times \text{transmission factor} \qquad \text{(1-B-1)}$$

where

$$\text{contact pressure} = \frac{\text{gross weight (lb)}}{\text{area of tracks in contact with ground (in}^2\text{)}}$$

weight factor:

gross weight				
	< 50,000 lb	=	1.0
50,000	– 69,999 lb	=	1.2
70,000	– 99,999 lb	=	1.4
	> 100,000 lb	=	1.8

$$\text{track factor} = \frac{\text{track width (in)}}{100}$$

grouser factor:

grouser height			
	< 1.5 in	=	1.0
	> 1.5 in	=	1.1

$$\text{bogie factor} = \frac{\text{gross weight (lb)}/10}{\text{total number of bogies on tracks in contact with the ground} \times \text{area of one track shoe (in}^2\text{)}}$$

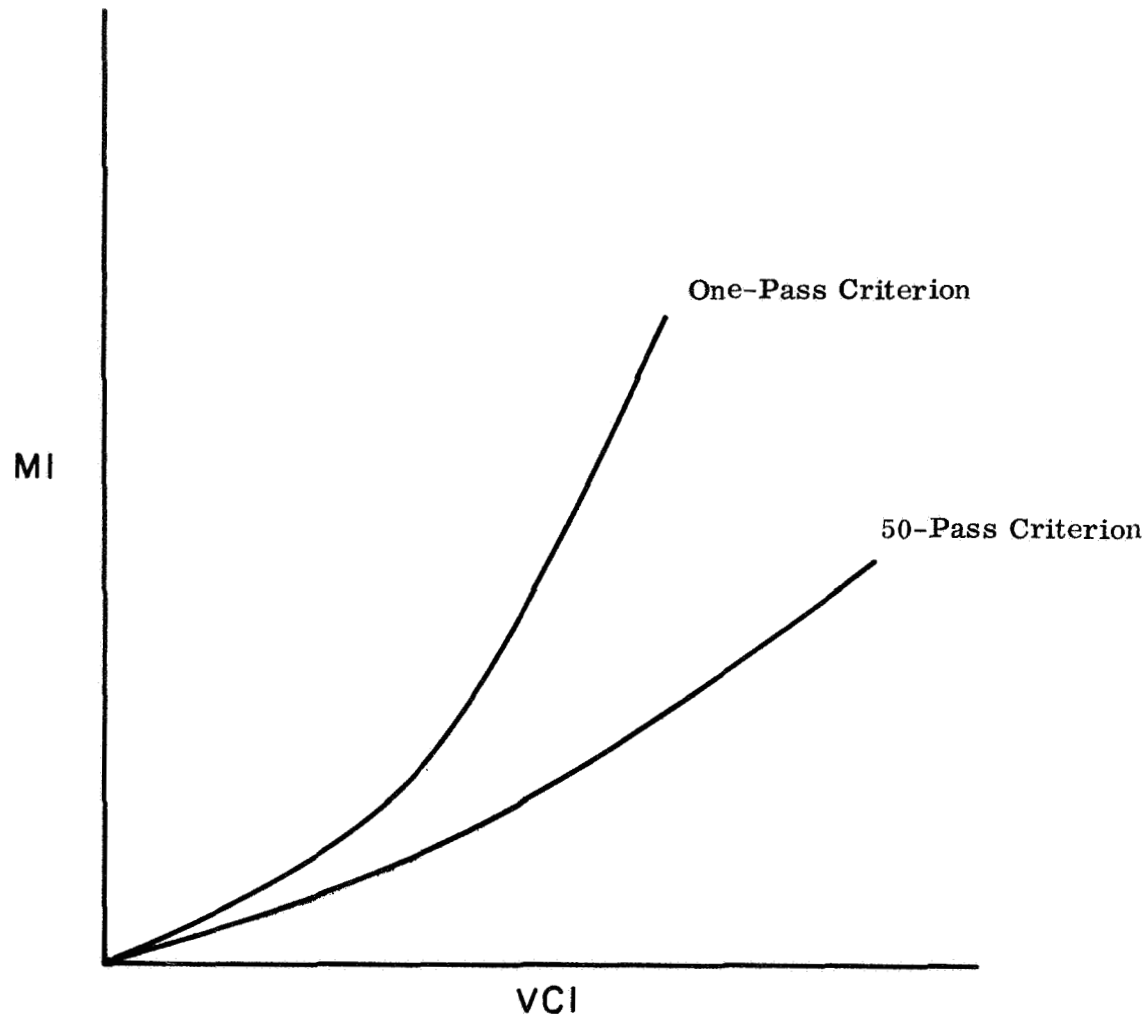

FIG. 1-B-1. Form of (MI) vs (VCI) Relationship

$$\text{clearance factor} = \frac{\text{clearance (in)}}{10}$$

engine factor: engine output > 10 hp/ton = 1.0

< 10 hp/ton = 1.05

transmission factor: hydraulic = 1.0

mechanical = 1.05

Wheeled Vehicles

$$MI = 0.6\left(\left(\frac{\text{contact pressure factor}}{\text{tire factor}} \times \text{weight factor} \times \text{grouser factor} + \text{wheel load} - \text{clearance factor}\right) \times \text{engine factor} \times \text{transmission factor}\right) + 20 \qquad (1\text{-B-2})$$

where

$$\text{contact pressure factor} = \frac{\text{gross weight (lb)}}{\text{tire width} \times \text{rim diameter} \times \text{number of tires}}$$

weight factor: gross weight > 35,000 lb = 1.1

15,000 — 35,000 lb = 1.0

< 15,000 lb = 0.9

$$\text{tire factor} = \frac{1.25 \times \text{tire width (in)}}{100}$$

grouser factor: with chains = 1.05

without chains = 1.0

$$\text{wheel load} = \frac{\text{gross weight (kips)}}{\text{number of wheels}}$$

$$\text{clearance factor} = \frac{\text{clearance (in)}}{10}$$

engine factor: engine output > 10 hp/ton = 10
< 10 hp/ton = 1.05

transmission factor: hydraulic = 1.0
mechanical = 1.05

Field tests have been used to determine the approximate relationship between a vehicle's maximum tractive effort or the maximum slope negotiable in a given soil and the quantity (RCI - VCI). Fig. 1-B-2 shows the form of this relationship (Roth, 1960).

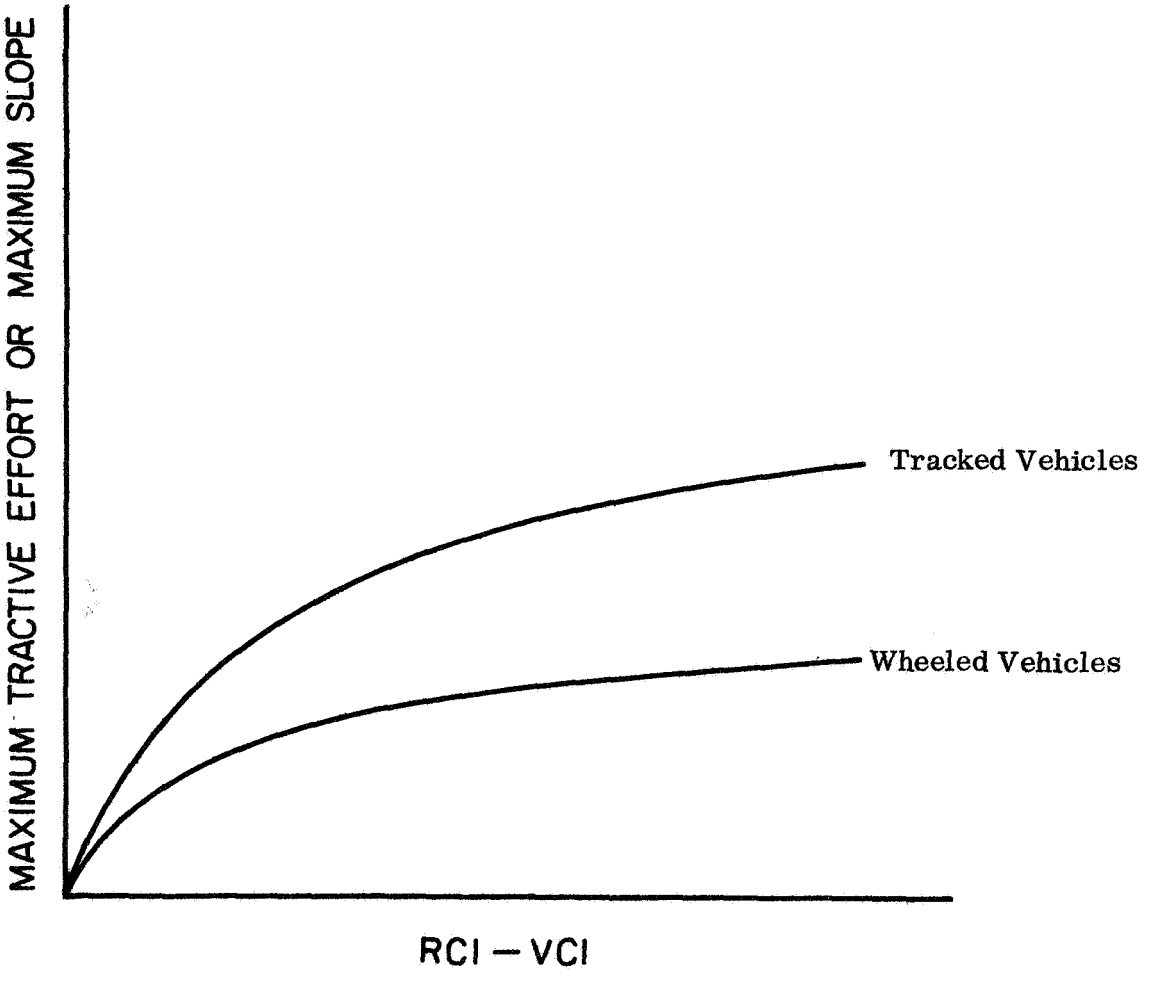

FIG. 1-B-2. General Form of the Tractive Effort and Negotiable Slope vs Difference Between Rating Cone Index and Vehicle Cone Index Relationship

C H A P T E R 2

FRICTION AND ADHESION IN ULTRAHIGH VACUUM AS RELATED TO LUNAR SURFACE EXPLORATIONS

By

J. Frisch and U. Chang

CHAPTER 2

FRICTION AND ADHESION IN ULTRAHIGH VACUUM AS RELATED TO LUNAR SURFACE EXPLORATIONS

(J. Frisch and U. Chang)

I. INTRODUCTION

It is known that an ultrahigh vacuum environment produces significant effects on such mechanical phenomena in materials as friction, adhesion, tensile behavior, fatigue life, etc. Among them friction and adhesion, which are closely related to surface properties, are most significant because the vacuum environment gives cleaner surfaces than the atmospheric environment. The surfaces in air are covered with oxides, moisture and other contaminants which prevent intimate contact of the two materials, thus acting as lubricants between the two contacting surfaces. A vacuum environment largely eliminates these effects.

Generally, coefficients of friction and adhesion increase considerably in vacuum, which implies that more power might be required to operate vehicles on the moon's surface where the environment is estimated to be a vacuum of approximately 1×10^{-14} Torr. Lunar vehicle design will require information both on rolling and sliding friction and on adhesion under such vacuum conditions.

While some data are available on sliding friction and adhesion under extreme conditions of temperature and vacuum, little work has been done on rolling friction over simulated lunar materials in vacuum. As a consequence the following task was indicated as part of Contract NSR 05-003-189: "Review of friction and adhesion problems. Recommendations for improved design of existing apparatus for determination of frictional and adhesion characteristics of different metallic and nonmetallic materials under high vacuum and at high and low temperatures."

Since significant purpose for such experiments may be the determination of power requirements for vehicles on the moon, recommendations have been formulated for experiments to determine rolling friction between

model wheels and simulated lunar rocks as a simulation of vehicle movement on the moon. Subsequent experiments could include the determination of rolling friction between model wheels and simulated soil samples. A review of studies on friction and adhesion is given first which includes data useful for the design of future experiments.

This review is followed by a brief report of four preliminary tests on adhesion in vacuum with copper and aluminum on obsidian. These tests were performed in order to determine the test capability of an existing force dynamometer and to determine the magnitude of adhesion, outgassing of rocks, polishing techniques for the specimens, and the time required to pumpdown to pressures at 10^{-10} to 10^{-11} Torr with these materials.

Included is a design for rolling friction tests utilizing the equipment already available. The design emphasizes a multi-test configuration without disturbing the vacuum to assure the same environmental conditions. Also included are provisions for initiating ion bombardment of rock specimen to simulate solar wind conditions.

II. REVIEW OF STUDIES AND EXPERIMENTS RELATED TO MOBILITY IN ULTRAHIGH VACUUM

A. Lunar Environment (After Fields et al., 1967)

Pertinent aspects of the lunar environment as they may influence friction and adhesion characteristics of materials are summarized briefly below.

1. Surface environment

a. Vacuum. Estimated lunar surface pressure ranges from 1.3×10^{-10} N/m^2 to below 1.3×10^{-12} N/m^2 ($1 \times 10^{-12} \sim 1 \times 10^{-14}$ Torr). Some of the probable atmospheric constituents include water, carbon dioxide and hydrogen.

b. Thermal conditions. The maximum and minimum temperature on the lunar surface are approximately 400° K and 70° K which are the temperatures of the lunar day and night respectively.

c. Solar wind and cosmic debris. The atmospheric condition allows α particles and protons of the solar wind to strike the lunar surface. Also a strong erosional process on the lunar surface probably occurs due to the impact of micro-meteoroids. Thus surface cleaning by sputtering and grit blasting or erosion may occur both for lunar materials and for spacecraft components.

d. Lunar gravity. The acceleration of gravitation on the moon is 1.62 to 1.63 m/sec^2 or approximately 1/6 that on earth.

2. Surface properties. Extensive information on lunar surface properties is given in Volume 1, Chapter 2 of this report.

B. Friction in Ultrahigh Vacuum

Although frictional behavior between metal specimens in vacuum environment has been studied in detail (Frisch, 1965, 1966, 1967), not much information on friction between metals and non-metals is available. Few theoretical explanations of friction between metals and non-metals have been attempted, but most investigators believe that the mechanism which describes metal friction and the adhesion mechanism, may also apply to metal/non-metal friction. To understand the basic mechanism of friction between metals and non-metals, more investigations are required.

1. Types of surface bonds. The exact nature of solid silicate adhesion in vacuum is not completely known, however possible types of bonding might include primary bonding (ionic-covalent) of the lattice structure, metallic bonding, molecular bond (Van der Waals bond), and electrostatic attraction due to electrostatic surface charges. Fig. 2-1 shows the relative importance of different bond types in several materials. Characteristics of the different bond types are summarized in Table 2-1.

2. Surface properties. Before deciding which type of bond is most effective for silicate-metal adhesion, it is necessary to know details of the characteristics of both surfaces. A freshly produced silicate surface as shown in Fig. 2-2 should adjust to a stable state by

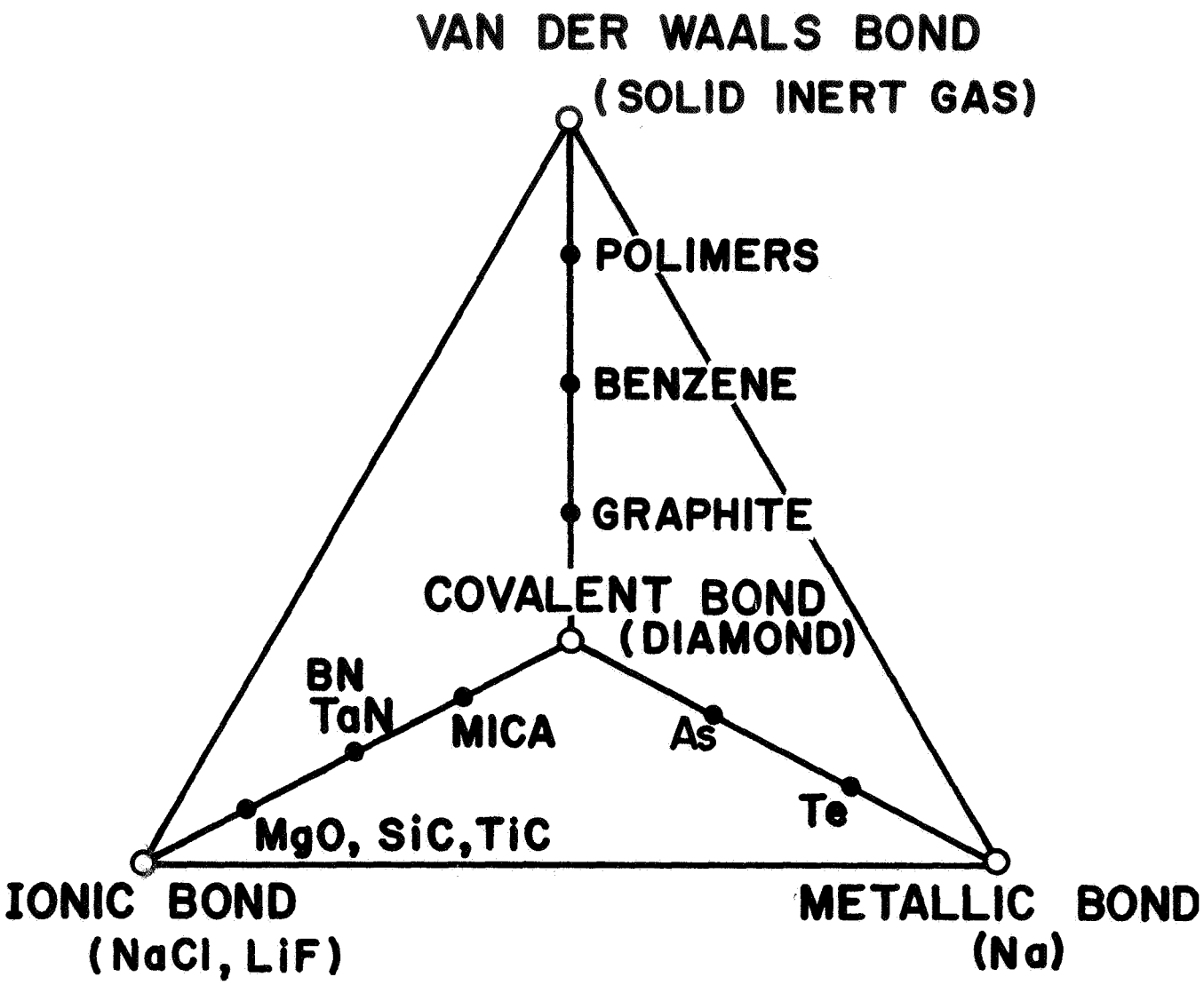

FIG. 2-1. Various Types of Bonding

TABLE 2-1

POSSIBLE BONDS (39, 50, 51)

		Type of Bond	Source	Magnitude	Directionality	Effective Radius	Silicate Examples
ATOMIC BOND	PRIMARY BONDS	Ionic	Electrostatic attraction of positive and negative ions	Very strong 30 ~ 200 Kcal/mole	Non-directional	Very long	Most silicates show partly covalent partly ionic
		Covalent	Share their outer electrons	Very strong	Directional	Short	But silicon forms bonds that are partly covalent, partly metallic.
		Metallic	Share all the valence electrons	Strong	Non-directional	Long	
	SECONDARY BONDS	Molecular (Van der Waals)	Displacement of charge within electrically neutral atoms or molecules	Very weak (abt. 1/10 of hydrogen bond)	Non-directional	Short	
		Hydrogen	Dipole attraction with hydrogen atom as positive end	Weak 10 or 20 Kcal/ Kcal/mole	Directional	Very long	Kaolinite
OTHER PHYSICAL BONDS	ON SURFACE	Electrostatic charges	Electrostatic attraction of the charges produced on the surface	Depends on the amount of charges	Non-directional	Extremely long	Rubbed silicate powders
		Wedge effect	Physical wedge locking	Depends on the surface configuration but not very feasible if surface is pretty smooth	Non-directional	Short	
		Absorbed surface film	By the action of surface film (water, vapor, etc.)	Weak	Non-directional	Short	Clay

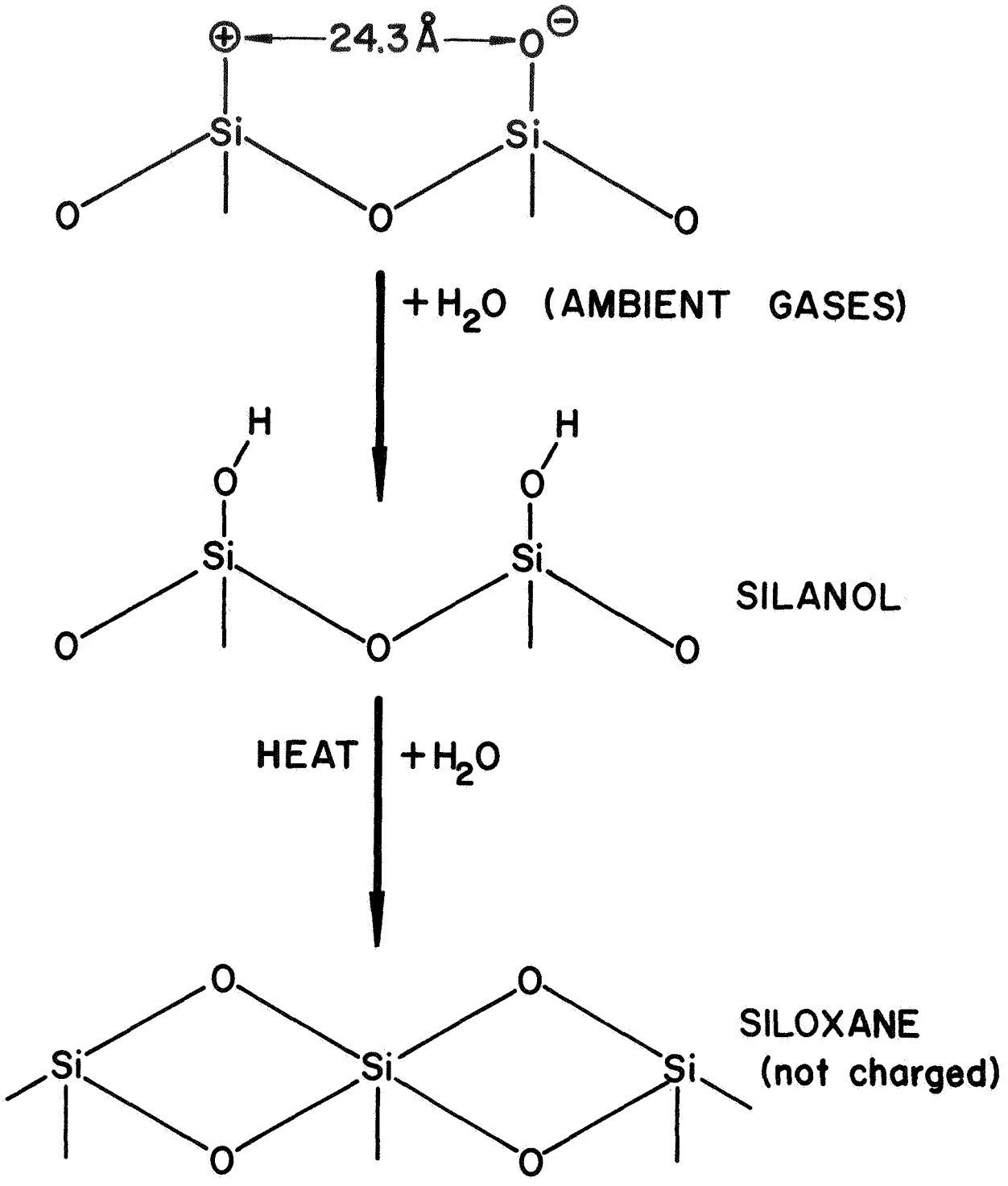

FIG. 2-2. Typical Silicate Surfaces

adsorbing ambient gas molecules. The freshly exposed silicon ions will satisfy their charge and coordination demands by first attaching the ambient gases like water vapor to form silanol. The desorbed surface is siloxane of hydroxyle group (Bromwell, 1965) which is stable. If the new surface is formed in absolute vacuum some surface distortion caused by the necessity for cation screening could occur.

The exact nature of the surface state of lunar soil is not known yet, but reasonable bounds are expected as more information becomes available. The lower bound would be a surface whose charge and coordinate demands are satisfied by having some degree of adsorbed material present. The adsorbed materials could be the kinds of gases present during the formation of lunar rocks. The upper bound would be one whose charge and coordinate demands are not satisfied. The lower bound appears more reasonable for the soil on lunar surface. The lower bound can be represented by air-formed surfaces while the upper bound by vacuum-formed surfaces. Considering the erosive effect of solar wind and cosmic debris on the lunar surface, the best simulation might be a surface slightly etched and then bombarded by ion particles. Such an erosion process gives the appearance of a finely etched surface.

3. Theory of friction. The coefficient of static friction is defined by:

$$\mu_s = \frac{T}{N} = \tan \phi_s \qquad (2\text{-}1)$$

where

T = tangential force to initiate sliding

N = normal load

The coefficient of kinetic friction, μ_k is the ratio of the tangential force, required to continue sliding, to normal load. μ_k is usually smaller than μ_s, because the bonding between two sliding surfaces is a function of time.

Modern theory (Bowden and Tabor, 1954) explains the basic friction mechanism as bonding of contacting asperities. The real area of contact, A_r, to support the normal load N can be expressed:

$$A_r = \frac{N}{q_u} \tag{2-2}$$

where

q_u is yield pressure or essentially the bearing capacity of the metal. The relation $q_u = 3\,\sigma_t$ has been suggested for most metals, where σ_t is the yield stress. Then:

$$\mu_s = \frac{T}{N} = \frac{A_r \cdot \tau_m}{A_r \cdot q_u} = \frac{\tau_m}{q_u} \tag{2-3}$$

where

τ_m is the shear strength of the material.

However, actual systems do not exhibit this simple relationship. Therefore, Bowden and Tabor's theory of dry friction analyzes the deformation of typical asperity junctions as sliding ensues. For an idealized model of asperity junction, the Von Mises yield condition in the two dimensional case can be represented as:

$$p^2 + 3S^2 = \sigma_t^{\,2} \tag{2-4}$$

where

p = compressive stress

S = shear stress

σ_t = tensile yield stress

For a three dimensional case the relation is:

$$p^2 + \beta S^2 = \frac{\beta}{3} \sigma_t^2 \qquad (2\text{-}5)$$

where

β is a constant shape factor

Bowden and Tabor (1954) suggest a value of $\beta = 9$ based on experimental evidence. During the initial stage $\sigma_t \simeq p$ for the two dimensional case when $S \simeq 0$. The plastic flow of the asperities, with combined tangential and normal load, causes an increase in contact area of the asperities and also brings other asperities into contact.* This "junction growth" will continue until the increased contact area is large enough to support the combined tangential and normal load. As the tangential load increases, failure may occur at the asperity interface. The interfacial shear strength, S_i, can be related to the shear strength of the asperity material, τ_y, by a constant $K \leq 1$ such that $S_i = K\tau_y$. Therefore, the yield condition for the three dimensional case can be written as:

$$p^2 = 9S_i^2(K^{-2} - 1) \qquad (2\text{-}6)$$

$$\frac{S_i}{p} = \frac{1}{3(K^{-2} - 1)^{1/2}} \qquad (2\text{-}7)$$

---

* Note: It would be a worthwhile experiment to perform metal - non-metal adhesion tests to determine this condition. With a constant normal load, two types of adhesion tests could be performed. After applying a tangential force below the friction force for a given interval, the adhesion force would be measured. This value could then be compared with the one obtained when a prior tangential force is not applied. For the asperity theory to be applicable the former value should be the larger one.

The coefficient of kinetic friction will be:

$$\mu_k = \frac{T}{N} = \frac{S_i \cdot A_r}{p \cdot A_r} = \frac{S_i}{p} = \frac{1}{3(K^{-2} - 1)^{1/2}} \qquad (2\text{-}8)$$

The factor K depends on the cleanliness of the surface. For a perfectly clean surface K = 1 which makes $\mu_k \to \infty$. The effect of K on μ_k is shown in Fig. 2-3.

4. Coefficient of friction. From the preceding discussion μ should be an apparent function of the degree of surface contamination, which is represented by the factor K. No velocity term is included in the expression of μ but the "junction growth" can be thought of as a function of time (Bowden and Tabor, 1954) and S_i or τ_y is strain rate sensitive. The real contact area is assumed as decreasing with increasing relative velocity of the two specimens and accordingly, p as well as S_i also increases. These two effects are of a compensating nature. At very high speed the temperature of the interface increases. If the yield pressure p of the cold substrate remains constant while the interfacial shear stress S_i drops, lower values of $\mu = \frac{S_i}{p}$ are obtained than at lower velocity. However, μ is not sensitive to the temperature increase of the bulk material. Generally, the coefficient of friction is constant at all velocities, but may show a slight decrease with increased velocities.

Over a wide range of values the effect of normal load on μ is known to be negligible, however p can be increased with larger normal loads as a result of work hardening. From Equation 2-8, it might be expected that μ_k decreases with increases of the normal load N. The stress field formed by dislocation pile-ups from normal deformation may not seriously affect the dislocation movements in the shear plane for tangential forces, because the slip plane of the normal deformations may be different from that of the tangential deformations.

The combined stresses of the normal and tangential forces may cause failure to occur on a plane other than the interface of the asperities. Experimental investigations by Cocks (1966) have shown that

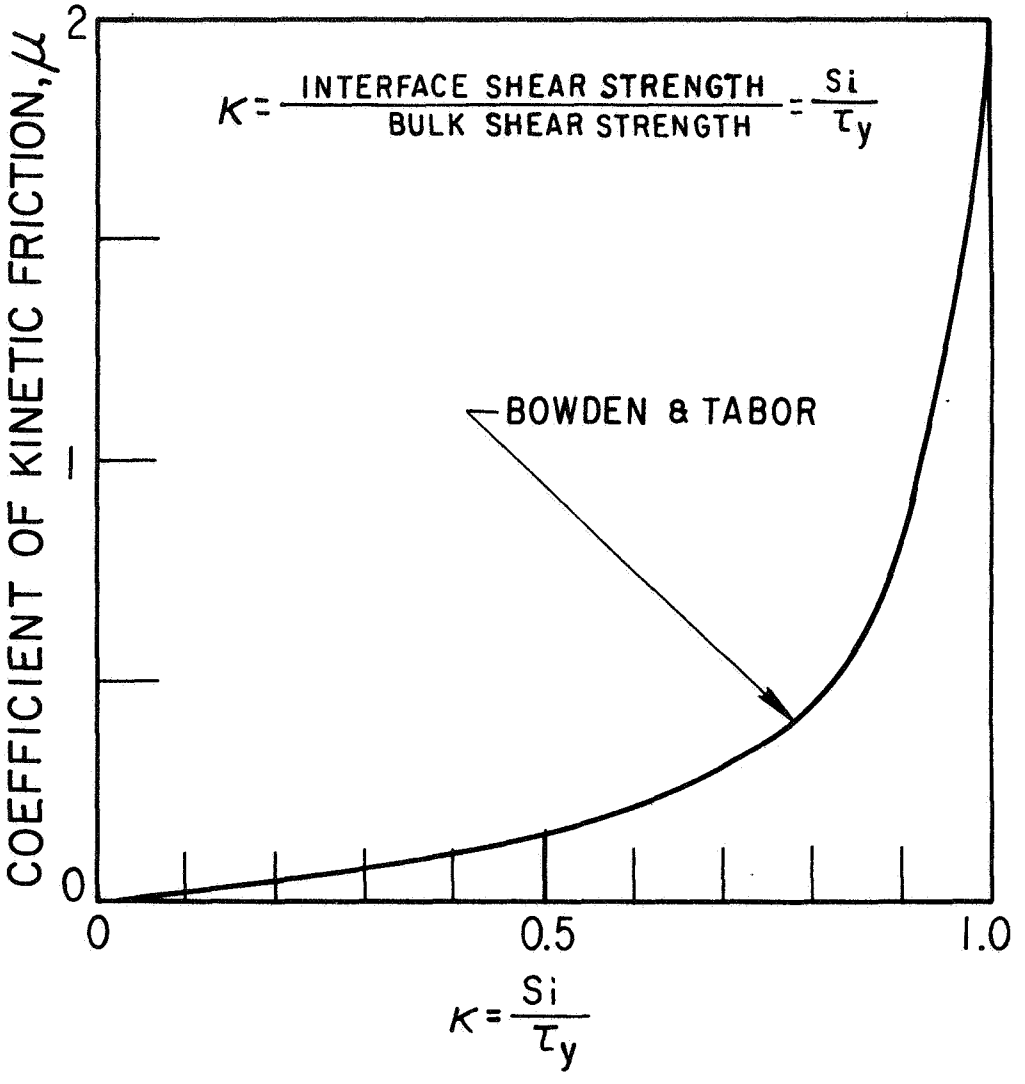

FIG.2-3 COEFFICIENT OF FRICTION μ AS FUNCTION OF K

the plastic deformations at asperity junctions can form "wedges" as shown in Fig. 2-4 and failure may occur at the root of the junction.

For a quantitative explanation of the mechanism of friction in materials whose asperities yield elastically rather than plastically, a knowledge of the real contact area A_r is required. For a perfectly elastic material the diameter, d, of the contact area A_r between a plane and spherical tip according to Hertz is:

$$d = (\delta NR)^{1/3} \tag{2-9}$$

where

N = normal load

R = radius of the tip

δ = a coefficient dependent on the geometry and elastic properties of the material

The contact area is thus proportional to $N^{2/3}$, which leads to the result:

$$\mu = \frac{T}{N} = \frac{\tau_y k N^{2/3}}{N} = \tau_y k N^{-1/3} \tag{2-10}$$

This is the case when the number of asperity junctions remains constant and increase their area relative to the normal load. But the actual case may be that both the number of asperities and the contact area of each asperity will increase with increases in normal load. It, therefore, is reasonable to expect that A_r may vary as N^n, where n is between 2/3 and 1, (Bromwell, 1966).

Surface contamination is the most critical factor affecting the value of μ. Adsorbed layers (Fig. 2-5) prevent pure metal-to-metal contact, decreasing the value of $\tau_y A_r$, which leads to a reduced value of μ. As shown before, a contamination-free surface would result theoretically in $\mu \to \infty$.

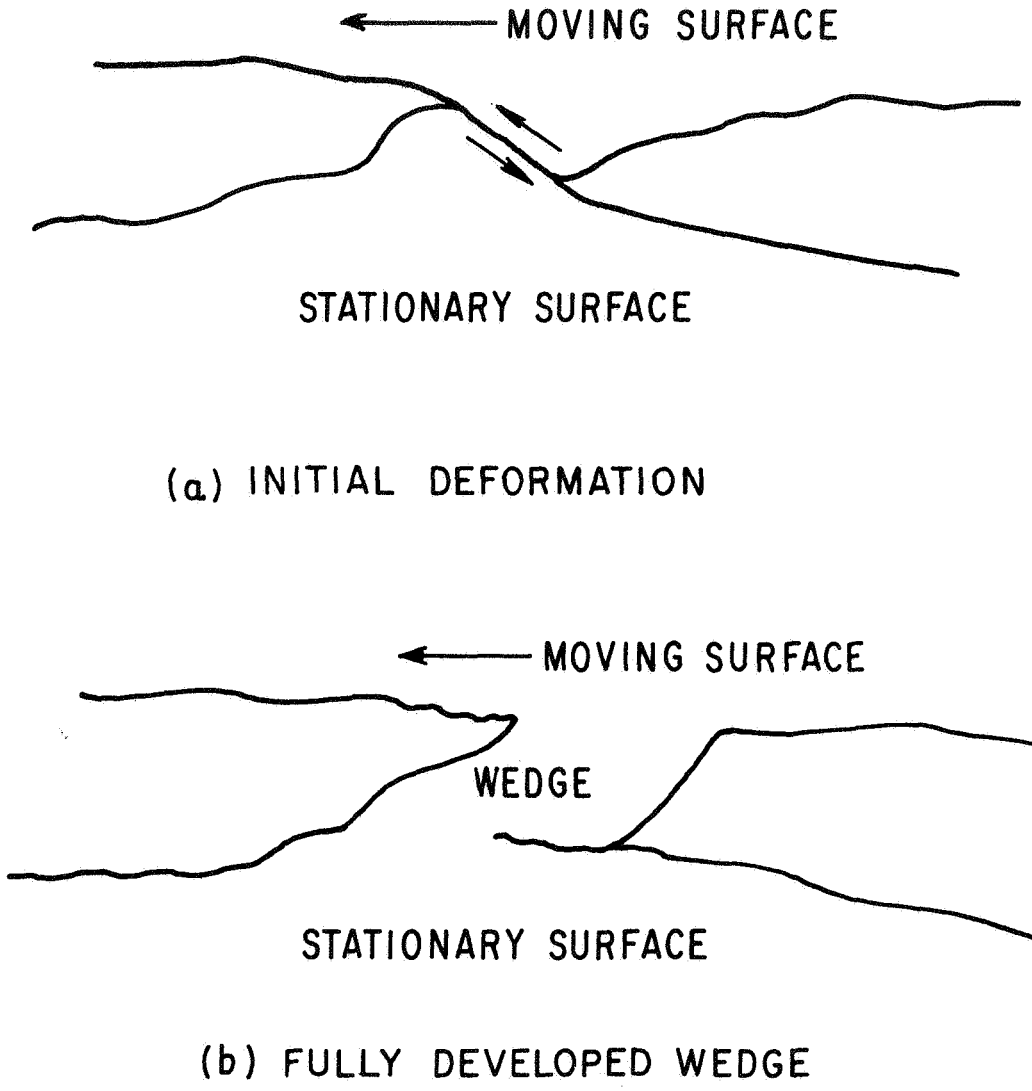

FIG. 2-4. Typical Mechanism of Wedge Formation Between Contacting Surfaces

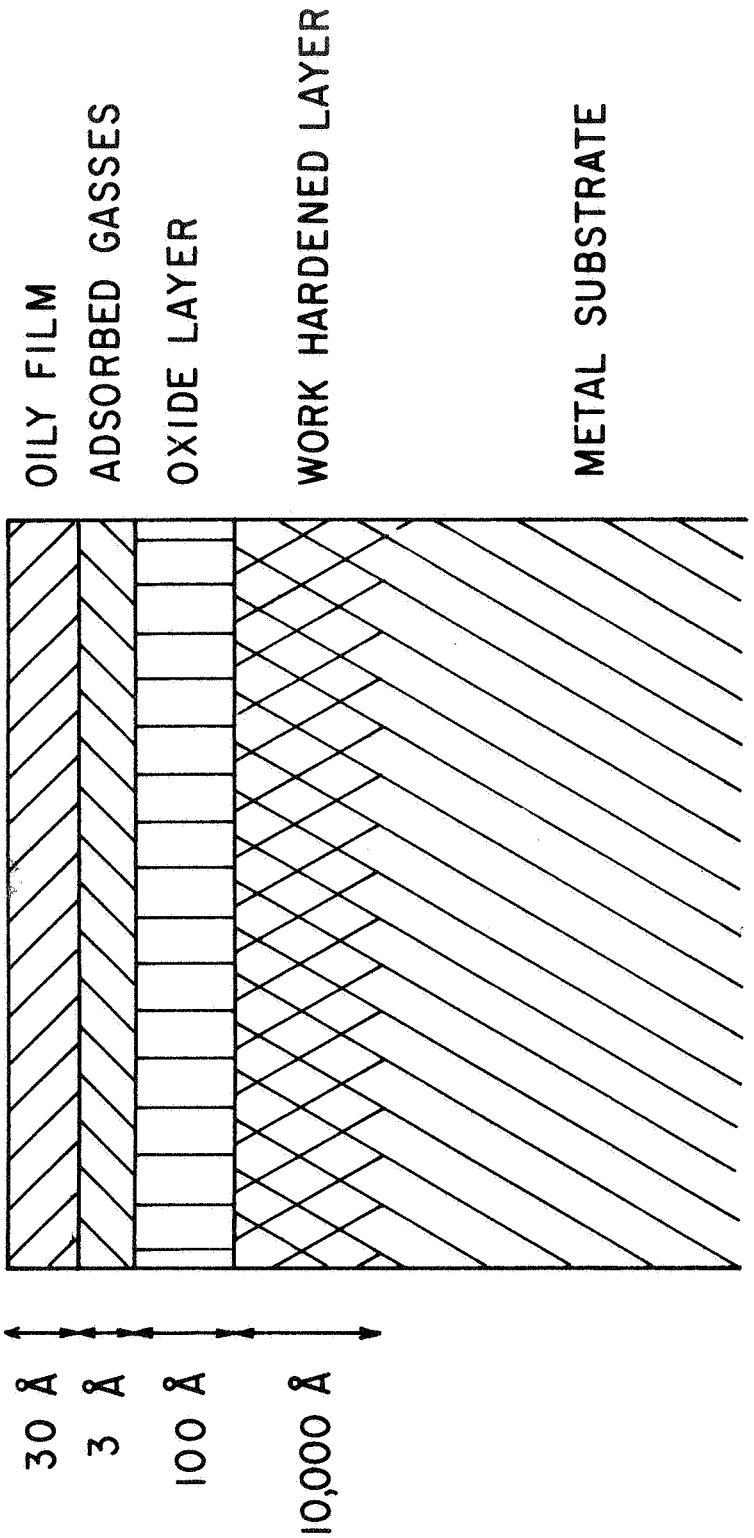

FIG. 2-5. Representative Diagram of Surface Layers (Salisbury et al., 1963)

Some studies (Penn, 1965, 1966) on the friction between metals and non-metals suggest that subsurface melting could occur at the asperities. It also attributes the decrease of μ_k at high speeds to the melted zone. Higher temperature at the asperities is thus expected to decrease μ_k since it helps in forming a molten zone.

Most non-metallic solid (namely "rocks") tends to have extremely strong covalent bonds, or combinations of covalent and ionic bonds between their molecules. Therefore, rocks cannot be expected to readily form a molten layer between the asperities. Even metals, the bonds of which are comparatively weak, do not form a molten layer during sliding. If the two sliding objects do form a molten layer, the coefficient of friction should be a function of temperature. If the experiment deals with the friction of metals on rocks, such a molten zone might be formed on the metallic side because of the weaker bond weaker interatomic bonds in metals in most rocks. If this is the case, a very thin film of metal should smoothly cover the rock asperities. However the material transfer observed in our experiments (see section does not show a film-like layer but rather imbedded particles on the non-metallic surface. This tends to indicate the irregular yield of local asperity junctions of the metallic part.

The most feasible explanation of the formation of asperity junctions may be "cold welding". If two molecules, which can form a bond between one another, are brought together within the effective radius of attraction, a strong bond can be formed. Usually the effective radius in covalent bonding is shorter than that of metallic bonding. Also, covalent bonds are highly directional while metallic bonds are not. This may be the reason why most non-metals show a lower value of μ_k than metals.

5. Friction between metals and non-metals. The mechanism of friction discussed in the preceding Section applies primarily to ductile metals which exhibit wide ranges of plastic deformation. Most non-metals show brittle fracture at small strains rather than plastic deformation, which introduces some doubt about the applicability of the "cold welding theory" to non-metallic friction.

Bromwell (1966) has suggested that frictional resistance of brittle materials, as for ductile metals, is due to cohesive forces acting at the contact points, and concluded that brittle materials would not exhibit "cold welding".

The study done by S.H. Penn (1964) shows that friction between interacting solids is primarily an adhesion phenomenon: The coefficients of friction for metals sliding on non-metals were greater in a vacuum than at atmospheric pressure. The temperature and vacuum dependency of μ_k may be of aid in finding out whether the mechanism of friction is mainly adhesion. Bromwell's conclusion was that neither the vacuum environment nor temperature alone increases μ of quartz blocks. μ_k of quartz crystals increases under high vacuum (higher than 10^{-8} Torr.) and high temperature (350° C.). The temperature dependence of μ was somewhat inconsistent, ranging from an increase of 30% to a decrease of 25%. The average values of μ_k decreased at high temperature. The temperature used in the experiment was not reported. On the other hand, Ryan (1967b), in his study of adhesion, concluded that adhesion increases considerably in a vacuum environment. He could not find any dependence of adhesion on temperature in his experiment with orthoclase. The basic mechanisms of friction between metals and non-metals will require further studies to obtain satisfactory explanations for the phenomenon. For the friction of particles and an aluminum disk slider it has been reported (Penn, 1965) that μ_k was inversely proportional to the average particle size, but the effect of normal load on μ_k was slight. The coefficient of friction of aluminum on quartz particles varied from 0.15 in atmosphere to .30 in ultrahigh vacuum. Between stainless steel and quartz particles μ_k was 0.14 in ultrahigh vacuum. The adhesion study by Ryan (1967b) also showed that stainless steel did not adhere to orthoclase in ultrahigh vacuum. Friction experiments with quartz blocks (Bromwell, 1966) demonstrated that for a smooth surface the coefficient of friction varies greatly according to the surface cleaning process, however for a rough surface it is almost constant. Generally μ_k for quartz blocks varied between 0.1 and 1.0 depending surface cleanliness.

In summary, the coefficient of friction, varies with normal load, temperature, vacuum, relative velocity between specimens, surface

condition, specimen configuration, surface preparation, crystallographic orientation, etc. In order for a certain value of μ_k to be meaningful, all these variables must be specified. Although the available data are not all entirely consistent, it does appear that hard vacuum surfaces are cleaner and the resulting frictional resistance in increased over that under atmospheric conditions.

C. Adhesion in Ultrahigh Vacuum

1. Review. Adhesion phenomena are closely related to friction problems while friction is measured by sliding of the junctions (shear displacement) whereas adhesion is measured by complete rupture of the junctions, in tension the resistance in each case is dependent on the intrinsic strength properties of the material and adsorbed films.

The coefficient of adhesion, f, is defined as the ratio of normal tensile force N' required for separation of two surfaces to the normal initially applied compressive force N.

$$f = \frac{N'}{N} \tag{2-11}$$

Stronger adhesion can be obtained by increasing the real area of contact, by removing the surface contaminants, and by reducing the (residual) elastic stresses. For an elastic material, the elastic recovery breaks most of the junctions when the applied force is removed.

Materials with a pronounced creep rate show a stronger adhesion as a result of compressive stresses according to the length of time the surfaces are kept in contact because creep increases the real area of contact and decreases the stored elastic energy. It is well known that surface contaminants, like oxide films, greatly weaken adhesion.

Experiments show that metals gain appreciable adhesion at elevated temperatures (Rabinowicz, 1965), at which the ductility is increased by a tangential stress superposed on the normal stress. This combined shear and normal force increases the real area of contact as a result of "junction growth".

Rabinowicz (1965) pointed out that adhesion is higher for materials with high surface energy. Semenoff (1958) has suggested that with clean metals another factor affecting adhesion is the mutual crystallographic orientation of the contacting surfaces. For dissimilar metals, the interfacial forces will probably be an average of the interatomic forces of each of the two members, so that the failure of the junction occurs within the weaker metals.

The adhesion in ultrahigh vacuum may be similar in mechanism except that the surfaces tend to be clean, so that we can expect much stronger adhesion than in air.

No mathematical theory of adhesion has been established successfully, especially for adhesion between non-metals and between metals and non-metals.

Ryan's study (1967b) on silicate adhesion constitutes a significant start on nonmetallic adhesion study in ultrahigh vacuum. From Ryan's study (1967b) previous investigations on solid-solid silicate adhesion are here briefly reproduced and summarized.

NAME	YEAR	SPECIMEN MATERIAL	PRESSURE	ADHESION FORCE	REMARK
(1) Tomlinson	1930	Glass + Quartz	Air	1 gr	No load history given
(2) Harper	1955	Quartz Spheres	Air	0.15 gr	" " "
(3) Salisbury	1963	Silicate Powders (5μ in dia.)	10^{-10} Torr	$2 - 3 \times 10^{-7}$ gr	Essentially no prior load
(4) Stein and Johnson	1964	Silicate Powders (140μ in dia.)	10^{-9} 10^{-10} Torr	30 gr	" " "
(5) Halajian	1964	Silicate Powder (∿ 40μ in dia.)	10^{-10} Torr	0.3 gr	

(6) Smith and Gussenhoven concluded that the adhesion between quartz was due to dispersion forces.

(7) Johnson and Greiner (1965) concluded that both dispersion forces and surface electrostatic charging were responsible for the observed adhesion.

(8) Blum et al. (1967) ground basalt in a vacuum of $10^{-6} \sim 10^{-9}$ Torr and found adhesion between the powder particles, unground rock and metals. This may be due to electrostatic charge on the surface.

Surveyor data shows that the lunar surface material is similar in composition to terrestrial basalt. Ryan (1967) measured the adhesion between some silicates and engineering materials which could be used on lunar missions. The specimen materials which he used were:

Silicates
- orthoclase ($KA\ell Si_3O_8$)
- hypersthene ($(MgFe)_2Si_3O_8$)
- hornblende
- bytownite
- obsidian

Engineering Materials
- Ti alloy (6Al • 4v)
- Pure Mg.
- Pure Be.
- Pure Al.
- Ceramic (Alumina)
- Stainless Steel

All these samples were prepared in air and went through a baking-out process at 100°C to 200°C for two to three days in the vacuum chamber. The adhesion force between silicate crystals (orthoclase (001)/ orthoclase) was as high as 0.4 grams with a 400 gm normal load, in vacuum of 2×10^{-10} to 4×10^{-10} Torr. The adhesion force between silicates and metals appeared to be almost 0.4 gram with approximately 700 grams of normal load at pressures in the 10^{-10} Torr. range.

The various combinations of specimens can be categorized into two types; Type A shows strong adhesion and material transfer from one specimen to the other and a sharp decrease in adhesion force at higher pressures. Type B maintain adhesion even at higher pressures but the adhesion forces were in the 1 to 2 mg range with a normal load of 1 kg. The latter type did not show material transfer between surfaces. Temperature variations of 100°K to 400°K did not affect the adhesion characteristics between silicates. Also of interest is the fact that no adhesion was detectable between stainless steel and orthoclase.

The tests with crystals cleaved in vacuum showed adhesion forces up to 8 grams which lasted for a considerable length of time. This high adhesion appeared to be due to the action of the normal atomic silicate bonding forces (lattice bonding).

By depositing silicate particles on aluminum, Salisbury et al. (1963) calculated adhesion of 3×10^8 dyne/cm^2 with the assumption that forces act only at particle points of contact. However assuming that the forces act at a distance, he obtained 750 dyne/cm^2. He also concluded that Van der Waal's forces and ionic and covalent bonds were probably responsible for high vacuum adhesion.

Adhesion forces of these magnitudes would not appear significant relative to the magnitudes of loading to be applied to the lunar surface, nor would they be of particular consequence per se as regards the thrust or motion resistance associated with lunar roving vehicles. This does not mean, however, that adhesion may be neglected in consideration of lunar operations. On the contrary, since the evidence is strong that small, but measurable adhesion forces do exist between unlike materials in high vacuum, there may be important consequences in terms of the surface contamination by small particle adhesion of instruments, windows, and mechanical systems. Further study of the importance of adhesion phenomena would appear warranted utilizing both terrestrial high vacuum simulations and observations during Apollo missions.

III. PRELIMINARY ADHESION EXPERIMENTS

A. Test Purpose

To explore the capability of the existing vacuum system in the Mechanical Engineering Laboratory of the University of California at Berkeley and obtain some information for designing and modifying a new system for rolling friction tests, 4 adhesion tests were performed. The first 3 tests were done with an OFHC* copper ring on obsidian blocks and the fourth test was done using aluminum and obsidian.

B. Test Procedures and Results

1. Test No. 1; Cu on large obsidian specimen. An OFHC ring specimen as shown in Fig. 2-6 was cut from a 1-inch thick plate machined to finish dimensions of 3/4" R × 1/8" width and 3/8" radius across the edge. Mechanical polishing of the surface was done with 600 grit emery paper followed by crocus cloth and jeweler's rouge. The specimen was degreased using an ultrasonic cleaner. Immediately before testing the specimen was chemically polished with acid (55% phosphoric acid, 25% nitric acid). This last polish was done to remove the so-called beilby layer which forms during previous polishing procedures.

Two obsidian specimens were cut with a diamond saw and polished with Norton Crystalline Grain 400 on lapping machine to dimensions, 0.43" × 0.28" × 0.3", and a weight of 1.475 grams. They were finished with (Centriforce Abrasive M 303) aluminum oxide powder. They were washed with acetone, etched with hydro-fluoric acid for 30 sec., rinsed with distilled water and kept under acetone.

a. Test procedure. The upper ring specimen was mounted on an aluminum holder and the lower obsidian block specimen was laid freely on a stainless steel plate which was covered with a thin film of molybdenum disulfide to prevent possible adhesion between the stainless steel plate and the obsidian specimen. The test configuration is shown in Fig. 2-7.

The force dynamometer strain gage bridge was connected to a carrier amplifier (Tektronix Type 3066) and the applied

---

*OFHC Copper: oxygen free high conductivity copper.

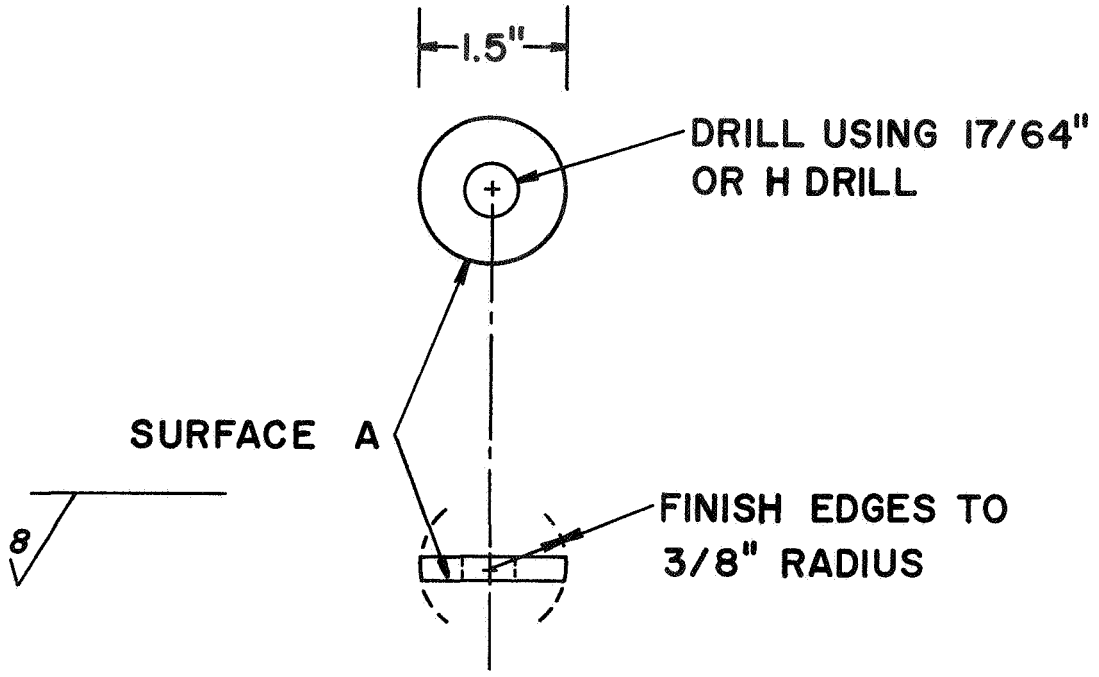

FIG. 2-6. Disk Specimen

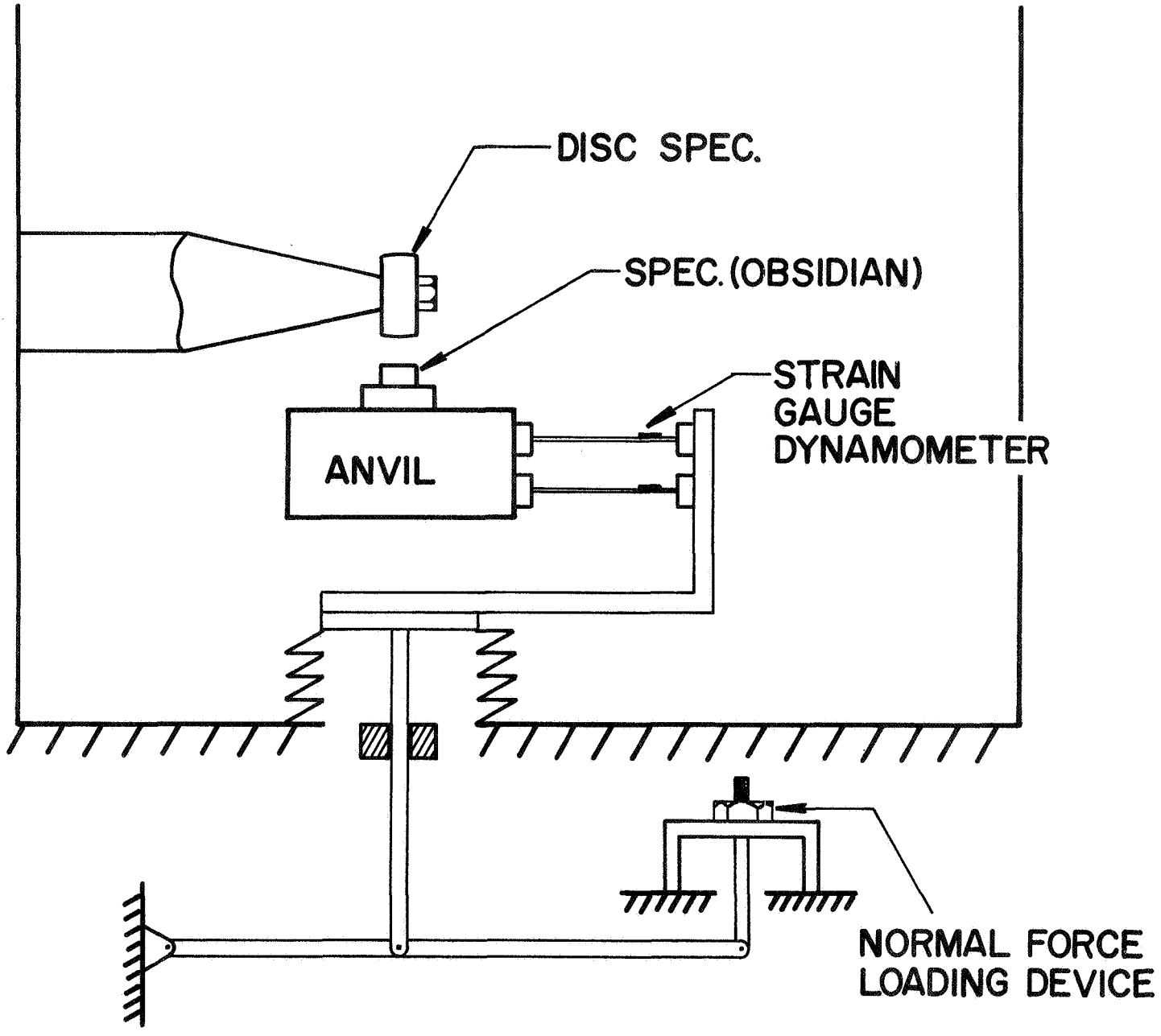

FIG. 2-7. Adhesion Test Apparatus

normal forces were read on a Dual beam oscilloscope. The test procedure involved raising the lower obsidian specimen slowly to make contact with the disk until a specified normal force was recorded by the dynamometer. The anvil was then slowly lowered to determine whether the obsidian specimen adhered to the metal disk specimen. Adhesion forces were not measured, but the tests were used to determine whether adhesion was great enough to support the weight of the lower specimen.

b. Pumpdown procedure. After the specimens were mounted in the chamber shown in Fig. 2-8, a mechanical roughing pump was used for pumpdown to 20 microns. A 75 liter/sec ion pump is then used beginning at a pressure of 10 microns.

As soon as the pressure was reduced below 10 microns the bake-out procedure was started as shown in Fig. 2-9. The chamber wall temperature was kept at 500° F for 12 hours. Cooling of the chamber to room temperature took about 8 hours. The pressure after cooling was usually in the lower part of the 10^{-9} Torr range, as measured with an ionization gage. A titanium sublimation pump brought the pressure into the 2 to 5 × 10^{-10} Torr range. Liquid nitrogen cooling of the copper shroud for the sublimation pump further reduced the pressure into the 10^{-11} Torr range, at which time the adhesion tests were started.

c. Results. Normal forces were equal to 10, 20, 30, 40 and 50 pounds applied but no measurable adhesion was detected. After opening the chamber, the obsidian specimen was found to have a crack along a 45 degree shear plane.

2. Test No. 2; Cu on small obsidian specimen.

a. Specimen preparation. The same OFHC copper ring was used as for Test No. 1 after it was again chemically polished. Preparation of the obsidian specimen followed the same procedure as used in the case of Test No. 1, however the dimensions were decreased to 0.27 × 0.20 × 0.05 inches (0.0905 grams). There was some fluctuation in vacuum during the test but the average pressure was 8.5 × 10^{-11} Torr. The temperature of the specimens was 90° F.

b. Test procedure. To prevent cracking of the obsidian the normal forces were limited to a maximum of 35 lbs, since it was found

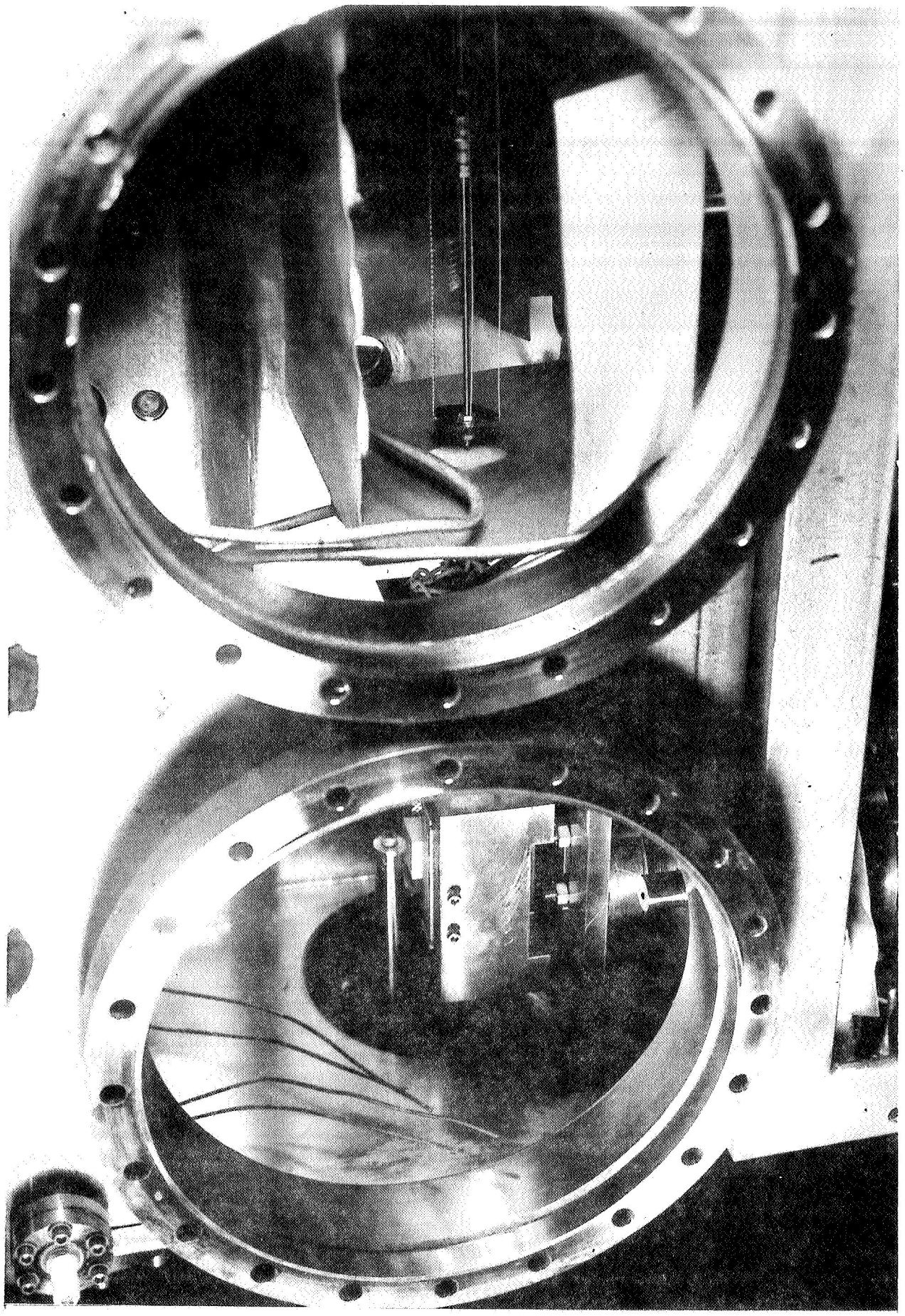

FIG. 2-8. Test Equipment Inside of Vacuum Chamber

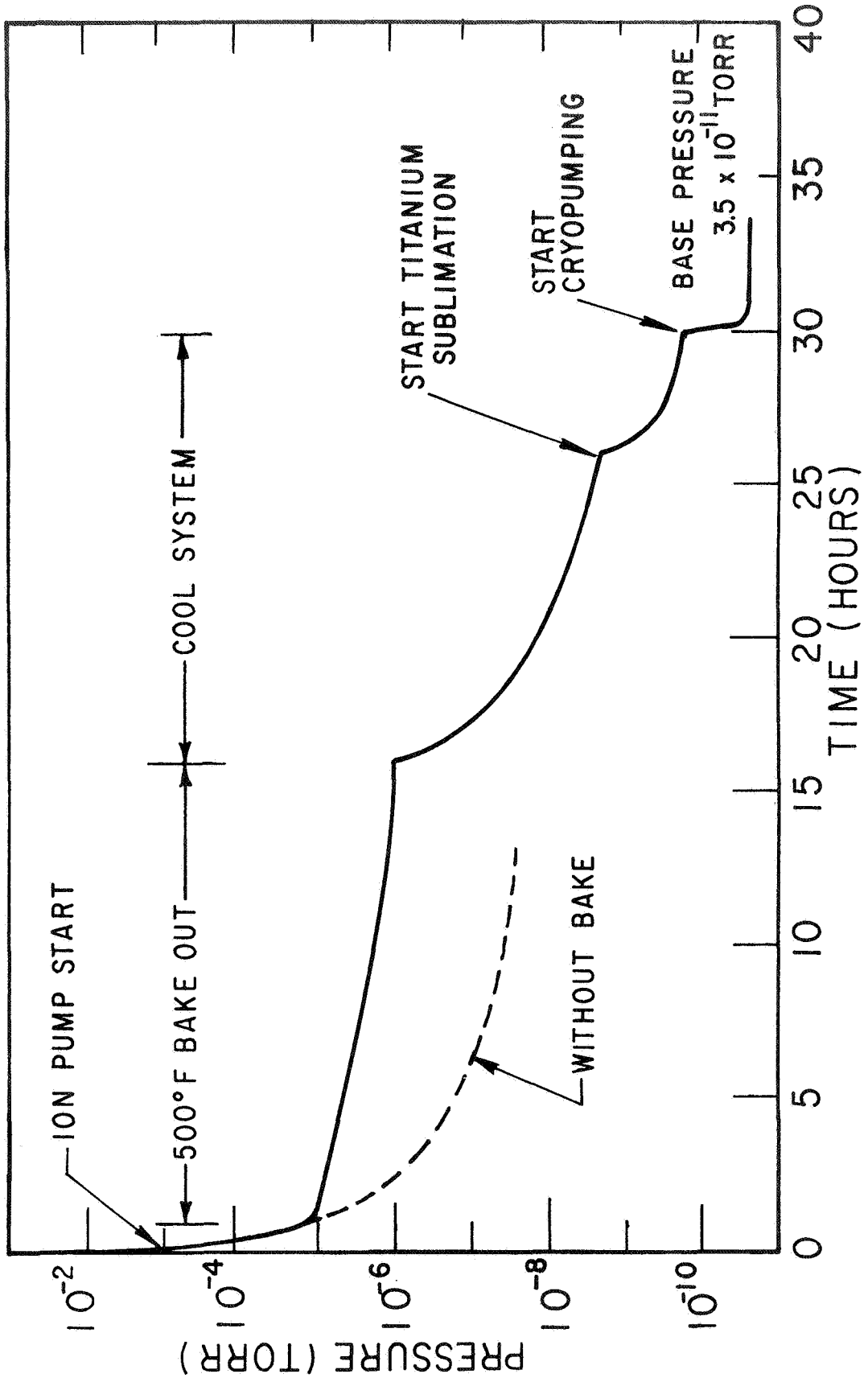

FIG. 2-9. Typical Pumpdown Performance

that a 40 lbs. normal force did not cause cracking in air.

c. Results. After applying a 35 lb. normal force a small amount of adhesion was observed, but not large enough to hold the weight of the obsidian specimen. After the test the obsidian surface contained copper particles imbedded in it, as shown in Fig. 2-10. Obsidian particles were not found on the copper disk.

3. Test No. 3; Cu on cleaved obsidian.

a. Specimen preparation. The same copper ring as in previous tests was used after chemical repolishing. In an effort to get cleaner and smoother surfaces obsidian cylinders of 0.175" dia. were cleaved with a stainles steel blade. Before cleaving, the obsidian cylinder was knotched along the desired cleavage plane. Most of the specimen surface had a mirror-like smoothness with some curvature. One obsidian disk weighing 0.131 grams was selected for this test.

After the normal procedure of pumpdown and bake-out, the pressure of the chamber during the test was 7.5×10^{-11} Torr and the temperature of the specimens was 100° F.

b. Test procedure. During pumpdown and bake-out the obsidian specimen moved slightly from its original position so that the copper disk could only touch one edge of the obsidian specimen.

c. Results. No measurable adhesion was detected.

4. Test No. 4; 2024 Al on cleaved obsidian.

a. Specimen preparation. A (2024) aluminum ring was machined to the same dimensions as the copper rings used in previous tests. The disk specimen was etched with a hydroxide solution of 16 grams NaOH and 90 ml of distilled water. The aluminum disk was dipped for five minutes in the hydroxide solution heated between 140° F and 160° F, and washed in water. The deposit of etching products was removed with concentrated HNO_3, followed by rinsing with distilled water.

A cleaved obsidian block of dimensions 0.175" diameter 0.1465 height (0.1264 gram) was cleaned with acetone before the test was initiated.

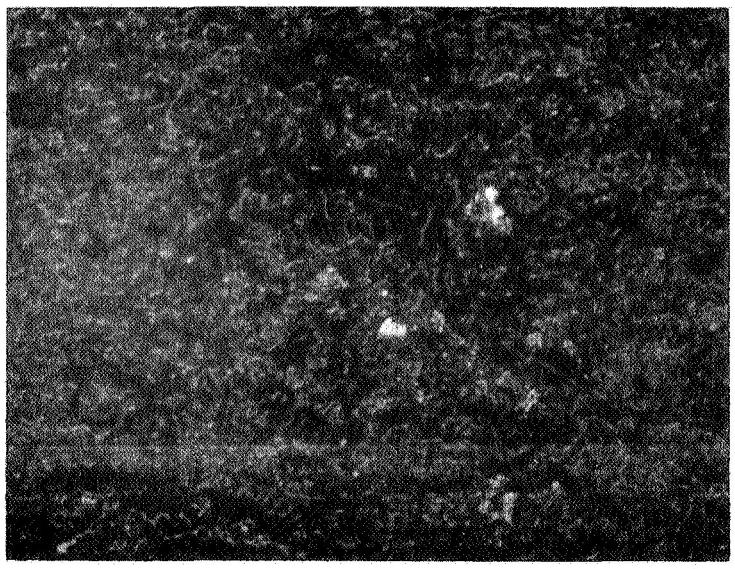

FIG. 2-10. Copper Particles on Polished Obsidian Specimen After Adhesion Test (20 × 20)

To obtain cleaner specimen surfaces, heater assemblies for both specimens were added as shown in Figs. 2-11 and 2-12. A special fixture for the obsidian block was added to prevent misalignment of the specimens due to external vibrations.

b. Test procedure. The obsidian was baked out at 950° F for 7.5 hours and the aluminum disk was baked out at 710° F for 8 hours. The vacuum during the test was at $4 \sim 8 \times 10^{-11}$ Torr. During the test the copper shroud in the chamber was cooled with liquid nitrogen. The specimen temperatures were 80° F. The tests were conducted using a 35 lb normal force between specimens.

c. Results. Some adhesion was observed in this test. The obsidian block adhered briefly to the aluminum after unloading and then fell away from the upper ring specimen. Microscopic examination of the obsidian surface, Fig. 2-13, showed embedded aluminum particles; however, obsidian particles were not seen on the aluminum disk surface. After the test, another observed phenomenon was adhesion of the aluminum disk to the OFHC copper plate which was in contact with it during the low pressure test condition.

Adhesion existed between the copper and aluminum after the test but the specimens could be separated easily after two hours in air.

C. Discussion and Conclusions

Because of the long pumpdown and bake-out procedures the average test time was approximately three to four days. Therefore in future experiments it would be desirable to utilize an apparatus that permits several tests without disturbing the vacuum environment. While it was found that the same obsidian specimen surface cannot be reused for further tests because of contamination which would affect subsequent test results, the metal ring may be used repeatedly.

Rolling friction might be increased due to stronger adhesion forces in ultrahigh vacuum. The wear problem in vacuum is considerably more serious than in air, because of lubrication problems and since material galling and transfer may be expected.

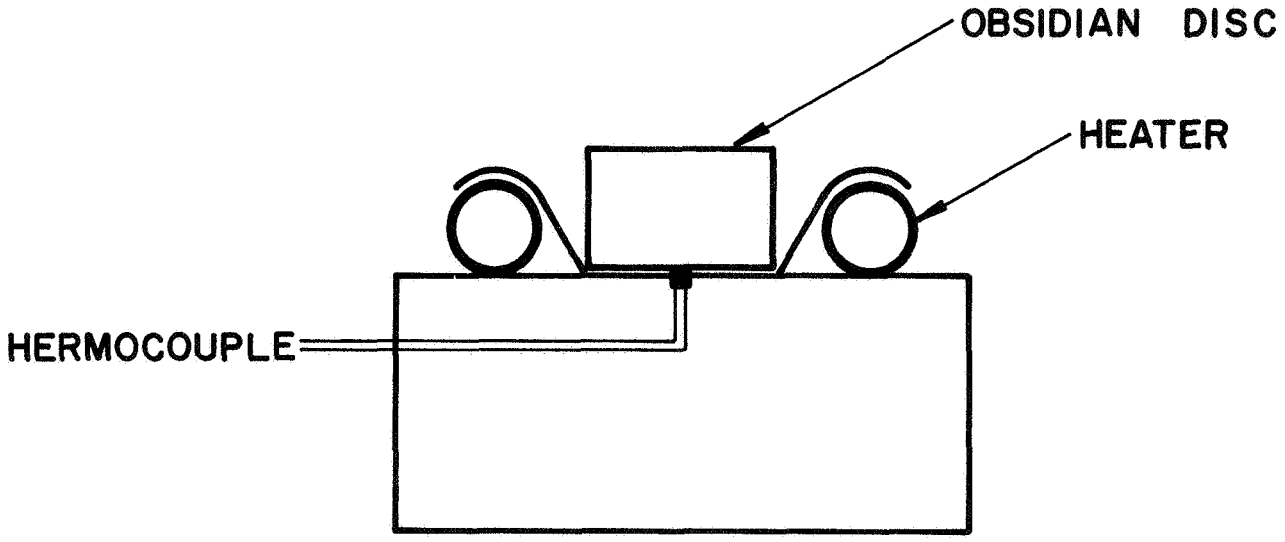

FIG. 2-11. Obsidian Specimen Heater Assembly

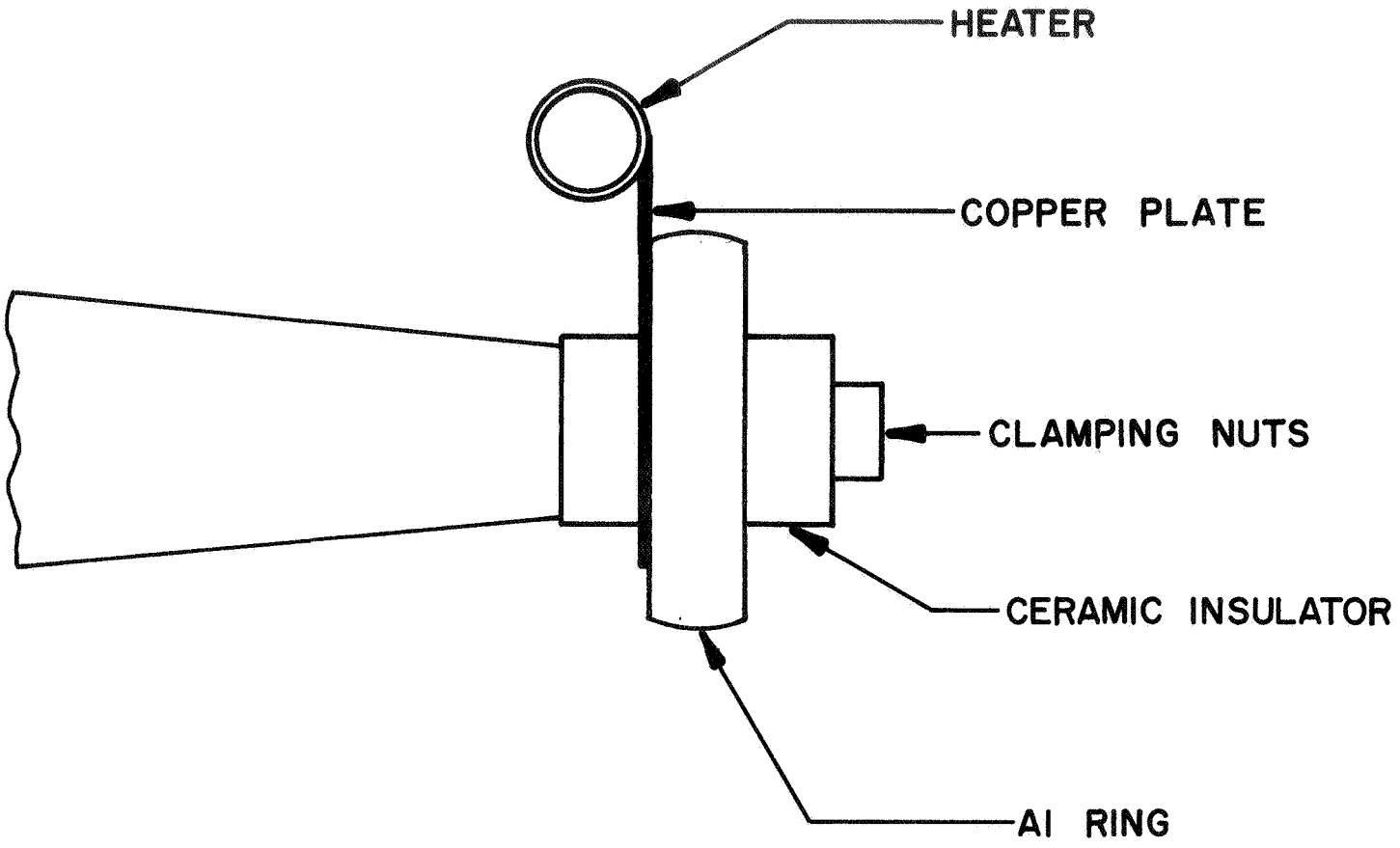

FIG. 2-12. Heater Assembly for Metal Disk

FIG. 2-13. Aluminum Particles on Cleaved Obsidian Specimen After Adhesion Test (20 × 20)

From the results of the review of past studies and the preliminary experiments described above it appears that:

1. High vacuum may cause an increase in frictional resistance.
2. Adhesion and metal transfer may occur under high vacuum conditions.

The available data are not entirely conclusive, however, and additional studies may be warranted. The remainder of this chapter is concerned with the design of test equipment that would be useful for further studies of the frictional and adhesional characteristics of materials in ultrahigh vacuum, with special reference to investigations of these effects in terms of the interaction between rolling metal wheels and non-metallic surfaces.

IV. TEST EQUIPMENT FOR THE STUDY OF WHEEL MOBILITY ON SIMULATED LUNAR MATERIALS IN ULTRAHIGH VACUUM

A. Introduction

The following sections report the project work concerned with theoretical considerations, load ranges, design calculations and experimental configurations relating to two approaches for the investigation of rolling friction phenomena and other parameters associated with vehicle wheel interaction with rock surfaces under simulated lunar environmental conditions.

1. Specimens and relative movement. There are numerous ways in which probable behavior of lunar vehicles might be studied in a vacuum environment. Any approach must consider the following factors:

Load input: pull force and torque
Specimen choice: material type size and shape
Relative movements of specimens:
wheel moves (input load applied to wheel),
support moves (input load applied to support)

The configuration of existing equipment (Odden, 1967; U. S. Army, 1966) favors use of rolling specimens on basalt surfaces for simulations of vehicle wheel interactions with the lunar surface.

Wheel sizes and shapes suitable for use in our existing vacuum chamber are shown in the experimental configurations and in Fig. 2-14.

Possible wheel materials are aluminum, stainless steel, titanium alloys and non-metals. Titanium alloys with their high strength and low weight and excellent mechanical properties at low temperature as well as aluminum alloy such as 6061 T6 and 347 stainless steel (Niobium - stabilized 1808) have been recommended (U. S. Army, 1966).

For initial tests, disc type wheels can provide information about the material without involving the additional influence of wheel geometry. Spoked wheels with differing spoke designs could provide information on possible benefits of large elastic deformations. The two different types of motive power, pull force and torque, should not show a significant difference in frictional characteristics or in energy consumption as long as no sliding takes place between the specimens. By using a pull force, the simulated rock can move against the wheel instead of the wheel being pulled along the rock specimen. For convenience the rock specimen will be translated linearly while the wheel rolls on it.

2. Expected normal load range. A normal load range for the metal wheel specimen should be selected such that the stresses at the contact area of the models are the same as those for real objects in a lunar situation. By assuming the same stresses at the area of contact, similar adhesion phenomenon may be expected for both model and prototypes. A modeling factor will still be necessary, however, since a "size effect" can not be avoided. As an example, an analysis for a sphere instead of a metal wheel is presented, and the stress field under the sphere is assumed to be uniform (Fig. 2-15). The stress under the sphere is given by:

$$\sigma = \frac{N}{\pi r^2 \sin^2 \theta} \qquad (2\text{-}20)$$

To assure geometric similarity, θ is denoted as $\theta_1 = \theta_2$ where the subscript $_1$ denotes a real object and subscript $_2$ the model.

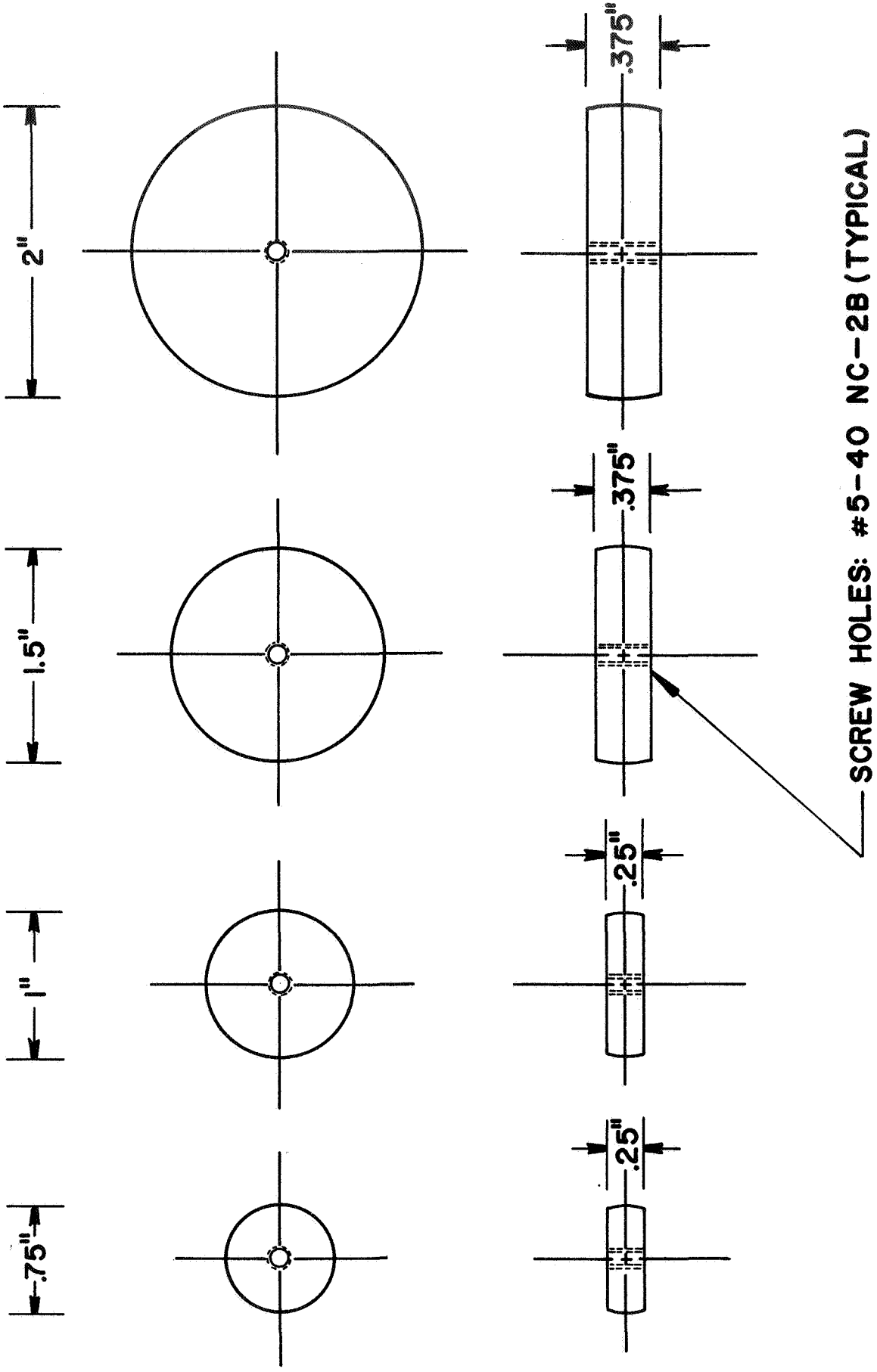

FIG. 2-14. Wheel Specimens

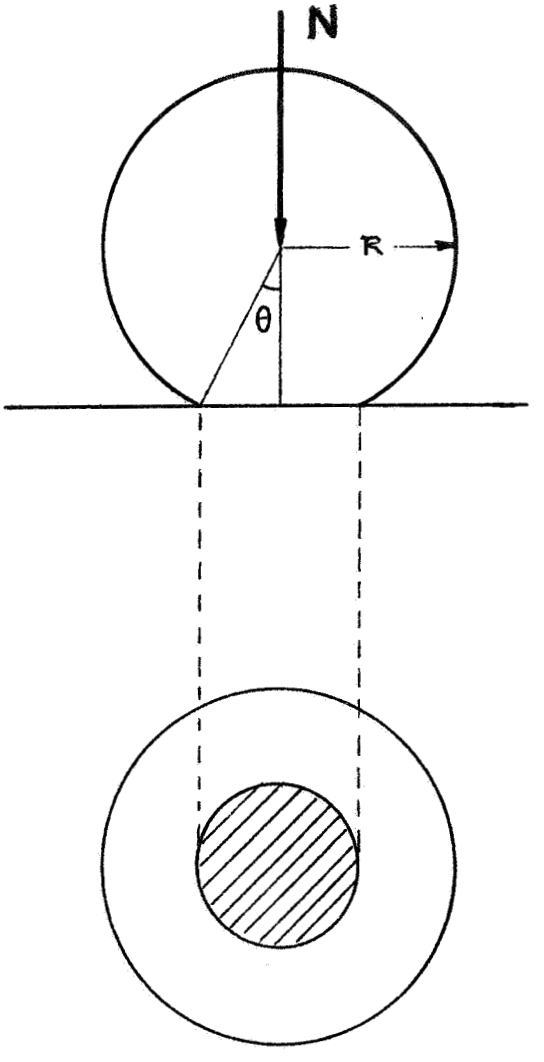

FIG. 2-15. Elastic Sphere on the Rigid Support

Then:

$$\sigma_1 = \frac{N_1}{\pi r_1^2 \sin^2 \theta_1} \quad , \quad \sigma_2 = \frac{N_2}{\pi r_2^2 \sin^2 \theta_2} \tag{2-21}$$

where:

N_1, N_2 = normal load

r_1, r_2 = radius of the contacting area

For the case when $\sigma_1 = \sigma_2$:

$$\frac{N_2}{N_1} = \frac{r_2^2 \sin^2 \theta_2}{r_1^2 \sin^2 \theta_1} = \frac{r_2^2}{r_1^2} \tag{2-22}$$

From the Hertz contact stress analysis and assuming elastic deformation of the sphere:

$$d = (\delta N r)^{1/3} \tag{2-23}$$

where:

d = the diameter of the circular contact area

N = the normal load

r = the radius of the sphere

$\delta = 12(1 - \nu^2)/E$

Again:

$$\sigma_1 = \frac{N_1}{a_1} = \frac{N_1}{\pi d_1^2} = \frac{N_1}{\pi (\delta W_1 r_1)^{2/3}} = \frac{{N_1}^{1/3}}{\pi \delta^{2/3} {r_1}^{2/3}}$$

$$\sigma_2 = \frac{N_2}{a_2} = \frac{N_2}{\pi (\delta W_2 r_2)^{2/3}} = \frac{{N_2}^{1/3}}{\pi \delta^{2/3} {r_2}^{2/3}} \tag{2-24}$$

if $\sigma_1 = \sigma_2$ then:

$$\frac{N_2^{1/3}}{N_1^{1/3}} = \frac{\pi\delta^{2/3} r_2^{2/3}}{\pi\delta^{2/3} r_1^{2/3}} = \left(\frac{r_2}{r_1}\right)^{2/3} \tag{2-25}$$

This again gives:

$$\frac{N_2}{N_1} = \left(\frac{r_2}{r_1}\right)^2 \tag{2-26}$$

Thus a "size effect" must be considered in extrapolating model test results to prototype conditions.

The dimensions of wheels for some proposed lunar vehicles are given in Table 2-2. While the first four wheel concepts in Table 2-2 are no longer being considered, the fifth is considered current for a dual mode (manned - unmanned) lunar roving vehicle.

As an example, consider a 30 inch diameter wheel and an assumed width of 10 inches, to support a load (lunar gravity) of 50 lbs (300 earth pounds).

Selecting an experimental wheel with 1 (one) inch diameter, and using the foregoing criterion:

$$\frac{N_2}{N_1} = \frac{r_1^2}{r_2^2} = \frac{d_1^2}{d_2^2} = \frac{1}{30^2} \tag{2-27}$$

$$N_2 = \frac{N_1}{900} = \frac{50}{900} = 0.0555 \text{ lb}$$

TABLE 2-2

Wheel Dimensions For Some Proposed Lunar Vehicles

	WHEEL		VEHICLE		
Reference	Diameter	Width	Number of Wheels	Total Weight	Speed
Odden, 1967	80 inches		4	3085 Kg	5 ∿ 16 Km/hr
Lancaster, 1967a	45 inches	10 inches	4	1000 lbs	
Lancaster, 1967b	45 inches	10 inches	4	700 lbs	6.5 ∿ 13 Km/hr
"Mimosa", 1966	2 meters	abt 0.52 meters	4	7894 Kgs	10 Km/hr
	30-35 inches	8-10 inches	4-6	750-1550 lbs	2 Km/hr - unmanned 15 Km/hr - manned

where:

N_2 is the normal load to be applied on a wheel specimen with 1 inch diameter.

A reasonable experimental normal force range would be 0.01 pound to 0.25 pound. Some experiments should be conducted at higher state of stress, however, in order to obtain better physical results on the wheel-rock interfaces.

3. Force analysis. If the rock specimen in Fig. 2-16 moves from left to right, the tangential force P_s read by straingage dynamometer will be:

$$P_s = P_R + P_B \tag{2-28}$$

where:

P_R = rolling friction between wheel and the rock

P_B = bearing friction

Figure 2-17 shows this relationship. The ball bearing can be thought of as two sliding rings, one is the effective inner race and the other is the effective outer race, with a coefficient of bearing friction μ_B. In Figure 2-16, N is the total normal load exerted on the wheel N^1 is the applied load plus the weight of the bearing saddle and the effective outer race. Therefore,

$$N^1 = N - W \quad \text{where } W = (\text{Weight of Specimen} + \text{Specimen Shaft} + \text{Effective Inner Race}) \tag{2-29}$$

If we introduce μ_R and μ_B then,

$$P_s = \mu_R \cdot N + \mu_B \cdot N^1 \tag{2-30}$$

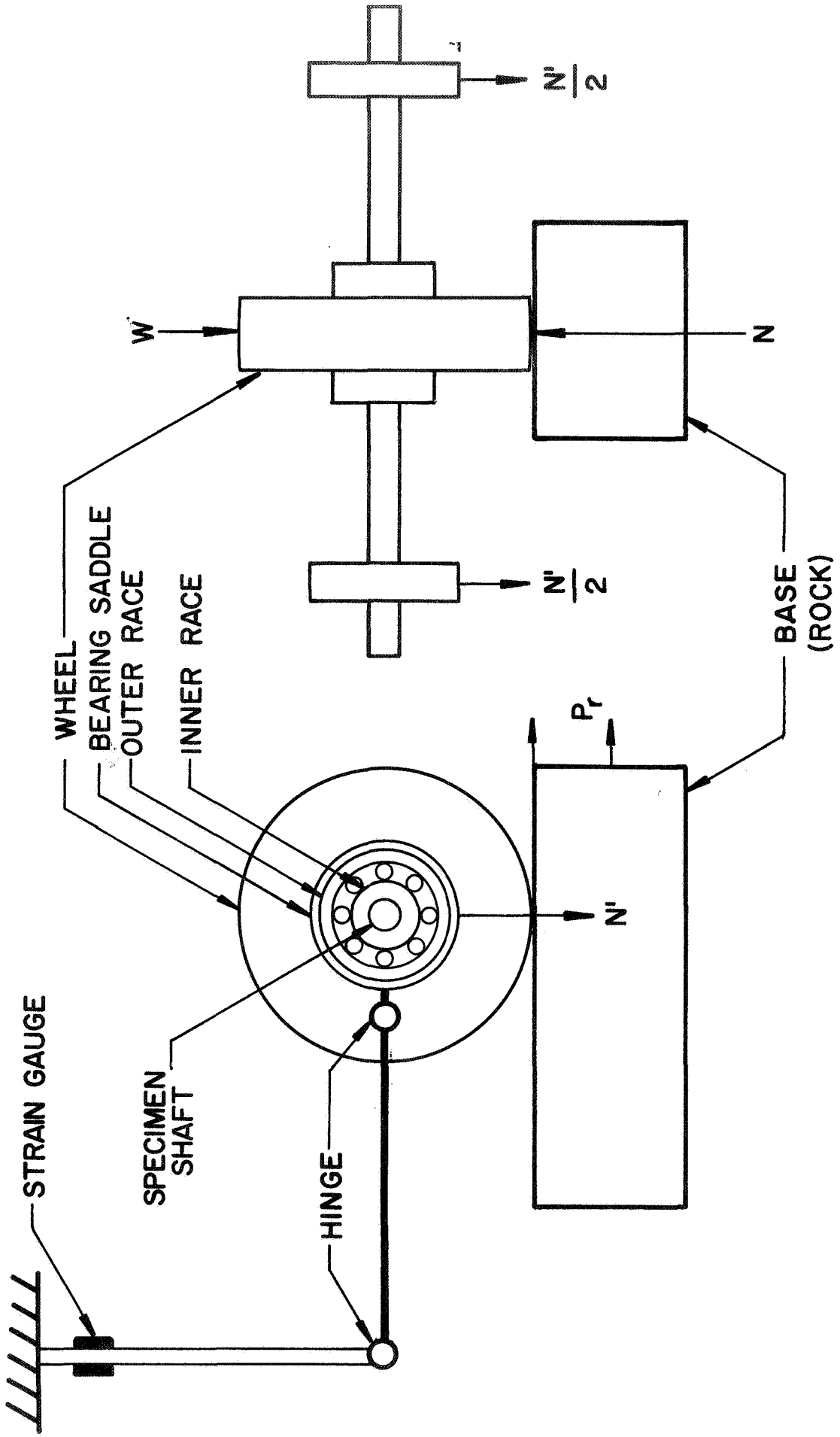

FIG. 2-16. Force Measurement Configuration

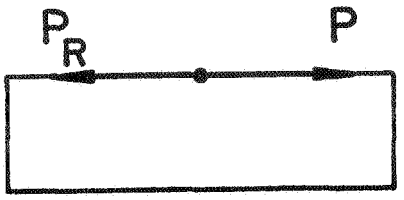

Base

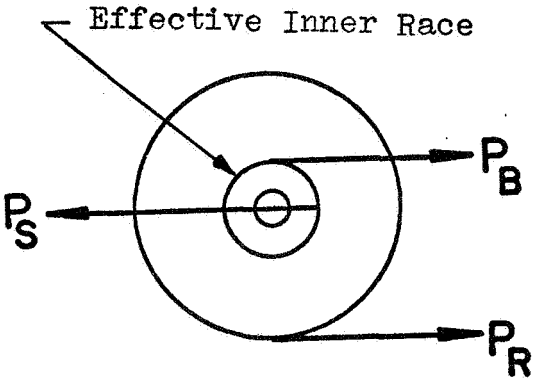

Wheel with Effective Inner Race Of Ball Bearing

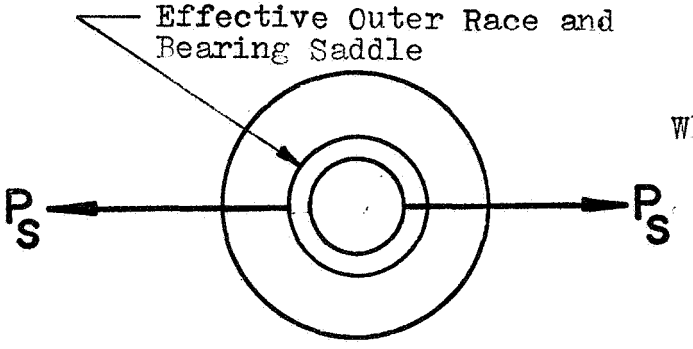

Wheel with Effective Outer Race of Ball Bearing and Bearing Saddle

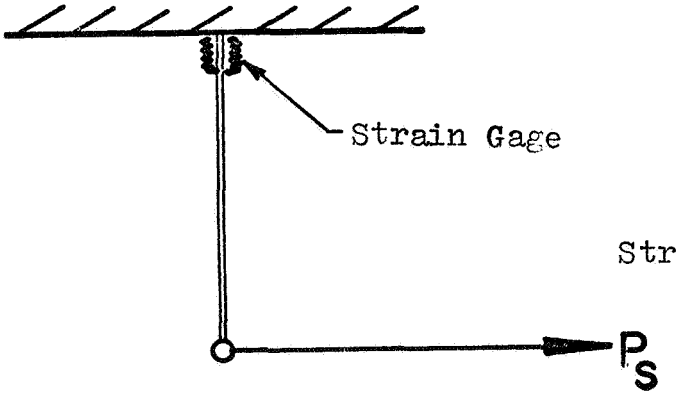

Strain Gage Dynamometer

FIG. 2-17. Tangential Force Analysis

where:

μ_R = coefficient of rolling friction between rock and wheel

μ_B = coefficient of bearing friction

The strain gage dynamometer will read the sum of the two friction forces, P_R and P_B. Either of two techniques can be used to find P_R from P_s.

a. If it is assumed that both μ_R and μ_B are constant in the normal load range of N_1^1 to N_2^1, the separation can be done analytically.

$$\mu_R \cdot N_1 + \mu_B \cdot N_1^1 = P_{s1} \tag{2-31}$$

$$\mu_R \cdot N_2 + \mu_B \cdot N_2^1 = P_{s2} \tag{2-32}$$

where:

$N_1 = N_1^1 + W$ and $N_2 = N_2^1 + W$

Suppose $N_2^1 = kN_1^1$ then,

$$\mu_R \cdot (N_1^1 + W) + \mu_B \cdot N_1^1 = P_{s1} \tag{2-33}$$

$$\mu_R \cdot (kN_1 + W) + \mu_B \cdot kN_1^1 = P_{s2} \tag{2-34}$$

yielding:

$$\mu_R = \frac{kP_{s1} - P_{s2}}{(k-1)W} \tag{2-35}$$

b. Another method for determining μ_R with the dynamometer is to place strain gages on the metal strips (see Fig. 2-19) which connect the bearing saddle (Part No. 12)* and the weight dish (Part No. 18). This strain gage dynamometer will read the bearing friction P_B. The readings should, however, be calibrated for each discrete value of normal load. Normal load can also be measured with these strain gages if they are connected to different bridge circuits.

B. Design and Modification of Experimental Equipment

This section describes how our existing facilities (Frisch et al., 1968), which have been used for the study of sliding friction between aluminum single crystals, could be modified for investigation of the frictional interaction between rolling metal wheels and nonmetallic surfaces. A schematic diagram of the overall experimental configurations is shown in Fig. 2-18.

1. Experimental vacuum chamber. Fig. 2-19 shows the details of the stainless steel vacuum chamber, which consists of the following assemblies:

a. Top flange configuration. The top flange subassembly consists of a top flange (Part No. 5)*, stainless steel bellows, threaded raiser (Part No. 1), raiser knob (Part No. 2), thrust ball bearing (Part No. 3), bearing base (Part No. 4), top disk (Part No. 7), strain gage dynamometer (Part No. 8), two connecting rods (Part No. 9), wheel specimen assembly (Parts No. 12, 13, 15), holder assembly (Part No. 10), weight dish (Part No. 18) and an electric feedthrough (Part No. 25). Parts numbered 1, 7, 8, 9, 10, 12, 13, 15 and 18 can be raised by turning the raiser knob (Part No. 2). The L-shaped hook of the holder assembly rotates the rachet wheel of the rock specimen assembly through an angle of 45 degrees, which enables the rock specimen to have a new surface for the wheel.

The ring connection of the wheel specimen assembly is actually disconnected when the wheel rides on the rock specimen. The

---

*For all part numbers, see Figs. 19, 20, and 21.

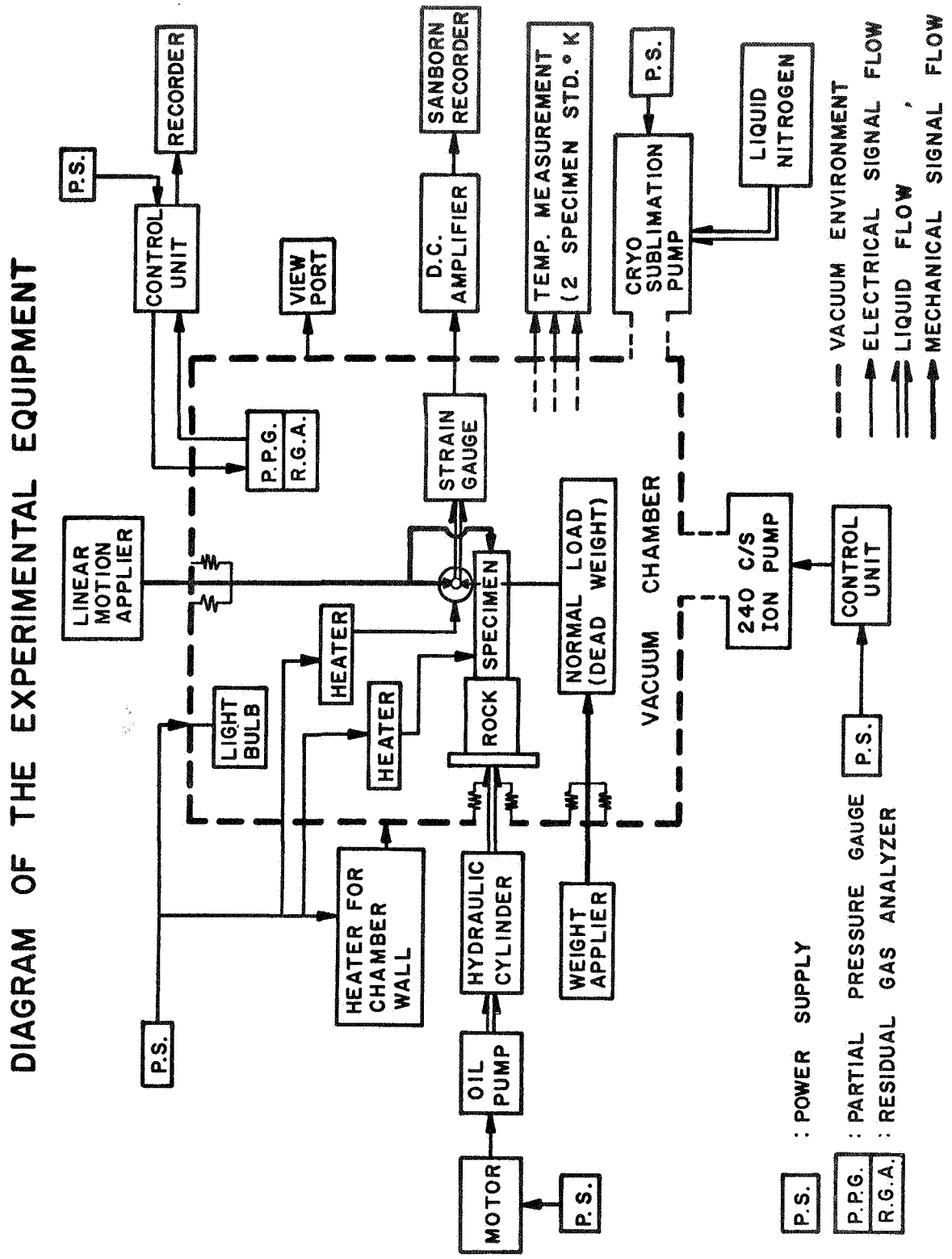

FIG. 2-18. Schematic Diagram of Experimental Equipment

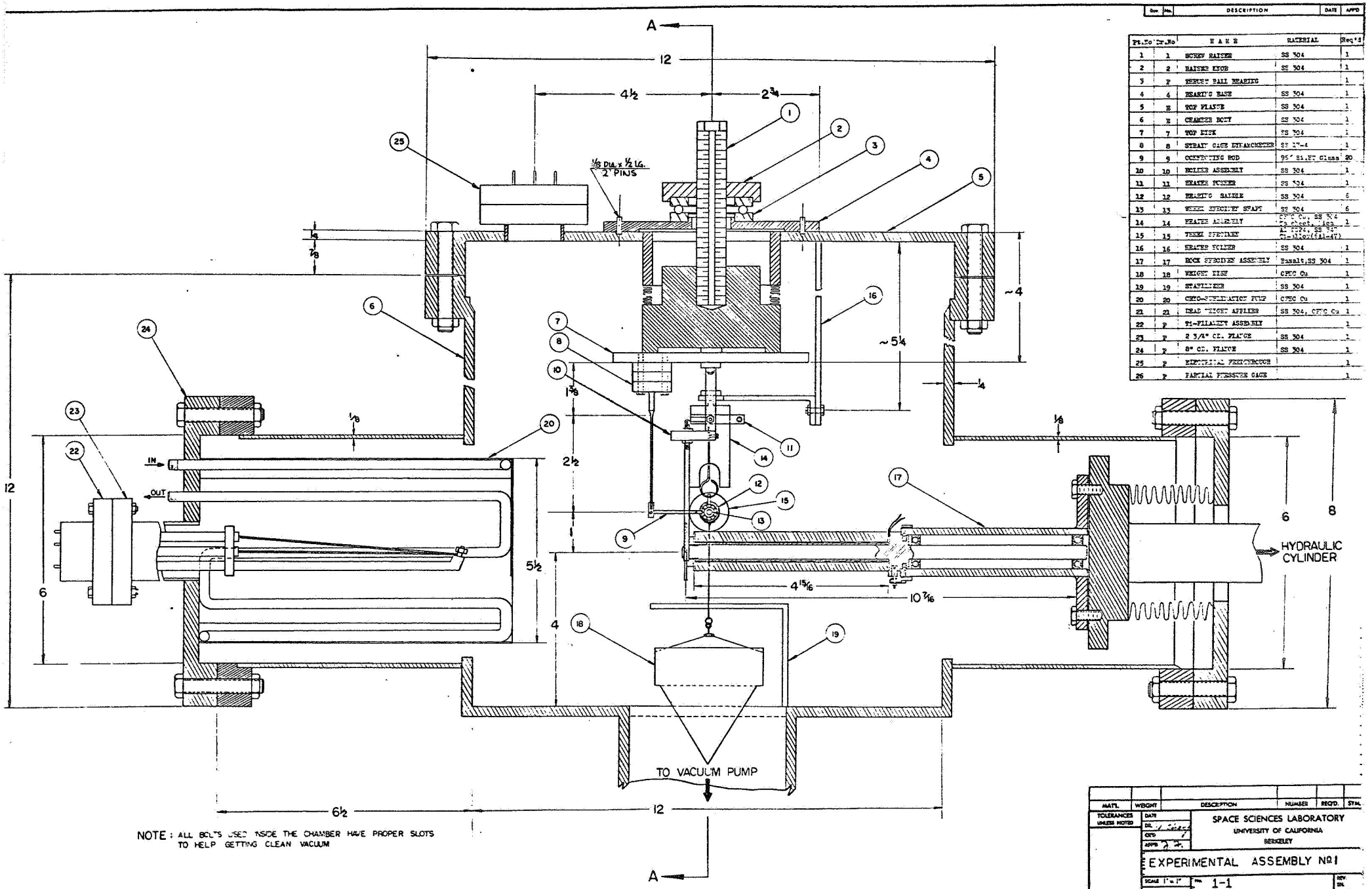

Pt.No	Dr.No	NAME	MATERIAL	Req'd
1	1	SCREW RAISER	SS 304	1
2	2	RAISER KNOB	SS 304	1
3	P	THRUST BALL BEARING		1
4	4	BEARING BASE	SS 304	1
5	5	TOP PLATE	SS 304	1
6	6	CHAMBER BODY	SS 304	1
7	7	TOP DISK	SS 304	1
8	8	STRAIN GAGE EXTENSOMETER	SS 17-4	1
9	9	CONNECTING ROD	95% Sil.Et Glass	20
10	10	HEATER ASSEMBLY	SS 304	1
11	11	HEATER PUSHER	SS 304	1
12	12	BEARING SADDLE	SS 304	6
13	13	WORM SPECIMEN SHAFT	SS 304	6
14	14	HEATER ASSEMBLY	OFHC Cu, SS 304 Ta sheet, Mgo	1
15	15	WORM SPECIMEN	Al 7075, SS 316 Ti-alloy(Ti-6Al-4V)	
16	16	HEATER HOLDER	SS 304	1
17	17	ROCK SPECIMEN ASSEMBLY	Basalt, SS 304	1
18	18	WEIGHT DISH	OFHC Cu	1
19	19	STABILIZER	SS 304	1
20	20	CHEMO-SOLIDIFICATION PUMP	OFHC Cu	1
21	21	DEAD WEIGHT APPLIER	SS 304, OFHC Cu	1
22	P	Ti-FILAMENT ASSEMBLY		1
23	P	2 3/4" CL. PLATE	SS 304	1
24	P	8" CL. PLATE	SS 304	1
25	P	ELECTRICAL FEEDTHROUGH		1
26	P	PARTIAL PRESSURE GAGE		1

FIG. 2-19. Front View of Experimental Assembly

wheel, therefore, has connection with only the strain gage dynamometer while the experiment is going on. The bearing saddle (Part No. 12) is connected to the strain gage dynamometer by a connecting rod (Part No. 9) which has pin joints at both ends. All of these parts are raised 1 inch from the position shown in Figs. 2-19 to 2-21, during the pump-down period.

b. Dynamometer design. The strain gage dynamometer shown in Fig. 2-24 consists of two bending beams with two strain gages mounted on each beam. Detailed dynamometer calculations are given in Appendix (A). This dynamometer is attached to the top disk (Part No. 7) for ease of replacement. The blocks between the dynamometer and top disk are for leveling the dynamometer when wheel specimens of different sizes are used. The bridge configuration in Fig. 2-24 is for recording the sum of the force $P = P_1 + P_2$, when P_1 and P_2 have different magnitudes. No temperature compensation is necessary for this bridge configuration.

c. Wheel specimen assembly. The wheel specimen is threaded to the center of an 1/8 inch diameter shaft, which has two miniature ball bearings press fitted at both ends as shown in Fig. 2-25. The bearing mounts are connected to the normal load fixture and dynamometer. The ball bearing can be lubricated with solid lubricants such as $TaSe_2$ or WSe_2. The stainless steel strips which connect the bearing mounts and the normal load fixture can be used as a strain gage dynamometer to determine the ball bearing friction. This dynamometer also can be used to obtain normal load values when the alternate loading configuration shown in Fig. 2-22 is used.

d. Rock specimen assembly. Fig. 2-23 shows the assembly for mounting the rock specimen. This assembly is attached to the hydraulic cylinder shaft which uses a metal bellows for the vacuum seal. The rock specimen shaft can be rotated 45 degrees for each time that the ratchet mechanism is operated, thus providing accurate indexing of the test surface relative to the disk. The shaft is covered with a ceramic indulator on which a tantalum foil heater is wound. This heater (for degassing the rock specimen) has a copper brush-switch which enables connection of the electric circuit. The temperature of the rock can be

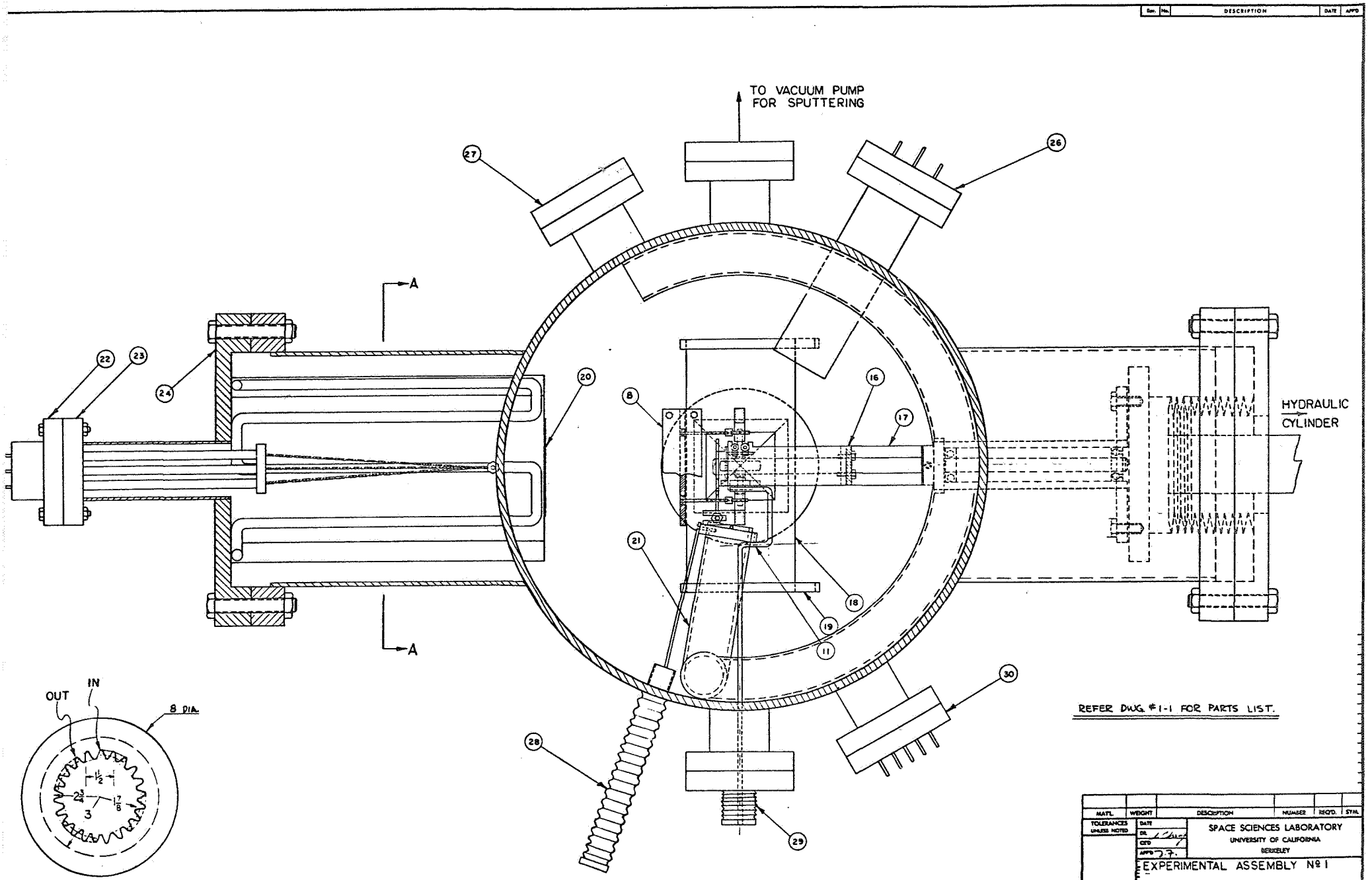

FIG. 2.20 Top View of Experimental Assembly

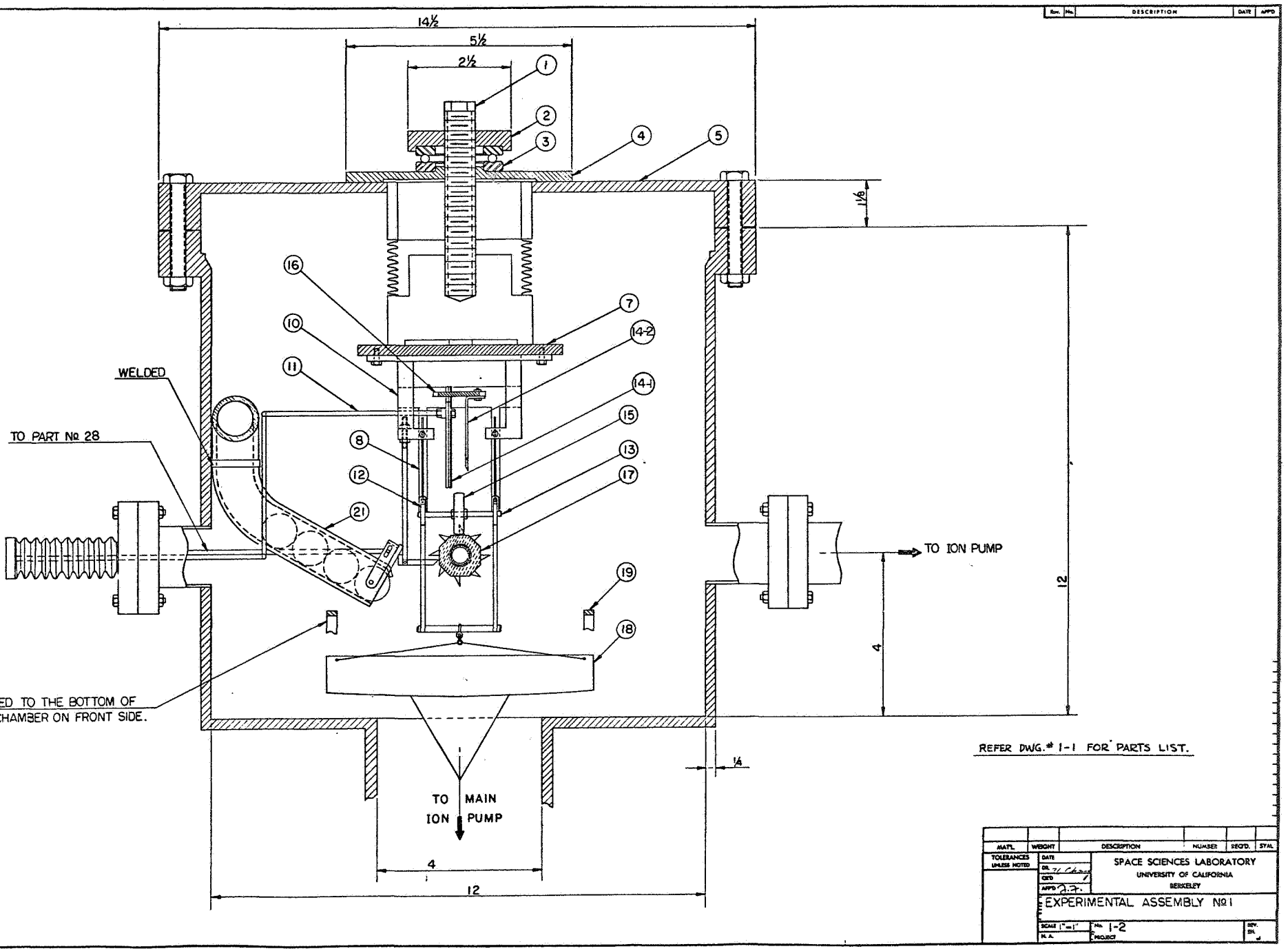

FIG. 2-21. Side View of Experimental Assembly

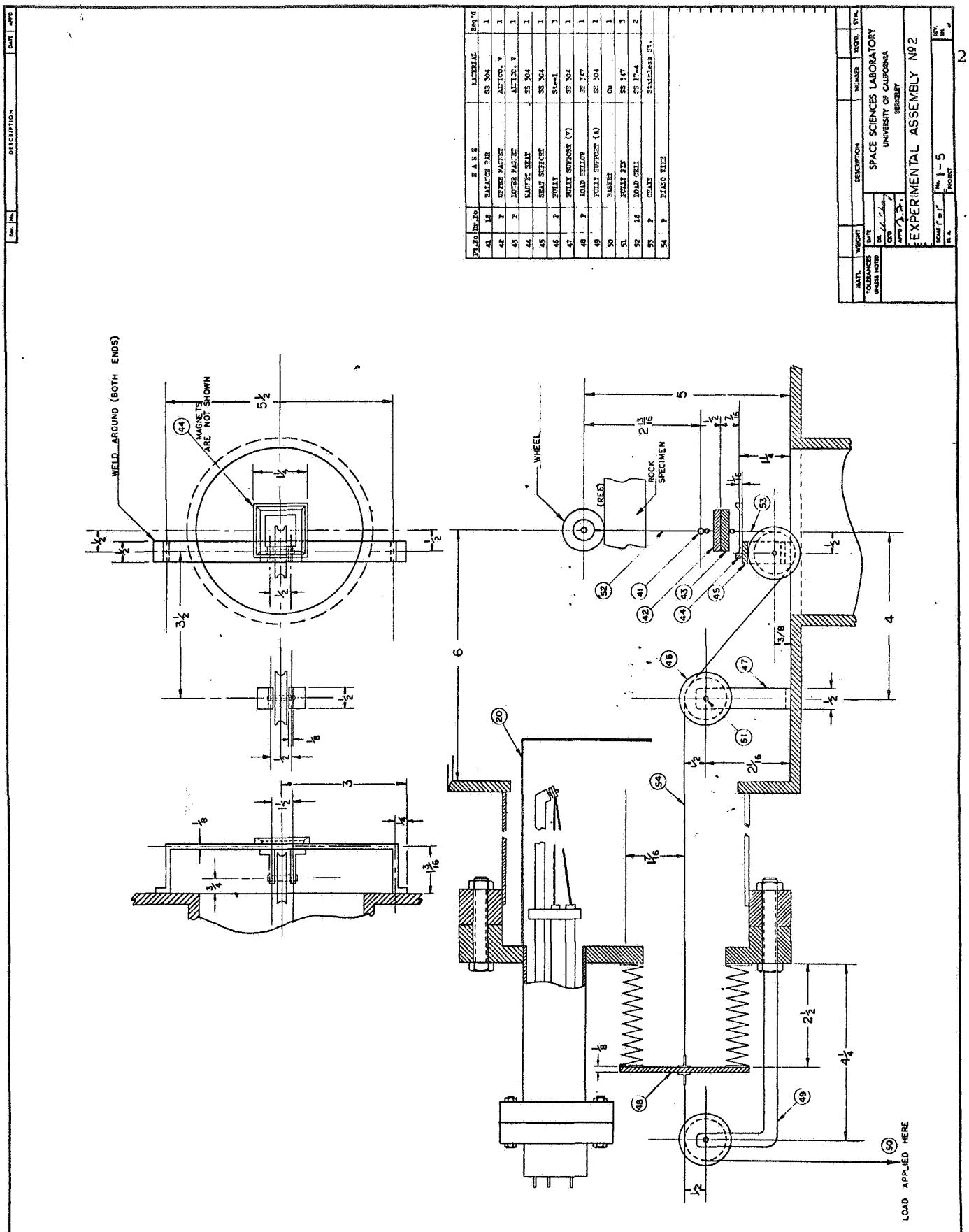

FIG. 2-22. Alternative Loading Configuration

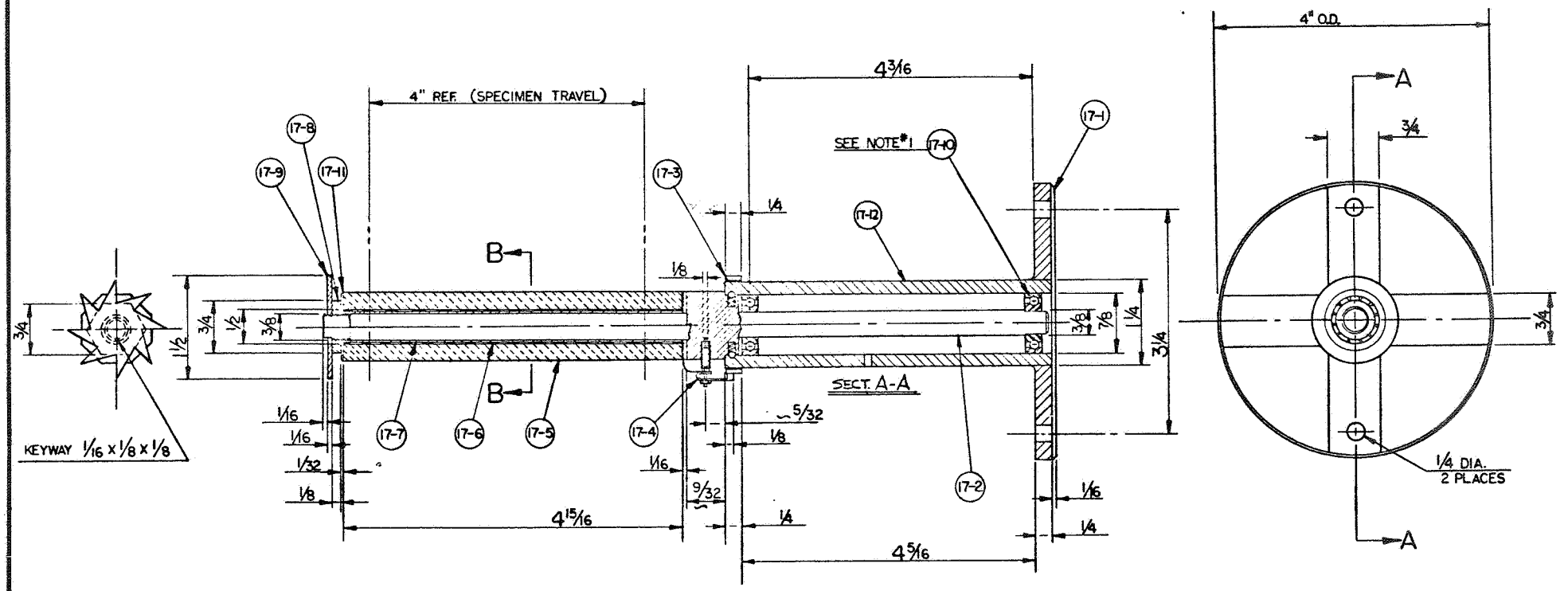

NOTES:

1. MINIATURE BALL BEARING (2)
   3/8 I.D. x 7/8 O.D. x 7/32 W
   (BARDEN PRECISION SK6K)

MAT'L	WEIGHT	DESCRIPTION	NUMBER	REQ'D.	SYM.
TOLERANCES UNLESS NOTED	DATE	SPACE SCIENCES LABORATORY UNIVERSITY OF CALIFORNIA BERKELEY			
	DR.				
	CK'D				
	APP'D				
		ROCK SPECIMEN SUBASSEMBLY			
	SCALE 1"=1"	No. 1-4			REV. SH.
	N. A.	PROJECT			

FIG. 2-23. Rock Specimen Assembly

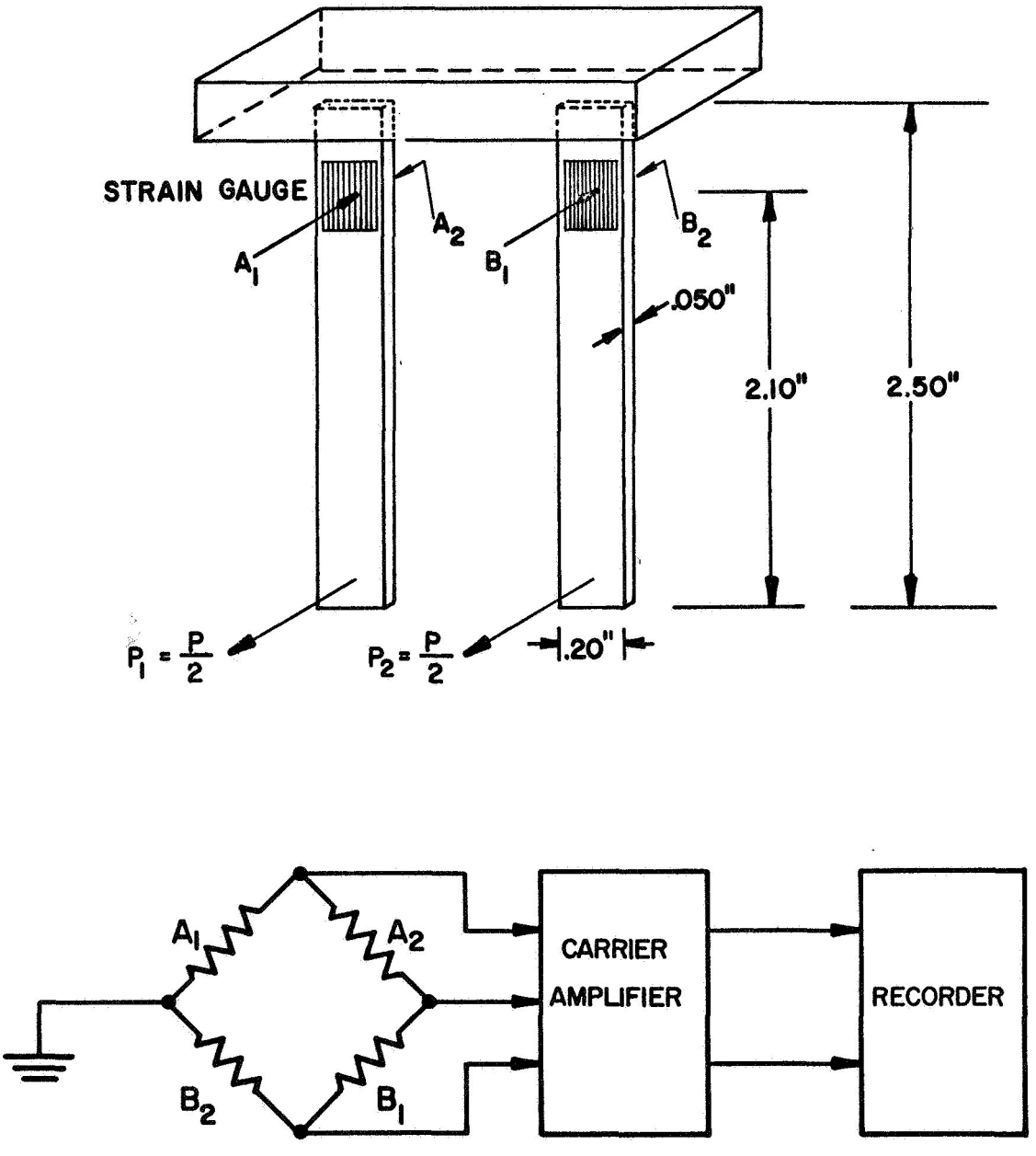

FIG. 2-24. Strain Gage Dynamometer and its Bridge Configuration

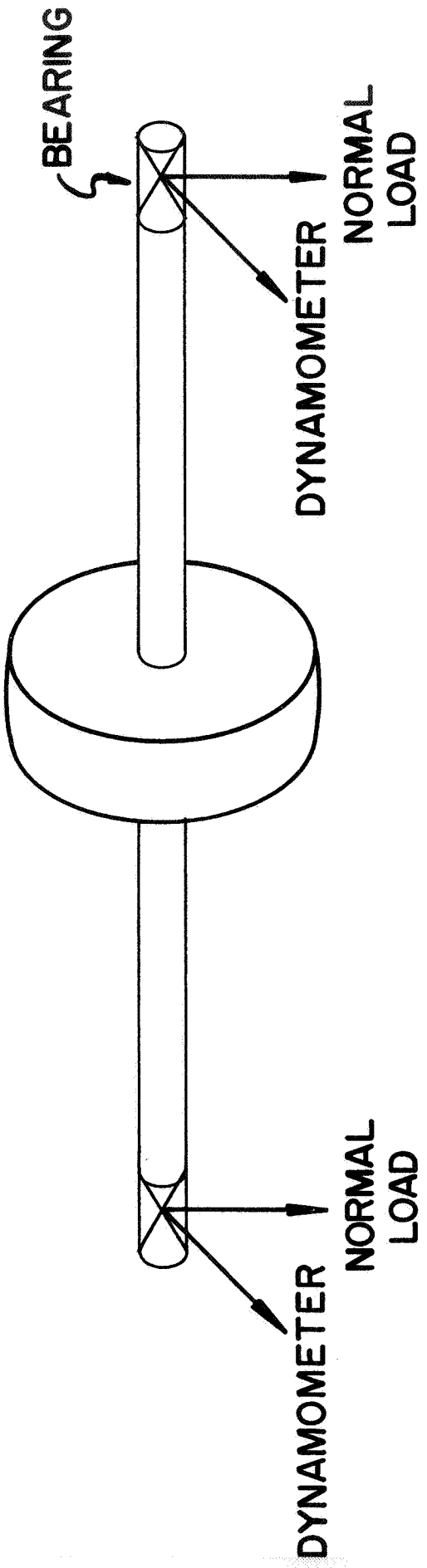

FIG. 2-25. Wheel Specimen Assembly

obtained with a thermocouple placed between the rock specimen and the shaft. The thermal expansions of the stainless steel shaft (α = 10.2 × 10^{-6} in/in °F) and the ceramics (α = 2 × 10^{-6} in/in °F) are such that the clearance between the ceramic insulator and the stainless steel shaft must be about 0.006 inches for a temperature change of 1500° F.

e. Normal load fixture. To provide capability for changing the normal load without opening the vacuum chamber, a loading device utilizing spherical weights has been designed. Each stainless steel sphere weighs 0.1 lbs giving discrete values of normal load from 0.2 lbs to 2.4 lbs. For stabilization 23 spheres are held inside a stainless steel tube, welded to the chamber wall, as a magazine for adding dead weight to the test configuration.

To increase the normal load, the pan with the spheres is lifted until it is stopped by the stabilizer. Additional spheres are dropped into the pan. It is expected that the chamber pressure may slightly increase due to some outgassing during this loading procedure. However, vibration will not be severe enough to cause serious pressure bursts.

f. Specimen heater. The heater for the wheel specimen is suspended by a holder which is welded to the top flange. This heater consists of a tantalum sheet with mica insulators on both sides. The mica sheets are then sandwiched between two metal sheets, one of which is stainless steel and the other OFHC copper. The copper sheet is placed on the side of wheel specimen. This heater assembly is pressed against the wheel specimen and the temperature of the wheel is obtained by means of a thermocouple.

2. Specimen details.

a. Configurations.

1) Disk specimens.

Materials: 2024 aluminum alloy
Titanium alloy (6 Al-4V)
Stainless steel (347 niobium stabilized 18-8)

Four different sizes, from 0.75 to 2 inch diameter, can be used as shown in Fig. 2-14. Alternative wheel designs could be used if desired.

2) Rock specimens.

Material: Basalt

The rock specimens can be a hollow octagonal column 1 inch × 4 15/16 inch long with a 1/2 inch hole. Each face of the octagonal column can be used as a test surface as shown in Fig. 2-23.

b. Preparation.

1) Wheel specimen. The specimens can be cut from 1/4 inch and 3/8 inch thick plate and finished to the dimensions shown in Fig. 2-14. Final mechanical polishing of the surface should be done using 600 grit emery paper, crocus cloth and jeweler's rouge. Specimens should be degreased using an ultrasonic cleaner and chemically etched immediately before the tests. Etching products can be removed with concentrated HNO_3 followed by a rinse in distilled water.

2) Rock specimen. Five (5) inch thick Basalt blocks can be drilled for a 1/2 inch hole and then cut with a diamond saw into 1.1" × 1.1" square columns with the drill hole along the longitudinal axis. The Basalt can then be shaped into an octagonal column, lapped with Norton Crystalline Grain 400 and polished with Centriforce Abrasive M 303 to final dimensions. This octagonal column can be degreased by an acetone wash, followed by a 10 second etch with a mixture of approximately 30 per cent (by volume) hydrofluoric, 30 per cent glacial acetic, and

40 per cent fuming nitric acid (Ryan, 1967b). The purpose of this etch is to remove surface dust contamination. This etch should be followed immediately by distilled water washes and then by oven drying in a loosely sealed glass container.

3. Pumpdown and bake-out procedure for vacuum system. After mounting a specimen in the vacuum chamber, pumpdown with a 10 cu. ft./min. mechanical roughing pump should be continued until the pressure drops to 10 microns. A cold trap can be used to prevent back-stream contamination. The main ion pump of 200 liter/sec. capacity should then be turned on. When the pressure drops into the 10^{-6} Torr range, the whole chamber should be baked-out to 600° F for a period of approximately 12 hours. The rock specimens should be baked out at 500° F for 12 hours, but the bake-out temperatures of the wheel specimens should vary according to their thermal properties. For a stainless steel or titanium wheel the temperature may reach 900° F without a change of properties, but for 2024 aluminum alloys the proper bake-out temperature is 350° F.

All these temperatures are far below the temperature needed to remove chemically adsorbed oxides, but are adequate to desorb physically adsorbed molecules. However, it may be feasible to use ion sputtering, briefly described in Appendix (C), to obtain cleaner surfaces. The titanium filament of the cryo-sublimation pump (Part No. 20) will be used to lower the chamber pressure after the chamber has cooled to room temperature. The copper shroud of the cryo-sublimation pump can be cooled by circulating liquid nitrogen. The expected chamber pressure, using this sequence of pumping techniques is approximately 5×10^{-11} Torr.

4. Data reduction and evaluation. The monitoring of the experiments utilizes already available thermocouples, strain gage dynamometer, residual gas analyzer and other pertinent instrumentation. The primary objective will be the determination of the normal and pull forces, their ratio during rolling and sliding motion, μ_R and μ_S, respectively as well as velocities, torques and surface conditions. The evaluation should relate the measured variables to the friction coefficients,

considering the elastic-plastic deformations during relative surface motion. The wheel size effect will hopefully, be significant enough to provide input data for modeling purposes relative to lunar vehicles.

5. Design summary. The rock specimen which will be pulled by means of a hydraulic cylinder along the rotating wheel is designed to rotate after each traverse so that it can provide a new surface for the next experimental test. In this way, several tests can be performed for each vacuum pump-down. This technique then makes it possible to do eight tests under the same vacuum environment, and provides data for analysis of the effect of normal load, temperature, etc., on the friction coefficient. To obtain lower pressures and cleaner surfaces, a cryo-sublimation pump and specimen heater assemblies are provided. Better simulation of lunar rock may be accomplished with the redesign of existing sputtering equipment.

Further equipment modification to include tests on soil samples rather than rock specimens, would be relatively simple once the described equipment has been constructed.

6. Alternative experiment for rolling friction. If the experimental results show that the coefficient of rolling friction μ_R is essentially independent of normal load and the relative velocity between the specimens, it may be worthwhile to obtain a more precise value of μ_R using another technique.

Frictional energy is essentially a dissipation energy which decreases the amount of stored energy in the system. Therefore if we can measure the stored energy of the system before and after a frictional displacement, the charge in stored energy represents the energy dissipated by friction. Therefore we can calculate the friction force by measuring the stored energy and the path of the system under consideration. As shown in Fig. 2-26 the technique is to release a spherical ball on the two inclined surfaces, and to measure the positions of the ball at its maximum height for every cycle, during rolling. Photographs will show a continuous shadow of the track of the ball as well as the maximum positions (Fig. 2-27). The turning points can be clearly shown, each frame containing 2 maximum positions of the ball.

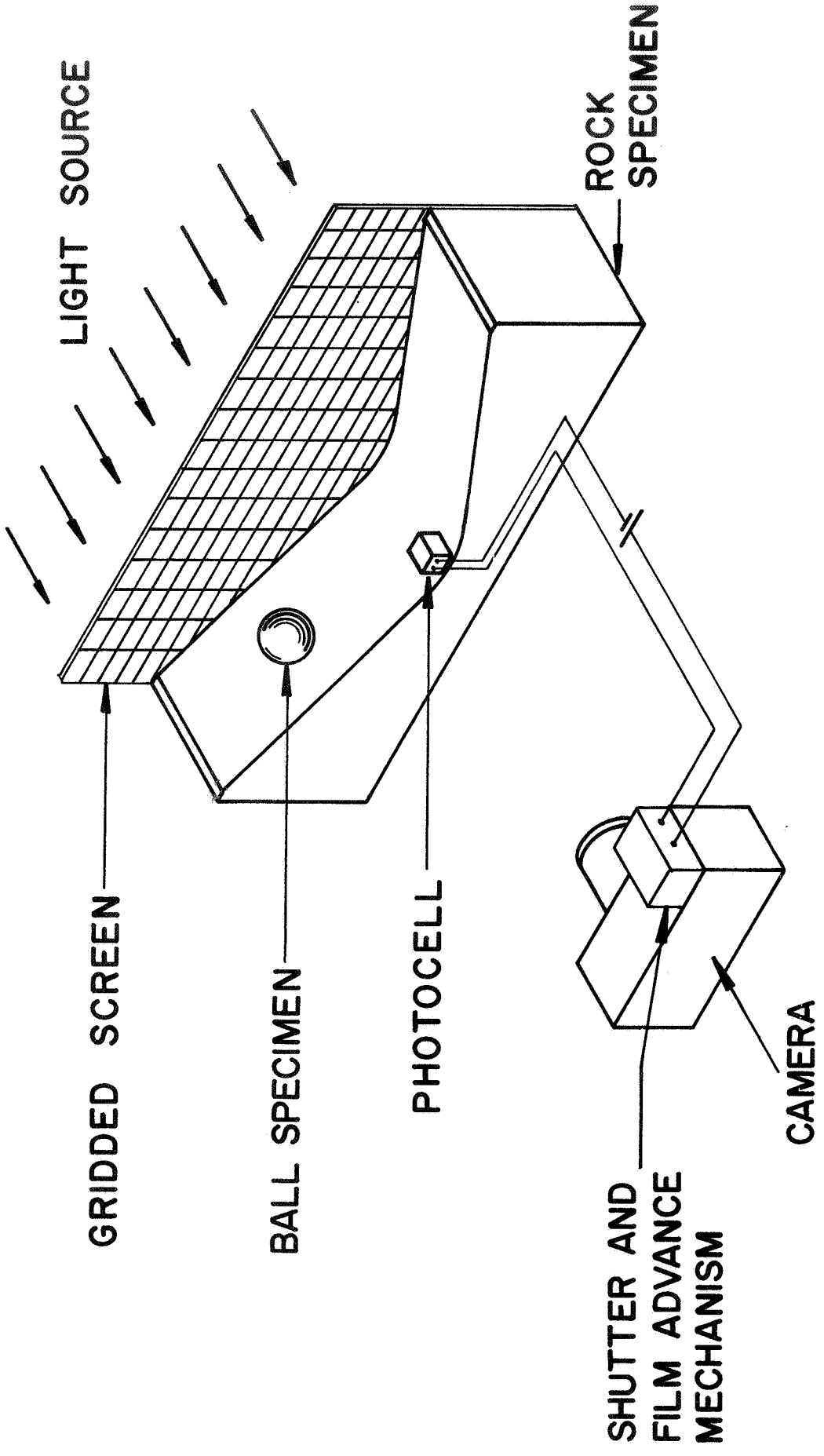

FIG. 2-26. Arrangement for the Alternative Method of Measuring Rolling Friction

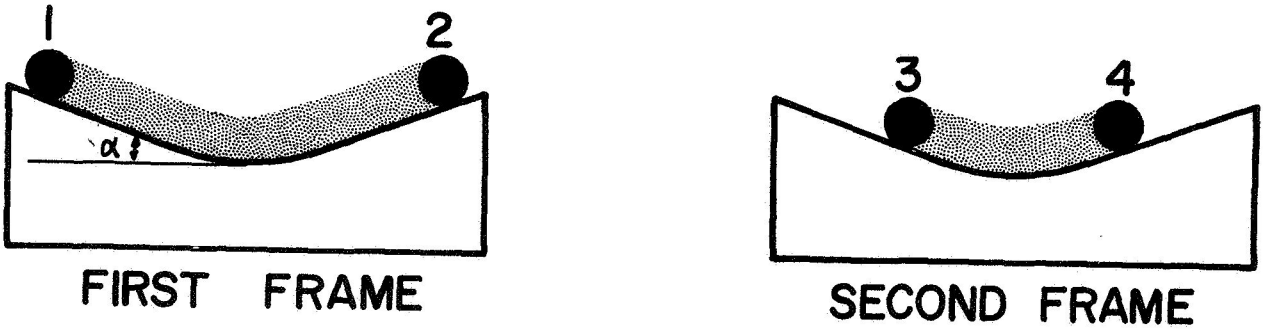

FIG. 2-27. Typical Pictures Taken by the Camera

The maximum positions and the inclined angle are then used to determine coefficient of rolling friction by the following analysis. Energy W dissipated by friction is:

$$W = \int F \cdot dx \tag{2-28}$$

where:

$F = \mu_R \cdot Mg \cdot \cos \alpha$ and M is the mass of the ball.

If in Fig. 2-28 F (friction force) is constant along AB and CD, and the mean friction force along BC is Fm, then from conservation of energy,

$$Mg(h_0 - h_1) = F(l_{11} + l_{12}) + Fm \cdot l \text{ ..... along AD} \tag{2-36}$$

$$Mg(h_1 - h_2) = F(l_{21} + l_{22}) + Fm \cdot l \text{ ..... along DE} \tag{2-37}$$

Equation (2-36) − Equation (2-37) and $l_{12} = l_{21}$ gives:

$$Mg(h_0 - 2h_1 + h_2) = F(l_{11} - l_{22}) \tag{2-38}$$

$$\therefore \quad F = \frac{Mg(h_0 - 2h_1 + h_2)}{l_{11} - l_{22}} \tag{2-39}$$

The above equations are based on the assumption that there is no sliding between the ball and the rock. Substituting $F = Mg \cos \alpha$ gives:

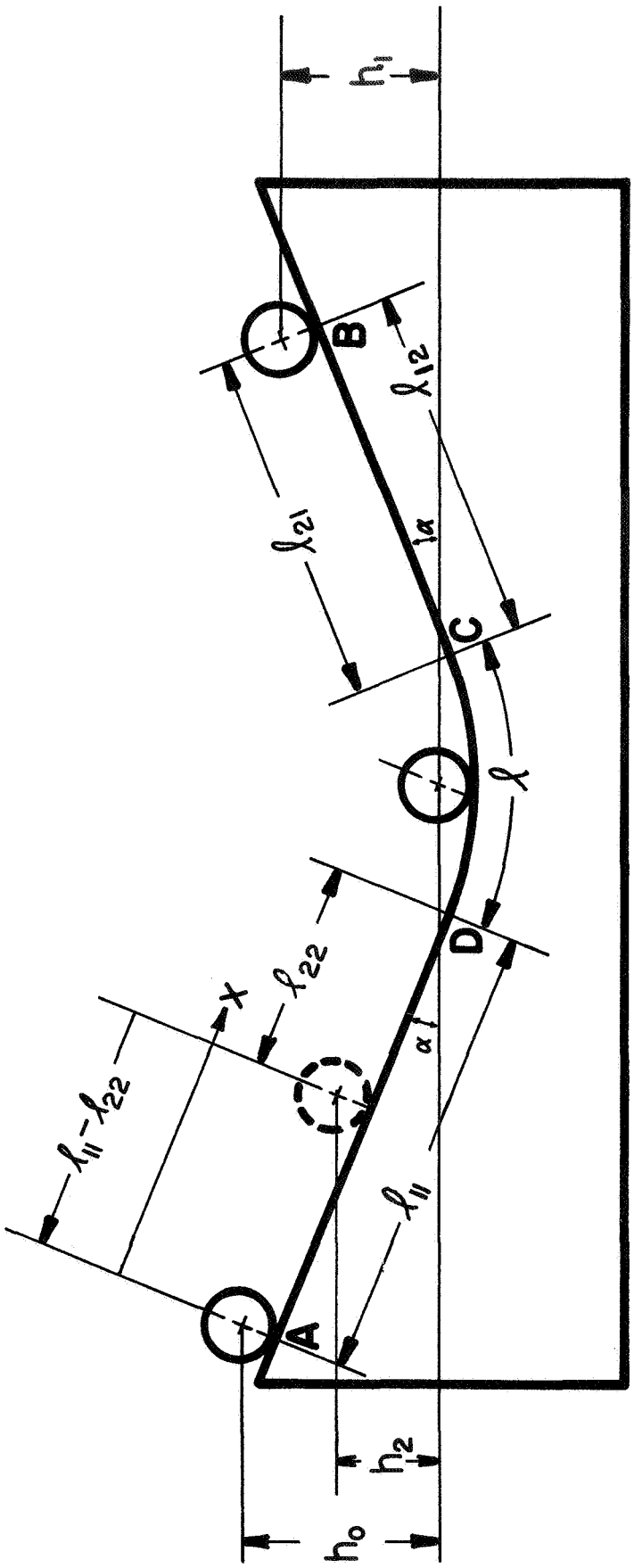

FIG. 2-28. Rolling Friction between a Spherical Ball and an Inclined Surface

$$\therefore \quad \mu_R = \frac{(h_0 - 2h_1 + h_2)}{(l_{11} - l_{22}) \cos \alpha} \tag{2-40}$$

This last expression for μ_R contains terms for the positions of the ball and the angle α of the inclined surface. A series of μ_R can be calculated by this method and each value of μ_R represents the coefficient of rolling friction at the average velocity of the ball in each cycle of movement. An advantage of this expression is that it does not involve the curved surface BC.

To assure that sliding does not occur between the two specimens, the angle α must be less than the angle of sliding friction.

The rock specimen and the ball can be placed inside the vacuum chamber for determination of the coefficient of rolling friction between the metal ball and the rock under simulated lunar conditions.

V. SUMMARY

This chapter has presented a review of the studies on friction and adhesion phenomena in vacuum between some engineering materials and simulated lunar rocks. It also describes possible experiments on rolling friction of wheels for lunar vehicles on a simulated lunar surface to aid in the estimation of power requirement for future lunar locomotion. An experimental configuration has been designed to determine coefficients of rolling friction relative to the applied load, temperature, wheel size and wheel velocity. Preliminary tests in vacuum on the adhesion between obsidian and copper as well as aluminum were performed, and are reported.

REFERENCES

1. Bekker, M. G. (1961), "Evaluation and Selection of Optimum Vehicle Types Under Random Terrain Conditions", General Motors Corporation, Defense Division, Report No. ER61-107, April.

2. Bekker, M. G. (1962a), "Mechanics of off-the-road Locomotion", Delivered at an Ordinary Meeting of the Institution of Mechanical Engineers in London, Paper No. AD L2/63, November 13.

3. Bekker, M. G. (1962b), "Land Locomotion on the Surface of Planets", ARS Journal, Vol. 32, No. 11, November.

4. Bekker, M. G. (1963), "Mechanics of Locomotion and Lunar Surface Vehicle Concepts", Automotive Engineering Congress, Detroit, Mich., January 14-18.

5. Bowden, F. P. and Rowe, G. W. (1959), "The Adhesion of Clean Metals", Proc. Roy. Soc., No. A 233.

6. Bowden, F. P. and Tabor, D. (1954), "The Friction and Lubrication of Solids", Oxford Press.

7. Bromwell, L. G. (1965), "Adsorption and Friction Behavior of Materials in Vacuum", M.I.T. Department of Civil Engineering Report, March.

8. Bromwell, L. G. (1966), "The Friction of Quartz in High Vacuum", M.I.T. Soil Mechanics Division Research Report No. R66-18, May.

9. Cocks, M. (1966), "Shearing of Junctions Between Metal Surfaces" Wear, Vol. 9.

10. Fields, S. A., et al. (1967), "Problems and Techniques of Lunar Surface Mining", NASA TMX-53560, January 10.

11. Frisch, J., et al. (1965), "Friction in Ultrahigh Vacuum", Institution of Engineering Research, University of California, Berkeley, Report No. MD-65-8, September.

12. Frisch, J., et al. (1966), "Friction in Ultrahigh Vacuum - Preliminary Tests on Aluminum Surfaces", College of Engineering, University of California, Berkeley, Report No. MD-66-2, April.

13. Frisch, J. and Pfaelzer, P. F. (1967a), "Ultrasonic Welding of Metals in Vacuum", College of Engineering, University of California, Berkeley, UCLRL Report No. MD-67-3, December.

14. Frisch, J., et al. (1967b), "Metallic Friction and Adhesion in Ultrahigh Vacuum", College of Engineering, University of California, Berkeley, Report No. MD-67-2, April.

15. Frisch, J., et al. (1967c), "Strain Gage Dynamometer Performance in Ultrahigh Vacuum", Presented at 1967 SESA Spring Meeting, Ottawa, Ontario, Canada, Paper No. 1209, University of California, May.

16. Frisch, J., et al. (1968), "Anisotropic Friction Betwen Aluminum Single Crystals in Ultrahigh Vacuum", College of Engineering, University of California, Berkeley, Final Report No. MD-68-1, May.

17. Halajian, J. D. (1962a), "Laboratory Investigation of Moon-soils", Grumman Aircraft Engineering Co., I.A.S. Paper No. 62-123, June.

18. Halajian, J. D. (1962b), "Vehicle-soil Mechanics on the Moon", Grumman Aircraft Engineering Corporation, Report No. ADR 04-04-62.2, October.

19. Hasseltine, E. H. (1967), "Study of Metallic and Dielectric Sputtering by Neutron Activation and Electron Microprobe Analysis", Ph.D. Thesis, University of California, Berkeley.

20. Jaffe, L. D. (1967), "Surface Structure and Mechanical Properties of the Lunar Maria", Jrnl. of Geophysical Research, Vol. 72, No. 6, March.

21. Johnson, R. W. (1963), "Lunar Locomotion", Lunar and Planetary Systems Development, General Electric Company, February 27, 1962, Reprinted July 24.

22. Johnson, R. W. and Greiner, J. M. (1965), "Chemical Bonding and Shear Strength of Silicate Systems Under Lunar Conditions", Paper presented to the Fourth Annual Meeting, Working Group on Extra-terrestrial Resources, Colorado Springs, General Electric, Missile and Space Division, November 30 to December 2.

23. Kramer, I. R.; Shen, H. K. and Podlaseck, S. E. Jr. (1966), "The Influence of a Space Environment on the Mechanical Behavior of Metals", Exp. Mechanics, January.

24. Lancaster, T. A. (1967a), "LSSM Evolution", Lunar Surface Exploration Selected Abstract for NASA Santa Cruz Summer Study, BSR-2147, Ann Arbor, Michigan, July 29 to August 12.

25. Lancaster, T. A. (1967b), "Basic LSSM Description and Capability", Lunar Surface Exploration Selected Abstract for NASA Santa Cruz Summer Study, BSR-2147, Ann Arbor, Michigan, July 29 to August 12.

26. Magie, P. M. (1966), "A Review of the Properties and Potentials of the New Heavy Metal Derivative Solid Lubricants", Presented at the 21st ASLE Meeting, May 2 to 5.

27. Mimosa Data Sheet (1966), "Manned Roving Vehicle Cabin - Three Men", Lunar Exploration Equipment Data Sheet, No. 2423, December.

28. Mimosa Data Sheet (1967), Lunar Exploration Equipment Data Sheets, No. 1421, March 1.

29. Mimosa Summary Digest (1967), Study of Mission Modes and System Analysis for Lunar Exploration. Report No. LMSC-A847940, Final Report, Lockheed Missile & Space Company, April 30.

30. Moffatt, W. G. et al. (1964), "The Structure and Properties of Materials", Vol. 1, J. Wiley & Sons.

31. Mohr, G. (1967), "Determination of the Coefficient of Friction Between Metals and Nonmetals at Ultrahigh Vacuum", Interim Progress Reports No. 0284-13 through -37, Grumman Aircraft Engineering Co., July 1965 - July 1967.

32. Odden, R. B. (1967), Mobile Lunar Surface Laboratory, Lunar Surface Exploration Selected Abstract for NASA Santa Cruz Summer Study, No. BSR-2147, Ann Arbor, Michigan, July 29 to August 12.

33. Penn, S. H. (1964), "Determination of the Coefficient of Friction of Metals on Nonmetals at Ultrahigh Vacuum", Grumman Research Department Report, Final Report No. 0284-5, May 15.

34. Penn, S. H. (1965), "Determination of the Coefficient of Friction Between Metals and Non-metallic Slides at Ultrahigh Vacuum", Grumman Aircraft Co., Report RE-205, March.

35. Peters, J. D. (1964), "Suitable Lunar Landing System Considering the Bearing Capacity and Failure Modes of Lunar Surface Materials", Arnold Engineering Development Center, DCS/Research, Arnold AF STN, Tennessee.

36. Rabinowicz, E. (1965), "Friction and Wear of Materials", John Wiley & Sons, Inc., New York.

37. Rosenberg, D. and Wehner, G. K. (1962), "Sputtering Yield for Low Energy He+ -, Kr+ -, and Xe+ - Ion Bombardment", Jrnl. of Appl. Phys., Vol. 33, p. 1842, May.

38. Ryan, J. A. and Baker, M. B. (1967a), "Adhesional Behavior of Air and Ultrahigh Vacuum Formed Silicate Surfaces in Relation to the Moon", ASTM Special Technical Publication No. 431.

39. Ryan, J. A. (1967b), "Experimental Investigation of Ultrahigh Vacuum Adhesion as Related to the Lunar Surface", Contract No. NAS7-307, Douglas Aircraft Co., September.

40. Salisbury, J. W., et al. (1963), "Adhesive Behavior of Silicate Powders in Ultrahigh Vacuum", Presented at the 44th Annual Meeting of American Geographical Union, Washington, D.C., April 17 to 20.

41. Scott, H. G. (1962), "Sputtering of Gold by Low Energy Inert Gas Ions", Jrnl. of Phys., Vol. 33, p. 2011, June.

42. Semenoff, A. P. (1958), Sxvativanye Metallov, Mashgiz, Moscow.

43. Smith, C. S. (1962), "Materials", Scientific American, Vol. 217, No. 3, September.

44. "Space Lubricant Myth" (1968), Industrial Research, March.

45. U.S. Army (1966), Vehicle Lunarization Study, No. M-274 "Mule" Vehicle, Vol. 1, Summary, April.

46. U.S. Army (1966), Department of the Army Office, Chief of Engineers, Vehicle Lunarization Study, No. M-274 "Mule" Vehicle, Vol. 11, Appendix, April.

47. Vaughn, O. H. (1967), "Lunar Environment: Design Criteria Models for Use in Lunar Surface Mobility Studies", NASA TMX-53661, September 28.

48. Vey, E. and Nelson, J. D. (1963), "Studies of Lunar Soil Mechanics", Final Report, IITRI Project No. M272 for NASA, Washington, D.C. July.

49. Wehner, G. K. (1963), "Sputtering Effects on the Lunar Surface", Electronics Division of General Mills, Inc., Minneapolis 13, Minn., Contract No. NASW-424.

LIST OF SYMBOLS

A_r	real contact area
E	modulus of elasticity
f	coefficient of adhesion
N	normal force
N'	normal separating force in adhesion
p	compressive stress
P	friction force
P_s	dynamometer force reading
q_u	yield pressure
r	radius of contact area
S	shear stress
S_i	interfacial shear strength
T	tangential force
W	normal load
Z	section modulus
β	shape parameter
δ	$= \frac{12(1-\nu^2)}{E}$
ϵ	strain
μ_B	coefficient of bearing friction
μ_K	coefficient of kinetic friction
μ_R	coefficient of rolling friction
μ_S	coefficient of static friction
ν	Poisson ratio
σ_t	tensile yield stress
ϕ	friction angle

APPENDIX

A. ROLLING FRICTION DYNAMOMETER DESIGN

1. Design Constraints

a. Normal load range: 0.2 to 2.4 lbs.

b. Diameter of the wheel specimen: 3/4 to 2 inches.

c. Maximum allowable dynamometer length: > 3 inches.

d. Loading condition: short-term static loads.

e. Amplifier sensitivity: 1μV.

2. Design of Strain Gage Dynamometer

a. Minimum force. It is known that the coefficient of friction in ultrahigh vacuum is considerably higher than under normal atmospheric conditions. Roughly compared to air, a vacuum environment causes twice the coefficient of friction. Relative to the designed experiment, the friction coefficient for antifriction needle bearings is 0.0045* and the coefficient of rolling friction between steel wheels and rails is about 0.006. These values might be considered as a reasonable anticipated lower bound for the coefficient of rolling friction between the rock and the wheel specimen in vacuum. Choosing $\mu_R = 0.006$ as a lower limit for the expected coefficient of rolling friction in vacuum, the minimum force the dynamometer will be subjected to is:

$$Fmin = \mu_R \cdot Nmin = 0.006 \times 0.2 = 0.0012 \text{ lbs} \qquad (2\text{-A-}1)$$

b. Maximum force. In general, rolling friction can not be greater than the sliding friction between the solids, and the coefficient of sliding friction becomes the upper bound for the coefficient of rolling friction. The coefficient of sliding friction, μ_S, between aluminum and

---

* Arvid Palmgren, "Ball and Roller Bearing Engineering", SKF Industries, p. 39, Philadelphia, 1945.

basalt has been reported as 0.6 (Fields et al., 1967). Therefore the expected maximum force for the dynamometer would be:

$$Fmax = \mu_S \cdot Nmax = 0.6 \times 2.4 = 1.44 \text{ (lbs)} \qquad (2\text{-A-}2)$$

c. Dynamometer configuration. The force F acting on the dynamometer has a very low minimum value. The simplest dynamometer configuration which satisfies the requirements for reliable measurements is the cantilever beam type which uses bending strain to measure the applied force. As shown in Fig. 2-29 two cantilever beams are used, one for each side of the wheel shaft. The beam is 2.5 inches long and 0.20 inches wide for a 1/8 inch resistance strain gage. The strain gages for this application are selected for their sensitivity and reliability in vacuum applications (Frisch, et al., 1967b).

Four strain gages, one on each side of the two beams, can be used to form a temperature compensated bridge.

d. Material. 17 - 4 PH stainless steel, with proper elongation, strength and creep properties is used for the beam.

e. Minimum strain of the cantilever beam. The section modulus of the cantilever beam shown in Fig. 2-29 is:

$$Z = \frac{bh^2}{6} = \frac{0.2h^2}{6} = 0.0333h^2 \qquad (2\text{-A-}3)$$

where:

b is the width and h is the thickness.

The bending moment at the gage section in Fig. 2-29, is:

$$M_s = \frac{F}{2} \times (2.5 - 0.4) = 1.05F \qquad (2\text{-A-}4)$$

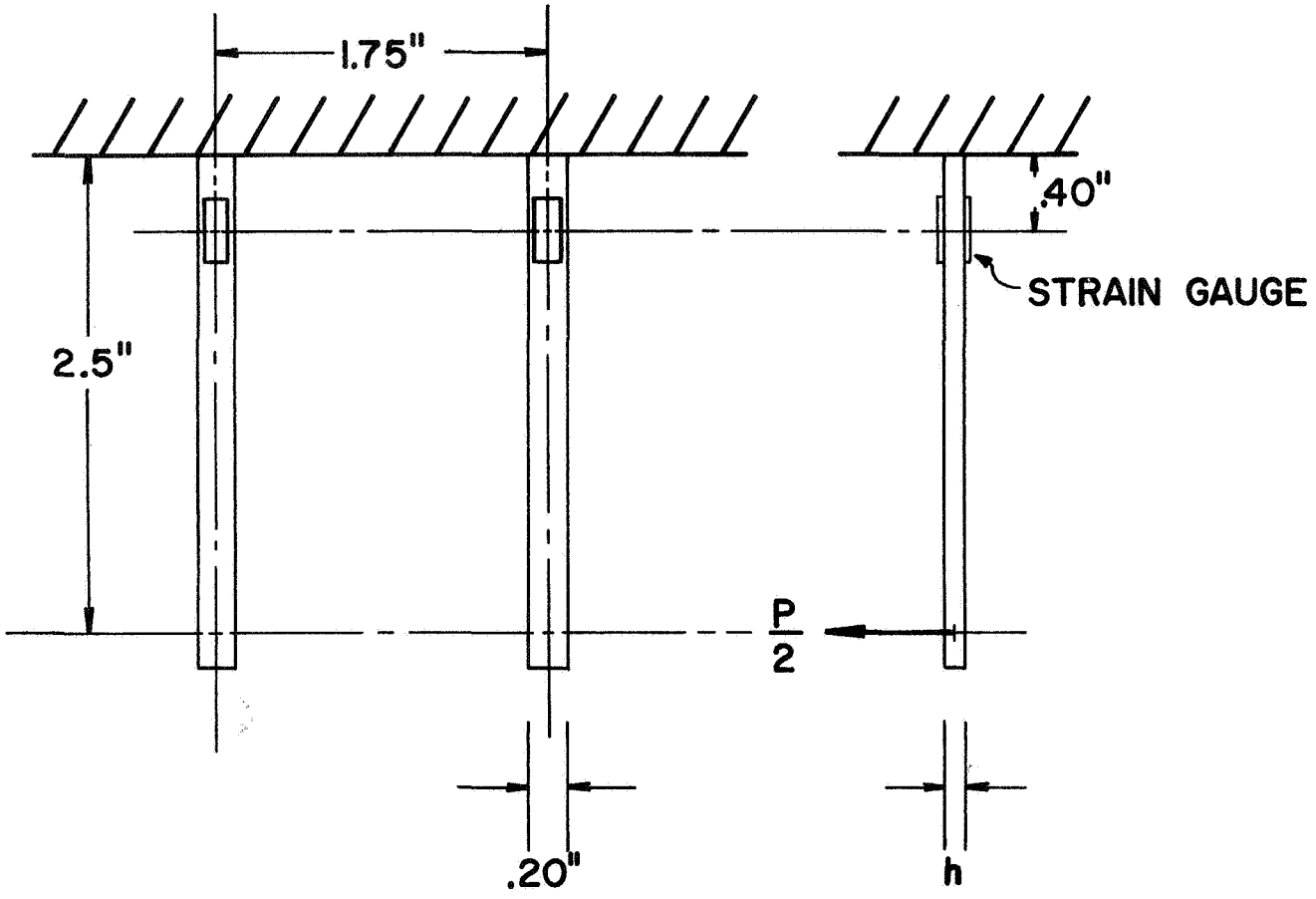

FIG. 2-A-1. Dynamometer Beam Configuration

The corresponding bending stress at the surface is:

$$\sigma_s = \frac{M_s}{Z} = \frac{1.05F}{0.0333h^2} = 3.15\,\frac{F}{h^2}\ \text{psi} \qquad (2\text{-A-}5)$$

The bending stress at the free surface with minimum force Fmin = 0.0012 (lbs) is:

$$(\sigma_s)\text{min} = \frac{3.15 \times 0.0012}{h^2} = \frac{0.0378}{h^2}\ \text{psi} \qquad (2\text{-A-}6)$$

Young's modulus of 17 - 4 PH stainless steel is: $E = 28.5 \times 10^6$ psi which gives the strain ε_s when $(\sigma_s)\text{min}$ is applied.

$$\varepsilon_s = \frac{(\sigma_s)\text{min}}{E} = \frac{0.0378/h^2}{28.5 \times 10^{-6}} = \frac{1.32 \times 10^{-9}}{h^2} \qquad (2\text{-A-}7)$$

f. Thickness of the cantilever beam. The formula for bridge output voltage into a known load is:

$$E_0 = \left(\frac{\varepsilon_s \cdot VG \cdot n}{4(R + r)}\right) r \qquad (2\text{-A-}8)$$

where:

ε_s = shear strain per gage
V = bridge supply volts
G = gage factor
n = number of active gages
R = nominal gage resistance
r = load resistance

As the standard oscilloscope input resistance is 1 megaohm, the previous formula can be simplified to give a very close approximation.

$$E_0 \frac{\varepsilon_s \cdot VGn}{4} \tag{2-A-9}$$

For the proposed design the following values will be used:

V = 12 volts

G = 2.0

n = 4, and $(\varepsilon_s)\min$ was $\frac{1}{h^2}(1.32 \times 10^{-9})$

Then:

$$(E_0)\min = \frac{1.32 \times 10^{-9}}{4h^2}(12 \times 2 \times 4)$$

$$= \frac{3.18 \times 10^{-8}}{h^2} \text{ Volts} \tag{2-A-10}$$

Since the noise level of the D.C. amplifier is 1μV, the minimum output voltage should be higher than 10 μV to have a signal to noise ratio higher than 10.

$$(E_0)\min \geq 10 \times 10^{-6} \text{ Volts}$$

$$\frac{3.18 \times 10^{-8}}{h^2} \geq 10 \times 10^{-6} \tag{2-A-11}$$

$$h^2 \leq 3.18 \times 10^{-3}, \quad h \leq 5.64 \times 10^{-2} \text{ inches}$$

g. For a 0.056 inch thick cantilever beam:

$$Z = \frac{bh^2}{6}$$

$$(\sigma_s)\max = \frac{Mmax}{Z} = \frac{Fmax \times 2.5}{2Z} = \frac{Fmax \times 2.5 \times 3}{bh^2} \qquad (2\text{-A-}12)$$

The allowable stress range for the dynamometer is usually 1/5 σ_t. Below this stress range, no permanent deformation is expected.

$$(\sigma_s)\max = \frac{1}{5}\sigma_t = \frac{Fmax \times 2.5 \times 3}{bh^2} \qquad (2\text{-A-}13)$$

Substituting the dimensions and the yield stress σ_t of 17 - 4 PH stainless steel 180,125 psi, the above Equation, Fmax is:

$$Fmax = \frac{180{,}125 \times 0.2 \times (0.056)^2}{5 \times 7.5} = 3.02 \text{ lbs} \qquad (2\text{-A-}14)$$

This value of Fmax is higher than the expected maximum rolling friction force and the cantilever beam thickness 0.056 inch is sufficient. To obtain better sensitivity at the lower limit, the thickness is changed to h = 0.050 inches and the allowable force Fmax is decreased to 2.4 lbs which is still larger than the expected maximum force of 1.44 pounds.

h. Strain gage heat dissipation. As a general guide, a bonded strain gage will not dissipate more than 250 milliwatts of continuous power. The dissipation for a 350 Ω bridge with a bridge supply of 12 volts will be:

$$W = \frac{E^2}{R} = \frac{144}{350} = 0.41 \text{ watts} \qquad (2\text{-A-}15)$$

Each 350 Ω bridge arm will, therefore, dissipate $\frac{0.41}{4}$ = 103 milliwatts, which is considered a safe design criterion.

B. BEARING LUBRICATION

In order to keep the friction in the wheel shaft bearings as small as possible, so-called space lubricants have been considered. These are self lubricating solids such as reinforced Teflon and Molybdenum Disulfide MoS_2. The advantage of solid lubricants is avoidance of outgassing and stability at high temperatures during the repeated bake-out cycles. In addition $TaSe_2$ (Magie, 1966) shows good vacuum stability, to be considered as well as the Dicronite* lubricant which appears to have a permanent lubricating quality.

C. SPUTTERING OF ROCK SPECIMENS

1. Solar Wind Simulation

The solar wind is known to be composed mainly of protons, electrons, α particles and other heavy particles. However the sputtering effect is due to proton and α particle bombardment. Some solar wind data (Wehner, 1963) that are useful for a rock sputtering technique are shown in Table 2-4. To design the sputtering equipment, sputtering-yield data are needed for proton and α particle bombardment of various metal and rock surfaces in the range of 1 to 20 Kev. The yield curve for He^+ ion bombardment reaches a very broad maximum at energies in the region 2 to 10 Kev and in a first approximation the maximum yield can be set at 3/2 the value found at 600 ev.

Also, the yields for light ions (e.g., hydrogen) are at least two orders of magnitude lower than those for more massive ions (Ne^+ or Ar^+) of the same energy (Wehner, 1963). Therefore it is advantageous to use heavier ions to shorten the sputtering time in the laboratory.

It may also be noted that SiO_2 sputters (volumewise) at roughly the same rate as Fe, while Al_2O_3 has a sputtering rate which is lower by a factor of five. Various rock samples show a thickness decrease which

---

* Dicronite Lubricants Co., MPB, Inc.

TABLE 2-A-1

SPUTTERING RATES UNDER SOLAR-WIND BOMBARDMENT (After Wehner, 1963)

Ion	Flux	Velocity	Energy	Yield(atoms/ion) (Normal incidence, smooth surface)	Sputtering Rate	
					Atoms/cm^2 · Year	Å/Year
Proton (solar wind)	$2 \times 10^8/cm^2$ · sec	600 km/sec	1850 ev	Cu: 0.03 Fe: 0.009 Stony Materials:	0.1×10^{15} 0.03×10^{15}	0.3 0.1 0.1
Proton (solar wind)	$2 \times 10^8/cm^2$ · sec for 1/60 of time	1000 km/sec	5000 ev	Cu: 0.04 Fe: 0.008 Stony Materials:	0.02×10^{15} 0.004×10^{15}	0.06 0.012 0.012
α - particle	$0.3 \times 10^8/cm^2$ · sec	600 km/sec	7400 ev	Cu: 0.4 Fe: 0.25 Stony Materials:	0.23×10^{15} 0.07×10^{15}	0.7 0.21 0.24
α - particle	$3 \times 10^8/cm^2$ · sec	1000 km/sec	20 kev	Cu: 0.2 Fe: 0.06 Stony Materials:	0.015×10^{15} 0.005×10^{15}	0.045 0.015 0.018

is about equal to or slightly higher than that of a medium sputtering rate metal such as Fe (Wehner, 1963). The sputtering rate itself is considerably higher if the beam strikes obliquely rather than at normal incidence.

Generally sputtering has the effect of smoothing the surface but polished surfaces show a higher degree of microscopic roughness after sputtering because differently oriented crystallites have different sputtering yields. Sputtering of oxide powders shows that the bombarded surface becomes enriched with metal. It appears that lighter atoms (i.e., oxygen) are more likely to escape from the surface than metal atoms. This matches the probability that lighter atoms excape from the moon's gravitational field.

2. Schematic Diagram for Rock Sputtering

The main problem in argon ion sputtering is the difficulty of removal by pumping of the argon gas after the sputtering. To minimize the load of pumping argon sputtering equipment can be designed in an auxiliary chamber, as shown in the diagram of Fig. 2-30.

The auxiliary chamber will be filled with pure argon until the pressure rises to 1×10^{-3} Torr while the filament is on. The outer magnetic coil permits the electrons to have longer helical path. This may increase the ionization rate of argon. Furthermore the argon ions can be partially trapped along the core. Then valve V_1 is opened and a voltage of -300 is applied to the OHFC copper plates to accelerate argon ions. After one sputtering cycle the rock specimen will be covered by Ar^+. To eliminate cation screening of Ar^+ the switch is connected to +30V to enable the electron bombardment of the rock specimen. By this method the Ar^+ can be neutralized, preceding the next cycle sputtering. This process is continued until the main chamber pressure reaches 1×10^{-3} Torr. After the sputtering process, the auxiliary ion pump for evacuating argon is started to bring the base pressure to 1×10^{-6} Torr, at which time it is almost saturated with argon. The main ion pump is started to evacuate the remaining argon. A chamber pressure of 1×10^{-9} Torr can be obtained using the auxiliary ion pump before starting the main ion pump (Frisch et al., 1968).

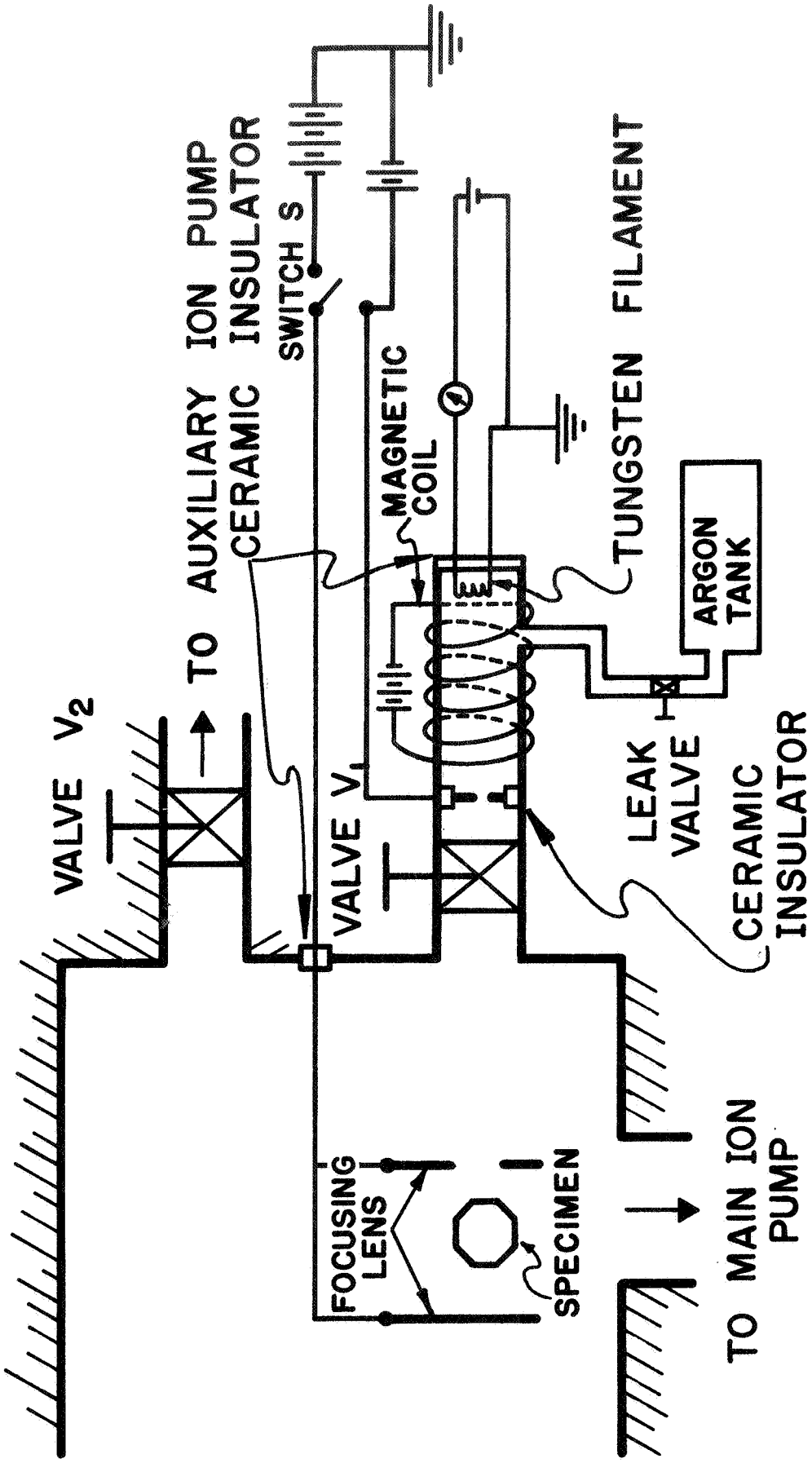

FIG. 2-A-2. Schematic Diagram of Ion-Sputtering Device

To estimate the sputtering rate of rock, the rock specimen will be replaced by an OFHC metal block of the same cross section as the rock specimen.

By measuring the current flowing through the copper block, the flux of incident argon ions can be calculated.

$$\text{No. of argon ion/sec} = \frac{\text{current (amp)}}{1.602 \times 10^{-19} \text{ (coulomb/ion)}} \qquad (2\text{-A-16})$$

However, the ion flux may be different for a metal target than a rock target. But as long as no voltage is applied to the target, the difference will be negligible. The sputtering ratio for rock can be assumed as 0.2 since this value is the usual one for oxides (Frisch et al., 1968). Therefore, about 1/5 of the number of argon ions which strike the rock corresponds to the number of rock atoms removed. The sputtering time will be determined from the thickness of the rock surface to be removed.

Currently used sputtering techniques for metals can be used for the wheel specimen (Frisch et al., 1968).

CHAPTER 3

UTILIZATION OF LUNAR SOILS FOR SHIELDING AGAINST RADIATIONS, METEOROID BOMBARDMENT, AND TEMPERATURE GRADIENTS

By

Francois E. Heuzé and Richard E. Goodman

CHAPTER 3

UTILIZATION OF LUNAR SOILS FOR SHIELDING AGAINST RADIATIONS, METEOROID BOMBARDMENT, AND TEMPERATURE GRADIENTS

(Francois E. Heuzé and Richard E. Goodman)

I. INTRODUCTION

Protection has to be provided for astronauts on the moon against three environmental factors: radiations, meteoroids and excessive temperature gradients. Extended stay times and payload constraints will require that some of the shielding materials be indigenous to the lunar surface. They are proposed here as lunar soils.

Present knowledge regarding each of the mentioned hazards is reviewed and a model selected. Lunar surface material properties used can be those selected by Smith and Mitchell (1968) from Surveyors and other pertinent experiment conclusions.

First estimates of shielding thicknesses are then established corresponding to a given set of assumptions whose validity is discussed. Further research needed is also outlined where it is felt that major uncertainties still exist for the establishment of final shielding specifications against a given hazard.

II. SHIELDING AGAINST RADIATIONS

A. Environment

Latest radiation environment analyses by NASA and the U. S. Air Force have been summarized by Burrell et al. (1968) and Curtis and Wilkinson (1968) as follows:

> Protons and electrons in the Van Allen belts (of no concern for on site lunar exploration).
>
> Solar wind (not discussed, since no appreciable dose is received behind any nominal shielding).

Galactic cosmic radiation (85% protons, 14% α particles, 1% heavier nuclei). Dose rate is approximately 10 rads/year without shielding.

Energetic solar cosmic radiation (protons and α particles). Maximum flare flux is about 10^9 protons/cm^2 above 30 mev.

It appears that lunar radiation shielding will have to be designed against energetic solar radiation for missions of extended duration (greater than one week).

B. Flare Predictions, Dose Rates, Shield Thicknesses

Based upon selection of solar flares obtained over the past 25 years, Burrell et al. (1968a) and Lahti et al. (1968) developed stochastic Monte-Carlo models for prediction of future events. Cumulative probability distributions of overexposure can then be obtained for missions of a given length as a function of dose rates and shield configurations. The procedure is as follows:

Compile actual solar flare data (n flares over a complete activity cycle).

Estimate total dose received during each flare behind shielding of given material and thickness.

Select mission length.

Input in computer program for stochastic model the previous dose estimates and have it generate N missions (several tens of thousands).

Smooth out the dose probability output for this particular mission and the particular shielding configuration(s).

Computations of references 2 and 6 are summarized in Table 3-1.

C. Discussion

We can assume that given the same input, two well conceived stochastic models will give the same overexposure probability outputs owing to their use of random numbers to the large number of missions

TABLE 3-1

STOCHASTIC MODELS FOR SOLAR FLARE EXPOSURE DURING INTERPLANETARY MISSIONS

	Burrell (1968-a)	Lahti (1968)
FLARE DATA	All 32 flares 1956 – 1963	Largest 20 flares 1956 – 1962
DOSE PREDICTION	Stochastic model by Norman (1967)	Stochastic model by Hildebrand and Lewis (1966)
SHIELD CONFIGURATION	Aluminum 2,5,10,20 g/cm^2 Polyethylene 2,5,10,30 g/cm^2	Aluminum 10,15,20,30,40 g/cm^2 Water 10,15,20,30,40 g/cm^2
MISSION LENGTH (examples given)	2 weeks 52 weeks	87 weeks* (Mars)
NUMBER OF MISSIONS GENERATED	20,000	40,000

*Program can account for dose dependence on distance from sun.

generated and to the final smoothing out of results. Thus, any discussion of reliability shall focus upon the input data. Shield thicknesses are given by a parameter with dimensions grams/cm^2. To convert to actual thickness of a given material, one must divide by the material density. It is stated (Burrell, 1968a) that, "in terms of these units, the penetration characteristics of charged particles are almost the same in all materials (hydrogen being the only exception)." This, according to Burrell (1968b), should not be taken as an engineering concept but rather as a qualitative statement explaining the use of the particular units g/cm^2.

With this in mind, computed doses for the the three major flares or clusters in the 1956-1962 cycle will be compared for different shield thicknesses and different materials. Table 3-2 is compiled from References 2 (p. 7) and 6 (pp. 10 and 21). For reasons of convenience, these results are plotted on Figure 3-1. This comparison calls for the following remarks:

1. Based upon results for one material (Al), doses for input data as given by different programs (References 5 and 7) are not significantly different. Let d be the dose, then six values are obtained for $\Delta d/d$, taken as $2(d_3 - d_4)/(d_3 + d_4)$

$$\frac{\Delta d}{d} = + 0.04, + 0.095, + 0.09, - 0.07, - 0.075, - 0.08$$

Relative errors are < 10% in this example. Thus it will be assumed that all together, input doses for the Monte-Carlo models are fairly well established as a function of recorded flares.

2. For all these materials, the respective influence of the three flares are reversed when the shield thickness is changed

	Total Dose in rads
for t_d = 10 g/cm^2	Feb 56 > Nov 60 > July 59
for t_d = 20 g/cm^2	Feb 56 < Nov 60 $\geq$ July 59

The implications of this fact are not clear to the authors.

TABLE 3-2

COMPARED DOSE ESTIMATES FOR TWO DIFFERENT MODELS,
TWO DIFFERENT THICKNESSES, THREE DIFFERENT MATERIALS, AND THREE SOLAR FLARES

MATERIALS	DOSES* (rads)							
	Al[2]**		Al[6]**		Polyethylene[2]**		Water[6]**	
THICKNESSES	t_d = 10	t_d = 20	t_d = 10	t_d = 20	t_d = 10	t_d = 20	t_d = 10	t_d = 20
FLARES OR CLUSTERS:								
February 23, 1956	50.20	24.80*	48.11	23.84*	35.7	16.5	38.32	18.07
July 1959	75.00	21.20*	67.55	18.94*	40.9	10.3	44.01	11.19
November 1960	68.80	23.75*	62.93	21.79*	40.8	13.0	44.32	14.13

* For considerations of energy brackets and characteristic rigidities, the reader is referred to References 2 and 6.

**Superscript indicates reference (Burrell or Lahti).

t_d = shield thickness in g/cm^2.

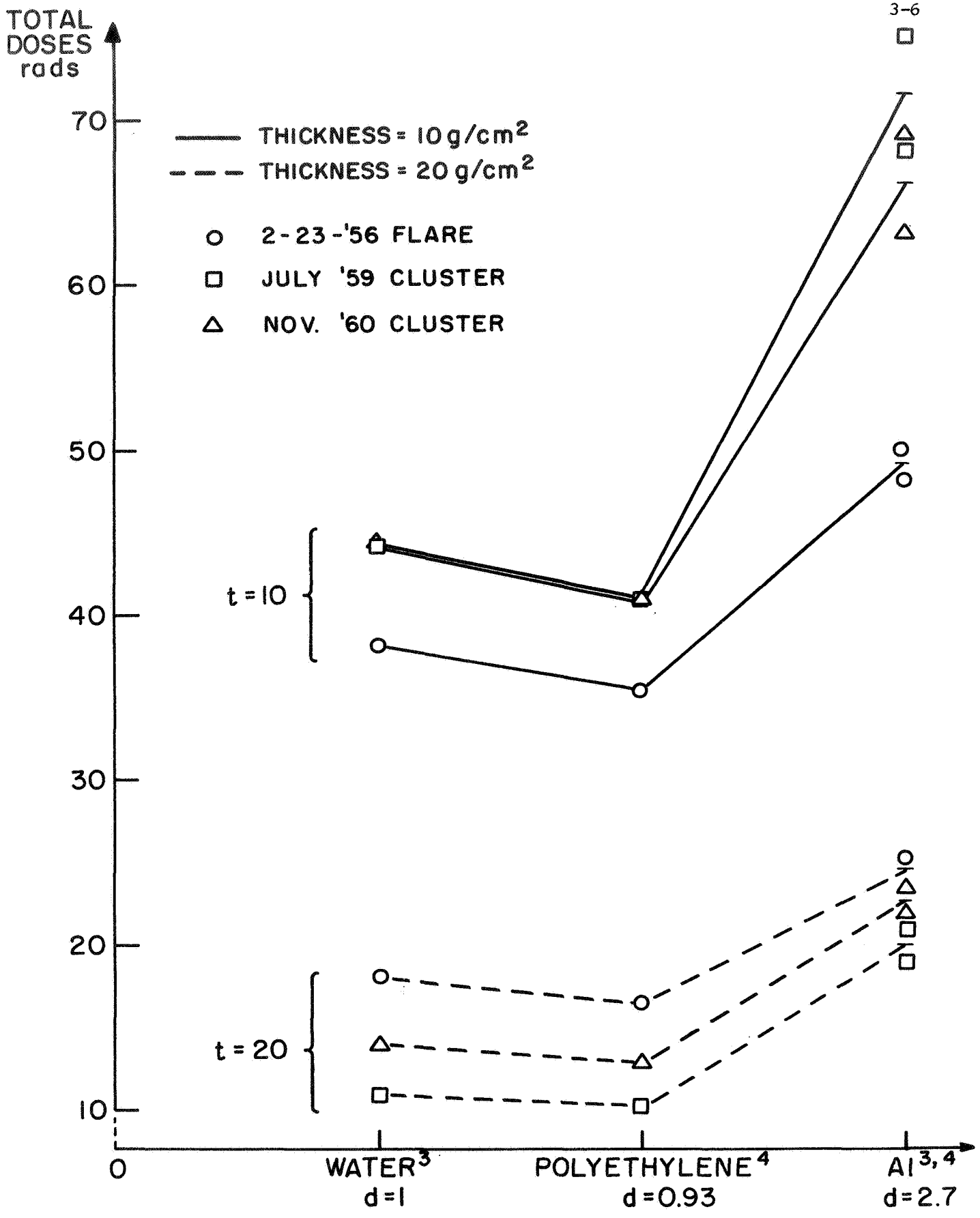

FIG. 3-1. Compared dose estimates for three major flares with different materials and thicknesses.

3. Aluminium is consistently least efficient and polyethelene most efficient of the above materials.

D. Applications — Examples

For engineering applications a first estimate of soil shield thickness will be based upon conservative "dimensionless" values; those for aluminum shielding. For non-hydrogenous materials aluminum is a good shield and might be close to lunar materials in atomic number (Burrell, 1968b).

The following computational procedures are then proposed:

1. Define mission duration (T days on site)
2. Select maximum allowable total dose D_{max}, from allowable daily dose d_{max} ($D_{max} = T \cdot d_{max}$)
3. Select desired probability, p, of no overexposure to the maximum allowable dose
4. Compute corresponding "dimensionless" aluminum shield thickness (by means of one of the available programs (Hildebrand, 1966; Norman, 1967)
5. Select a value for the average lunar soil shield density (the degree of soil compaction for instance can be introduced here)
6. Compute the corresponding required soil thickness

Example:

1. T = 52 weeks = 364 days
2. d_{max} = 0.2 rad/day; $D_{max} \simeq$ 73 rads/year
3. p = 99.99%
4. From Reference 3, p. 30, $t_{Al} \simeq 22$ g/cm^2
5. λ_{soil} = 1.35 g/cm^3 (soil similar to fine grained sand with high porosity, p = 50%, — no compaction)

$$6. \quad t = \frac{t_{Al}}{\gamma_{Al}} \cdot \frac{\gamma_{Al}}{\gamma_{soil}} = \frac{22}{2.7} \cdot \frac{2.7}{1.35}$$

$$t \simeq 16 \text{ cm of soil}$$

To further this example, results of similar computations are tabulated on Table 3-3 for different specifications.

E. Summary — Conclusions

Considering that the Monte-Carlo flare predictions tend to yield conservative numbers, these first estimates are believed to be safe. They have a built-in factor of safety owing to the following facts:

1. "Dimensionless" shield thicknesses used are those computed for aluminum
2. No biological cell regeneration is assumed
3. Moderate to high soil porosities (little to no compaction) have been considered. Higher compaction will indeed provide better protection for the same thickness
4. On site any cut and cover operation for shelter building will involve the use of some roof support and sealing of materials. They will come as an additional shielding unit

On the other hand. the estimates do not account for other radiation types (whose hazard is indeed much smaller). Wilson and Karcher (1966) have concluded that best protection against primary neutron flux and lowest secondary gammas is obtained in soils with high silicon and low iron content. It is encouraging to know that lunar soils are of this type. See Vol. I, Chapter 2, this report.)

III. SHIELDING AGAINST METEOROIDS

A. Environment — Model Selection

Meteoroids in the lunar environment can be characterized by four parameters: mass, density, velocity, and mass flux relationship. Determination of these parameters has been the object of a great many efforts (Cosby, 1965), and we shall try here to adopt a workable model taking into account this previous research.

TABLE 3-3

SOIL SHIELD THICKNESSES FOR GIVEN SPECIFICATIONS

	d_{max} rads/day	p %	t_{Al} g/cm^2	γ_{soil} g/cm^3	t_{soil} cm
2 Weeks	0.1	99.99	24*	1.00	24
	0.1	99.99	24*	1.50	16
	0.2	99.99	21*	1.00	21
	0.2	99.99	21*	1.50	14
1 Year	0.1	99.99	29*	1.00	29
	0.1	99.99	29*	1.50	19.5
	0.2	99.99	22*	1.00	22
	0.2	99.99	22*	1.50	14.5
20 Months	0.1	99.99	24**	1.00	24
	0.1	99.99	24**	1.50	16
	0.2	99.99	15**	1.00	15
	0.2	99.99	15**	1.50	10

*From Reference 2

**From Reference 6

After Bjork, et al. (1968), the bulk of currently available information regarding this environment is derived from four sources:

1. Photographic observations of the luminous trajectories of meteoroids earth's atmosphere, photographic meteors, mass = 10^{-2} to 1 gram
2. Radar observations of the ionization trails of meteoroids in the earth's atmosphere; radio meteors, mass = 10^{-6} to 10^{-2} gram
3. Rocket and satellite sounding board measurements of meteoroid impact momentum
4. Penetrating flux measurements by satellites such as those taken by Explorer XVI, Explorer XXIII, and by the Pegasus vehicles

A review of the most recent models for near earth and deep space is presented in Table 3-4. All of them propose a linear relationship between the logarithmic flux per unit time and unit surface, and the logarithmic meteoroid mass. Moreover, mass ranges are generally specified and the parameters of the linear relationship accordingly modified to allow for an added reduction in the flux when masses reach the extremes of the brackets considered. For our design specifications, we shall select here from all previous models, a conservative estimate giving the highest flux (sporadic + stream). According to Naumann's model (1966) the total mass influx will be considered negligible for $m \leq 10^{-8}$ gram.

This model does not give any further reduction of the flux for $m \leq 10^{-6}$ g and $m \leq 1$ g as could be done considering proposed mass influx distributions (Naumann, 1966; Bjork et al., 1967; Ross, 1968), which emphasize the influence of meteoroids with mass $10^{-6} \leq m \leq 1$ g. On the contrary we shall compensate for the reduction in flux of masses $m > 1$ g inherent to the logarithmic form of the expression by adopting a bilinear relationship.

TABLE 3-4

MODELS OF METEORITE ENVIRONMENT

REFERENCE	MASS (grams)	DENSITY g/cm^3	VELOCITY km/sec	PRIMARY MAS-FLUX RELATIONSHIP*	LOCATION
Burbank, et al. (1965)	10^{-14} to 1	0.5 (average)	11 to 72 (average 30)	log N_{sp} = − 1.34 log m − 15.36 log N_{st} = − 1.34 log m − 13.97	Near earth, cislunar and moon
Smith, R. E. (1965)	10^{-10} to 1	0.22 to 0.88 (average 0.44)	15 to 25 (average 20)	log N = − 1.0 log m − 14.54	Moon
Nauman, R. J. (1966)	10^{-6} to 10^{2}	1.7 (average)	20	log N = − 1.16 log m − 14.3	Near earth
Dohanyi, J. S. (1966)	10^{-2} to 1	0.26	20 (average)	log N = − 1.0 log m − 14.0	Near earth
Dohanyi, J. S. (1967)	10^{-8} to 10^{6}	—	—	log N = − 0.8 log m − 12.4	Deep space and moon
Bjork, et al. (1967)	10^{-2} to 1 10^{-10} tp 10^{-5}	0.26 0.36 (50%) 2.80 (50%)	20 to 72 (average 28)	log N = − 1.34 log m − 14.0 Log N = − 0.8 log m − 12.4	Near earth Near earth

*N = number of meteoroids/m^2/sec above mass m in grams N_{sp} = N sporadic N_{st} = N stream

Models presented in Table 3-4 apply to an omnidirectional flux (2 π steradians). For a shield of finite area on the lunar surface, the angle will be π steradians. Thus, with

$$10^{-8} \leq m \leq 10 \text{ grams}$$

$$11 \leq v \leq 72 \text{ km/sec}$$

$$0.26 \leq \pi \leq 2.8 \text{ g/cm}^3$$

$$\text{solid angle} = \pi \text{ steradians}$$

the following model is adopted:

$$\log_{10} N = -1.0 \log m - 12.7 \qquad 10^{-8} \leq m \leq 1 \text{ gram} \tag{3-1}$$

$$\log_{10} N = -0.8 \log m - 12.7 \qquad 1 < m \leq 10 \text{ gram} \tag{3-2}$$

where N is the number of impacts per m^2/sec above mass m in grams. Equations 3-1 and 3-2 are now expanded into Table 3-5. For different specifications of mission length T and shield area A, the table gives the probability P of having impacts above a given mass m_{max}, or conversely the maximum mass M_{max} corresponding to a 99.99% probability of no hit above M_{max} (equivalent to N_{total}/mission $\leq 10^{-4}$).

For example it can be seen both ways [Table 3-5(*)] that with the model we have proposed, a 100 m^2 shield over a one year period will have a probability of 99.99% of not seeing an impact greater than 10 grams.

TABLE 3-5

PROBABILITIES OF NO IMPACT ABOVE GIVEN MASS AND CRITICAL MASSES WITH 99.99% PROBABILITY, FOR DIFFERENT MISSION LENGTHS AND SHIELD AREAS

T	A(m^2)	m_{max}(g)	log N_{total}/mission	P	M_{max} (g) for 99.99% Probability
2 weeks	10	0.01	− 3.6	2.5×10^{-4}	
"	"	0.1	− 4.6	2.5×10^{-5}	
"	"	1.0	− 5.6	2.5×10^{-6}	0.027
"	"	10.0	− 6.4	4.0×10^{-7}	
6 months	10	0.1	− 3.5	3.2×10^{-4}	
"	"	1.0	− 4.5	3.2×10^{-5}	0.32
"	"	10.0	− 5.3	5.0×10^{-6}	
6 months	100	0.1	− 2.5	3.2×10^{-3}	
"	"	1.0	− 3.5	3.2×10^{-4}	4.2
"	"	10.0	− 4.3	5.0×10^{-5}	
1 year	10	0.1	− 3.2	6.3×10^{-4}	
"	"	1.0	− 4.2	6.3×10^{-5}	0.64
"	"	10.0	− 5.0	1.0×10^{-5}	
1 year	100	0.1	− 2.2	6.3×10^{-3}	
"	"	1.0	− 3.2	6.3×10^{-4}	(*) 10.0
"	"	10.0	(*) − 4.0	(*) 1.0×10^{-4}	

The problem is then to obtain shield specifications.

B. Design Constraints and Discussion

The shield design shall be adequate against two hazards: shield perforation and shield erosion. Methods of approach adopted by other investigators for metal and polyethylene shields (Bjork, 1963; McMillan, 1968; Fish, 1968) cannot be readily adapted to soil shields. However, some parameters of hypervelocity impacts in soils have been investigated which lead to the following approach.

We shall consider the following two constraints and discuss their implications:

1. The depth of the largest crater created either by primary or secondary impact shall be a fraction Δ of the shield thickness (thick target).

2. The total mass ejected from the shield by impact over the mission length shall be a fraction ϵ of the total shield mass.

a. The perforation constraint. With respect to primary impact, two new parameters must now be defined:

1. The ratio $\alpha = (m_{ej})_1/m$ of the primary mass ejected by an impact to the mass of the impacting meteoroid. Given α and the soil density, the volume ejected can then be computed.

2. The ratio β of crater diameter to depth. Given β and knowing the volume ejected, the crater depth can be computed. The assumption, however, has to be made that the primary crater is conical in shape. This is consistent with the use of a thick target in unconsolidated materials (Constraint 1).

Possible α values have been suggested by experimenters in hypervelocity impact (Gault, et al., 1963; and others) and discussed by Ross (1968). For a weakly cohesive fine quartz sand-like soil and for velocities up to 30 km/sec, maximum values for α are obtained in the mass range 10^{-2} to 1 gram; the consensus is in favor of $10^3 \leq \alpha \leq 10^4$.

Much effort (Bjork, 1963; Smith, 1965; Quaide and Oberbeck, 1968) has been devoted to obtaining representative β values; β is generally presented as proportional to the impact velocity raised to a power n (n being a fraction of 1) and depends upon the target strength. However, for lunar type soils and over a wide range of velocities, typical β bracket (Ross, 1968; Moore, 1967) may be taken as $1/3 \leq \beta \leq 1/5$ with $\beta = 1/4$ suggested as a most representative value for a cone-shaped crater.

The respective influence of primary and secondary impacts must also be assessed from the standpoint of penetration. As observed by Gault, et al. (1963), the great majority of secondary ejecta have a velocity smaller by about 2 orders of magnitude than the primary impact. Low velocity penetration equations could then be applied. They have been under investigation for several years and recently Moore (1967) proposed their application to lunar secondary craters. Quigley and Mitchell (1968) later modified Moore's equations. However, this is not necessary when relative penetration depths only are considered. In fact we are interested here in the mass and velocity of the largest fragment ejected. Gault, et al. (1963), have discussed this and proposed the following. For masses of primary impact $\leq$ 10 g (which is the upper limit we have adopted in our model), the mass of the largest fragment ejected M_{ej} is at most 1/10 of the total mass ejected in primary impact $(M_{ej})_1$. Thus

$$(m_{ej})_{max} \leq 10^3 M_{max} \qquad \text{with } \alpha \leq 10^4$$

$$(v_{ej})_{max} \leq 10^{-2} v_{max}$$

The kinetic energy of the largest fragment of ejecta is then smaller than 1/10 that of the primary impact and we shall infer that primary impacts only are relevant to the perforation constraint.

b. The erosion constraint. The total ejecta has now to be computed by integration over the impacting mass range considered to satisfy Constraint 2. From Equations 3-1 and 3-2, N can be rewritten as (dimensions, grams, meters, seconds)

$$N = \frac{m_i^{-k_1}}{10^{k_2}} \text{ per } m^2/\text{sec}$$

$k_1 = 1$, $k_2 = 12.7$ with $10^{-8} \leq m \leq 1$ g

$k_1 = 0.8$, $k_2 = 12.7$ with $1 < m \leq 10$ g

let $N^*(m_i)$ be the rate of change with respect to mass, of the number of impacts of mass m_i (per m^2/sec), i.e.

$$N(m_i) = \int_{m_i}^{\infty} N^* \cdot dm$$

therefore

$$dN = - N^* \cdot dm$$

also

$$dN = - \frac{k_1}{10^{k_2}} \; m_i^{-(1 + k_1)}$$

Thus, within a mass range $[m_i, m_j]$, the total mass influx M_{tot} per m^2/sec is with $m_i < m_j$

$$M = \int_{m_i}^{m_j} m \cdot N^*(m) \cdot dm$$

with

$$m \cdot N^* = \frac{k_1}{10^{k_2}} m^{-k_1}$$

We can compute for example the total mass influx for our model in the range $10^{-8} \leq m \leq 10$ g

$$M_{tot} = \int_{10^{-8}}^{1} \frac{m^{-1}}{10^{12.7}} dm + \int_{1}^{10} 0.8 \cdot \frac{m^{-0.8}}{10^{12.7}} dm$$

$$= 2.303 \frac{\log m}{10^{12.7}} \Bigg]_{10^{-8}}^{1} + 0.8 \frac{m^{0.2}}{0.2 \times 10^{12.7}} \Bigg]_{1}^{10}$$

$$= 20.78 \cdot 10^{-12.7} \text{ g/m}^2\text{/sec}$$

$$= 13.1 \cdot 10^{-6} \text{ g/m}^2\text{/year} \qquad 10^{-8} \leq m \leq 10 \text{ g}$$

REMARK: Based on Naumann's distribution (1965), Ross (1968) computed the total mass influx for Naumann's model with the following result:

$$M_{tot} = 40 \cdot 10^{-6} \text{ g/m}^2\text{/year for } 10^{-8} \leq m \leq 10^3 \text{ g}$$

The method described above applied to Naumann's model gives a value of

$$M_{tot} = 72.8 \times 10^{-6} \text{ g/m}^2\text{/year for } 10^{-8} \leq m \leq 10^3 \text{ g}$$

which differs from Ross.

More generally the same probability approach should be adopted for the erosion of a shield area A over a time length T, so that:

1. Once M_{max} is computed, then the total influx is

$$M_{tot} = \int_{10^{-8}}^{M_{max}} m \cdot N^* \, dm$$

2. If the probability p adopted for computation of crater depth is $p = (1 - 10^{-n})$ %, then with the same probability we shall have

$$(M_{ej})_{1_p} = 10^n \cdot \alpha \cdot M_{tot} \ g/m^2/sec$$

$$= 10^n \cdot \alpha \cdot M_{tot} \cdot T \cdot A \ grams$$

for the general mission specifications given.

Secondary impacts must also be considered from the standpoint of erosion. Ross (1968) has discussed this problem, and based upon results obtained by Gault, et al. (1963) adopted for $(M_{ej})_2$, total mass ejected by secondary impacts,

$$(M_{ej})_2 \leq (M_{ej})_1/10$$

Thus, we shall take conservatively for the total mass eroded

$$M_{ej} = 1.1\ (M_{ej})_{1p}$$

$$= 1.1 \cdot \alpha \cdot 10^{n} \cdot M_{tot}\ g/m^2/sec$$

3. $(M_{ej})_{mission} = 1.1 \cdot \alpha \cdot 10^{n} \cdot M_{tot} \cdot A \cdot T$ grams

c. Conclusions. Several remarks and conclusions are now presented from the preceding.

1. Our model has the same form as Naumann's. Thus not taking into account masses greater than 10 g underestimates the total mass influx by about 4%. This is negligible with respect to Constraint 2.

2. The selection of an upper limit for impacting masses will then have influence only on Constraint 1.

3. The proposed model appears to be quite conservative with respect to Naumann's total mass influx.

4. With respect to shield erosion and perforation primary impacts only will have to be considered.

5. In fact, within the mission lengths and shield areas considered, Constraint 2 will prove to be satisfied (see Table 3-6). Even if it were assumed that all the ejecta is lost (no fall-back upon shield), M_{ej} will be small compared to the total shield mass for any significant shield thickness (a few centimeters).

6. Topographic sheltering as defined by Ross (1968) will not have to be introduced since we are looking for a conservative estimate. Crater superimposition will not be considered critical

either since the shield will be designed according to the limits of confidence desired, against the largest primary impact which happens only once.

7. It is preferable, when a given sheltered area is needed, to obtain it through the use of separate shelters rather than with an unique one. For a given safety level, the largest impact considered will be smaller for smaller shields and the shield thickness reduced. In the case where α is selected as 10^4, the total amount of soil to handle will then also be reduced. If $\alpha = 10^3$, this amount will be the same.

8. Use of more numerous, smaller shelters is again more desirable with this model since it decreases the risk of total loss of available sheltered area.

Then, the only parameters to influence design will be α, β, γ, Δ, and ε.

C. Design Procedure — Examples

The following design procedure is now proposed for protection against meteoroids when mass does not exceed 10 g.

1. Define mission length T
2. Select shield area A
3. Select a safety level (expressed as the probability p of no impact above the maximum impact mass M_{max} against which the shield will be designed)

4. Compute M_{max} corresponding to p from the mass flux model. This is a first trial and error to determine which one of Equations 3-1 or 3-2 applies. If $M_{max} > 10$ g reduce A and recompute M_{max} (second trial and error)

5. Select $\alpha = (M_{ej})_{max}/M_{max}$

6. Compute $(M_{ej})_{max}$

7. Select soil density γ

8. Compute $V_{max} = (M_{ej})_{max}/\gamma$

9. Select β (ratio depth/diameter of crater)

10. Compute d_{max} (depth of largest crater)

$$d_{max} = \left(\frac{12}{\pi} \frac{V_{max}}{\beta^2}\right)^{1/3}$$

11. Select $\Delta = t/d_{max}$ $\Delta \geq 3$

12. Obtain the soil shield thickness t

13. Compute the total mass of the shield M_{shield}

14. Compute the total mass eroded M_{ej} corresponding to the flux $10^{-8} \leq m \leq M_{max}$ using Equation 3-3

15. Select ε (allowable erosion ratio of the shield)

16. If $M_{ej}/M_{shield} > \varepsilon$, increase Δ and recompute M_{shield} and M_{ej} (third trial and error)

Example

1. T = 6 months

2. A = 100 m^2

3. p = 99.99%

4. M_{max} = 4.2 g (from Equation 3-2)

5. $\alpha = 10^4$

6. $(M_{ej})_{max} = 4.2 \cdot 10^4$ g

7. $\gamma = 1.5$ g/cm^3

8. $V_{max} = 28 \cdot 10^3$ cm^3

9. $\beta = 4$

10. $d_{max} \simeq 19$ cm

11. $\Delta = 3$

12. t = 57 cm of soil

13. $M_{shield} = 85.5 \cdot 10^6$ g

14. $M_{ej} = 8.6 \cdot 10^5$ g

15. $\varepsilon = 0.1$

16. $M_{ej}/M_{shield} = 1\% < \varepsilon$
($\Delta = 3$ and t — 57 cm satisfy both constraints)

This sample computation is now expanded into Table 3-6 for different values of T, A, α, and γ (p = 99.99%, $\beta = 4$, and $\Delta = 3$ are fixed parameters). It can be seen that even with the lowest Δ, the perforation constraint is overwhelming. The erosion almost never exceeds 1% of the total shield mass.

D. Summary — Conclusions

Some major conclusions have already been presented above (Pages 3-19 and 3-20), and we shall add to them the following.

In the present state of the art, the above model and results are believed to be a workable tool for design of lunar soil shields against the meteoroid hazard. Estimates can be rendered conservative through adequate choice of parameters as follows.

The critical constraint has proven to be perforation; thus, any safety factor shall be built into the computation of d_{max}, where d_{max} is proportional to the other parameters as shown:

$\gamma^{1/3}$	$V^{1/3}$
$\beta^{-2/3}$	$M_{max}^{1/3}$
$\alpha^{1/3}$	$(M_{ej})_{max}^{1/3}$

It is recommended that α be taken as 10^4 before any further research proves it to be consistently smaller. The most conservative value for β would be $\beta = 3$. When the desired confidence level is increased, M_{max} is also increased and so are d_{max} and t.

This model could be used for short missions with $p > 99.99$ percent, but for one year missions with a shield area of 100 m^2, p is restricted to $p \leq 99.99$ percent by the corresponding $M_{max} = 10$ g. It is, however, felt that this upper limit on M_{max} represents a realistic weighing of hazards in lunar exploration.

The shield thicknesses considered will probably require, in extended missions, the handling of non-negligible masses of lunar soil; this problem has been discussed in previous chapters and by Fields et al. (1967).

Eventually, these thickness specifications are still much lower than those which would tend to provide the equivalent of one earth atmosphere for shielding (Corp et al., 1967) (750 cm or 25 feet for $\gamma = 1.35$ g/cm^3), and thus more within the realm of practicality.

TABLE 3-6. SPECIFICATIONS FOR SOILS SHIELD DESIGN AGAINST METEOROIDS.

T	A (m^2)	p = 99.9% n=4	M_{max} (gr)	α	γ (gr/cm^3)	β	d_{max} (cm)	t (cm) Δ=3	M_{shield} (gr)	M_{tot} (10^{-5} gr/m^2/yr)	$(M_{ej})_{mission}$ (99.99%)	$(M_{ej})_{mission}$ /M_{shield}
2 weeks	10	99.99	0.027	10^3	1.0	4	1.8	5.4	5.4×10^5	9.2	3.5×10^2	<1.0%
"	"	"	"	"	1.5	"	1.6	4.8	7.2×10^5	"	"	"
"	"	"	"	10^4	1.0	"	4.0	12.0	12.0×10^5	"	3.5×10^3	"
"	"	"	"	"	1.5	"	3.5	10.5	15.8×10^5	"	"	"
3 months	10	"	0.16	10^3	1.0	"	3.3	9.9	9.9×10^5	10.4	2.8×10^3	<1.0%
"	"	"	"	"	1.5	"	2.9	8.7	12.3×10^5	"	"	"
"	"	"	"	10^4	1.0	"	7.4	22.2	22.2×10^5	"	2.8×10^4	1.2%
"	"	"	"	"	1.5	"	6.4	19.2	28.8×10^5	"	"	1.0%
"	100	"	1.8	10^3	1.0	"	7.5	22.5	22.5×10^6	14.8	4.1×10^4	<1.0%
"	"	"	"	"	1.5	"	6.6	19.8	29.7×10^6	"	"	"
"	"	"	"	10^4	1.0	"	16.4	49.2	49.2×10^6	"	4.1×10^5	"
"	"	"	"	"	1.5	"	14.3	42.9	64.3×10^6	"	"	"
6 months	10	"	0.32	10^3	1.0	"	4.2	13.2	13.2×10^5	10.8	5.9×10^3	<1.0%
"	"	"	"	"	1.5	"	3.7	11.1	16.7×10^5	"	"	"
"	"	"	"	10^4	1.0	"	9.3	27.9	27.9×10^5	"	5.9×10^4	2.1%
"	"	"	"	"	1.5	"	8.0	24.0	36.0×10^5	"	"	1.6%
"	100	"	4.2	10^3	1.0	"	10.0	30.0	30.0×10^6	15.6	15.6×10^4	<1.0%
	"	"	"	"	1.5	"	8.8	26.4	39.6×10^6	"	"	"
	"	"	"	10^4	1.0	"	21.8	65.4	65.4×10^6	"	8.6×10^5	1.3%
	"	"	"	"	1.5	"	19.0	57.0	85.5×10^6	"	"	1.0%
1 year	10	"	0.64	10^3	1.0	"	5.3	15.9	15.9×10^5	11.2	12.3×10^3	<1.0%
"	"	"	"	"	1.5	"	4.7	14.1	21.2×10^5	"	"	"
"		"	"	10^4	1.0		12.6	37.8	37.8×10^5	"	12.3×10^4	3.3%
"		"	"	"	1.5	"	10.0	30.0	45.0×10^5	"	"	2.7%
"	100	"	10.0	10^3	1.0		13.4	40.2	42.2×10^6	16.4	18.0×10^4	<1.0%
"	"	"	"	"	1.5	"	11.8	35.4	53.1×10^6	"	"	"
"	"	"	"	10^4	1.0		29.2	87.6	87.6×10^6	"	18.0×10^5	2.0%
"	"	"	"	"	1.5		25.4	76.2	114.3×10^6	"	"	1.5%

IV. SHIELDING AGAINST TEMPERATURE VARIATIONS

A. Environment

Better knowledge of lunar surface temperature has been achieved through successful Surveyor missions (Lucas et al., 1966, 1967a, 1967b, 1968).

The diurnal variation (for a 28-day lunar "day") is taken to be 310° K (from 90° K to 400° K) at the very surface. Accordingly, protection has to be provided against these extreme temperatures. The solution discussed here will be the use of a shelter buried under a shield of lunar soils or rock, the thickness of which is to be determined so that temperature gradients under this shield will be minimum. The near constant temperature achieved below the shield might not be adequate for living quarters, but the problem of heating and insulation of the shelter will not be discussed here. We shall only try to provide a stable environment.

B. Lunar Surface Thermal Characteristics

Temperature gradients will decrease at depth in the soil shield according to the thermal properties and density of the soil. The following parameters are considered:

k = total thermal conductivity (radiative + conductive) joules/cm K

c = specific heat, joules/gr °K

γ = density, g/cm^3

Γ = thermal inertia = $(k\ p\ c)^{-1/2}$

δ = thermal diffusivity = $k/\gamma c$ = $k^2\Gamma^2$cm^2/sec

Reliable estimates have supposedly been obtained for Γ through the "high-resolution" sensors of Surveyors as opposed to telescopic observation data. We shall adopt (After Lucas and Harrison et al., 1968):

$$400 \leq \Gamma \leq 800$$

The density of lunar soils can also be restricted to a narrow bracket in the upper few meters (see Volume I, Chapter 2 of this report):

$$1 \text{ g/cm}^3 \leq \gamma \leq 1.5 \text{ g/cm}^3$$

However, the in situ thermal conductivity and specific heat of lunar soils and rocks, hence their diffusivity are not yet accurately known. Diffusivity will govern the rate and extent of the decrease of temperature fluctuations with depth.

C. Selection of a Soil Thermal Model

Many efforts have been devoted to the determination of k and c chiefly through experiments on simulated lunar soils in simulated lunar environment (pressure, temperature, and gravity) and construction of models with varying degrees of sophistication (Linsky, 1966; Jones, 1967), to reflect experimental or on site data.

Considering the above values adopted for γ and Γ, the product $k \cdot c$ is then:

$$1.05 \times 10^{-6} \leq k \cdot c \leq 6.2 \times 10^{-6}$$

Some average values proposed for k and c for powders and fine-grained simulated lunar soils in lunar temperature and pressure environment are summarized in the following Table 3-7.

Here we shall use average values of diffusivity, which amounts to adopting for these first estimates an acceptable temperature independant model. From the preceeding, values of the parameters will thus be:

$400 \leq \Gamma \leq 800$	$\text{cm}^2 \text{ sec}^{1/2} \text{ °K/cal}$
$1.0 \leq \gamma \leq 1.5$	g/cm^3

TABLE 3-7. SUMMARY OF PROPOSED K AND C VALUES FOR LUNAR SOILS

	Reference	Temperature Range	Average Value	Remarks
Total Thermal Conductivity, k joules/cm, °K	Bernett (1963)	200 - 360	6.6×10^{-6}	Size = 20 - 200 μ
	Buettner (1963)	260 - 360	3.2×10^{-5}	Size = 5 μ
	Watson (1964)	150 - 350	6.7×10^{-6}	Size = 100 μ
	Wechsler (1965)	280 - 330	6.6×10^{-6}	Size = 100 - 150 μ
	Clayton (1966)	---	2.1×10^{-5}	---
	A.D. Little (1966)	---	1.25×10^{-5}	---
	Jones (1967)*	---	---	---
	Harrison (1968)	---	1 to 2×10^{-5}	---
Specific Heat, c cal/g, °K	Linsky (1966)	$\propto T^{1/3}$	0.2	Average Values in 200 - 350 °K Range
	Clayton (1966)	T independ.	0.7	
	A.D. Little (1966)	depend. 10^{-4} T	0.7	
	Dulnev (1967)	T independ.	0.2	
	Halajian (1967)	T independ.	0.2	
	Jones (1967)*	---	---	
	Harrison (1968)	---	0.2	

* See Table 3-8.

$0.2 = c$ cal/g • °K

$5.2 \times 10^{-6} \leq k \leq 3.1 \times 10^{-5}$ cal/cm • sec • °K

$1.75 \times 10^{-5} \leq \delta \leq 1.55 \times 10^{-4}$ cm^2/sec

D. Decay of Temperature Fluctuations with Depth

One-dimensional diffusion equations can be used now, for temperature fluctuation computations in the shield provided we assume that the interface between bottom of soil shield and top of shelter insulation stays at the nearly constant temperature obtained at depth t in the semi-infinite medium. This implies adequate design of shelter insulation. All that will be achieved by the soil shield will be to eliminate temperature fluctuations on the outside of the shelter.

The temperature at the lunar surface can be expanded in a Fourier series of the form:

$$T(t, \theta) = \sum_{n=0}^{\infty} A_n \cdot \cos(n\omega\theta + \varepsilon_n)$$

where $\frac{2\pi}{\omega} = \tau$, the period of rotation of the moon about its axis.

The solution of the diffusion equation (Carslaw and Jaeger, 1959), is, at depth t,

$$T(t, \theta) = \sum_{n=0}^{\infty} T_n \cdot e^{-\xi t} \cdot \cos(n\omega\theta - \xi t + \varepsilon_n)$$

where

$$\xi = \frac{n\omega}{2\delta}$$

Local thermal anomalies will not be taken into account, and as suggested by others (Schlumberger Report, 1966), we will use an average model for lunar surface temperature, as a function of time θ,

$$T(0, \theta) = T_1 \sin \omega\theta \qquad 2m\pi < \omega\theta < (2m + 1)\pi \quad (m = 0, 1, 2, \ldots)$$

$$= -T_2 \qquad (2m + 1)\pi < \omega\theta \quad (m = 0, 1, 2, \ldots)$$

where temperature is measured relative to 240°K and $T_1 = 160°K$ and $T_2 = 150°K$. Then,diurnal waves establish an average temperature:

$$T_{av} = \frac{T_1}{\pi} - \frac{T_2}{2} + 240 \simeq 216°K$$

around which the temperature oscillates.

The amplitude of this oscillation decays exponentially with depth and the square root of frequency. This decay is different for the different harmonics of the variation. We shall use only the first three harmonics which are computed as:

$$T_1^* = \frac{T_1}{2} + \frac{2T_2}{\pi} = 175.5°K$$

$$T_2^* = -\frac{2T_1}{3\pi} = -34°K$$

$$T_3^* = +\frac{2T_2}{5\pi} = 19°K$$

so that the total fluctuation at depth t is:

$$\Delta T_{max}(t) = 2T_1^* e^{-\xi_1 t} + 2T_2^* e^{-\xi_2 t} + 2T_3^* e^{-\xi_3 t}$$

where:

$$\xi_1 = \frac{\omega}{2\delta} \qquad \xi_2 = \frac{2\omega}{2\delta} \qquad \xi_3 = \frac{3\omega}{2\delta}$$

and:

$$\omega = 2.5 \times 10^{-6} \text{ rad/sec}$$

$\Delta T(t)$ is presented for different values of δ at different depths in Fig. 3-2.

E. Summary - Conclusions

Jones (1968) has recently studied the same problem and presented twelve possible cases at the same thermal model of the lunar surface upper layer. Of these, the ones judged here the most likely with regard to our previous discussion of thermal parameters are presented in Table 3-8 together with models of this study.

Remark. Annual temperature fluctuations also exist on the lunar surface. However, for diffusivities lower than 10^{-3} cm^2/sec and at depths shallower than 100 cm, their amplitude is considerably smaller than the amplitude of diurnal waves (A. D. Little, 1967). Accordingly, they have not been considered here.

Conservative estimates for soil shielding will use the higher diffusivities. It is then proposed that the ranges of likely values to be adopted be as follows:

$$400 \leq \Gamma \leq 800$$

$$1.0 \leq \gamma \leq 1.5$$

$$1.75 \cdot 10^{-5} \leq \delta \leq 1.55 \times 10^{-4}$$

Accordingly, a soil shield of thickness 50 cm is believed to provide adequate protection against diurnal lunar temperature fluctuations if we accept a $\Delta T_{allow} = 1°K$.

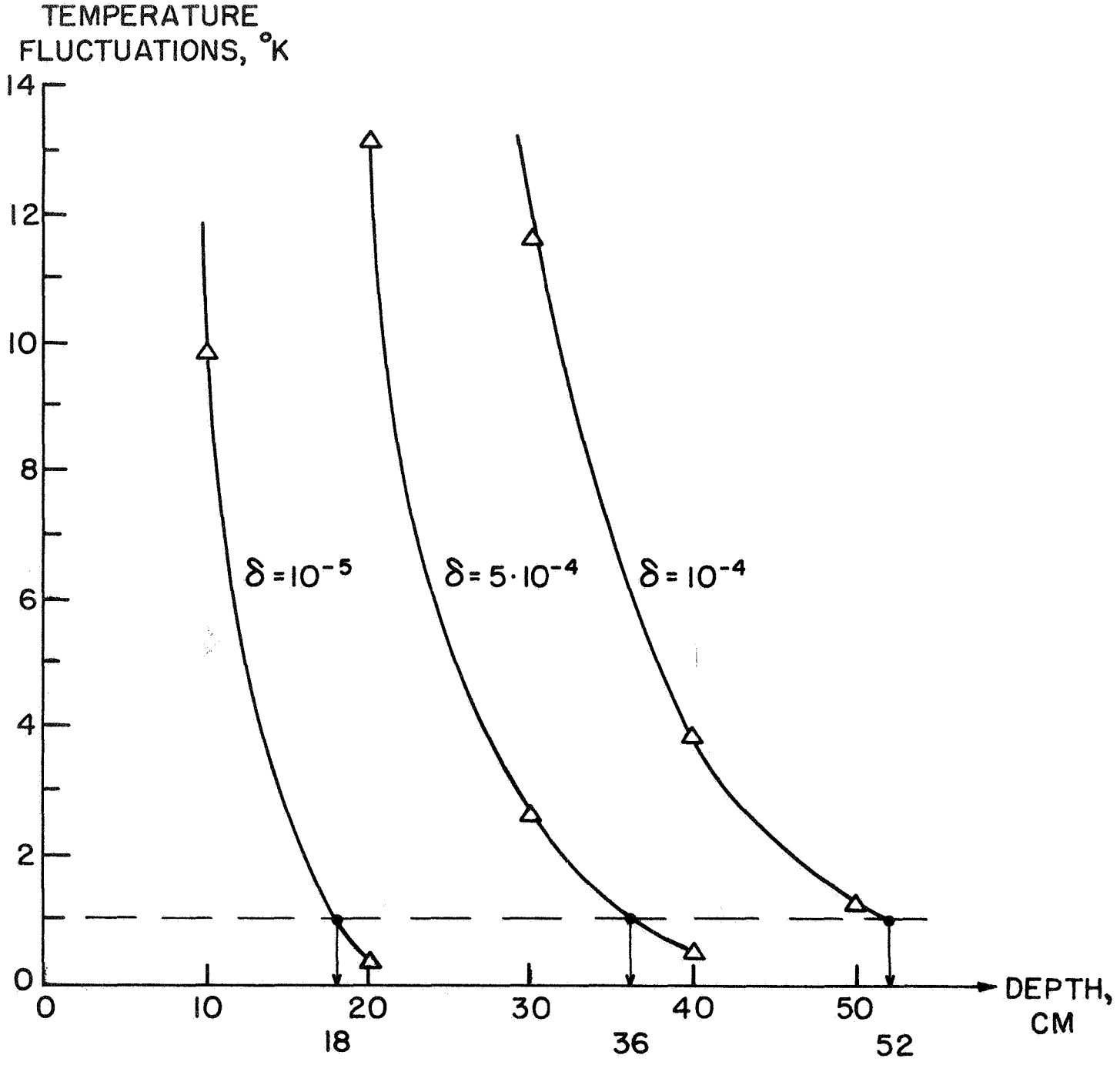

FIG. 3-2. Diurnal temperature fluctuations at depth, in lunar soils of different diffusivities.

TABLE 3-8. Depths Beneath the Lunar Surface at which the Total Diurnal Temperature Fluctuation Does Not Exceed 1°K for Different Values of Diffusivity

Reference	Model No.	T_0 °K	Γ	δ cm^2/sec	t cm
Jones (1967)	4	233	500	2.5×10^{-5}	25**
	5	224	757	1.1×10^{-5}	15
	6	223	800	6.0×10^{-5}	34
	10*	---	800	6.0×10^{-5}	36
	11*	---	700	5.0×10^{-5}	30
	12*	---	600	3.6×10^{-5}	26
This Report	1	216	400-800	1.0×10^{-4}	52***
	2	216	400-800	5.0×10^{-5}	36
	3	216	400-800	1.0×10^{-5}	18

* S = 1352 watts/m^2(solar constant, after Surveyor I)
** Estimated from figures of Ref. 36
*** From Fig. 3-2, this section.

V. SUMMARY - CONCLUSIONS

Detailed conclusions have been drawn separately for each of the hazards considered in this work. Recurring parameters vital to soil shield design have been assigned specific values or value brackets taking into account the most up to date knowledge of lunar surface properties, processes and environment. Overall results are shown in Table 3-9.

TABLE 3-9. Summary of Lunar Soil Shielding Study

Hazard	Characteristics of the Hazard	Method of Approach	Minimum Adequate Shield Thickness (t)
Radiation	Dependent on mission length Independent of shield area	Probabilistic	30 cm (1 year 99.99 %)
Meteoroids	Dependent on mission length Dependent on shield area	Probabilistic	90 cm (1 year 99.99 % 100 m^2 10 g)
Temperature Gradients	Independent of mission length (T > 28 days) Independent of shield area	Deterministic	50 cm (1° K)

The thickness t of the soil shield is in each case a function of the following parameters:

Radiation: $t(d_{max}, p, T, \gamma)$

Meteoroids: $t(M_{max}, p, T, A, \alpha, \beta, \Delta, \gamma)$

Temperature: $t(k, c, \Delta T_{allow}, \gamma)$

Since detailed design procedures have been presented, this work is a tool which can be applied to any given mission length, shield area, and desired level of risk different from the ones considered here.

REFERENCES

1. Smith, S. S. and Mitchell, J. K. (1968), "Recent estimates of lunar surface material properties", Department of Civil Engineering, University of California, Berkeley (prepared for Marshall S.F.C. on NASA Contract NSR 05-003-189), May.

Radiation

2. Burrell, M. O.; Wright, J. J.; and Watts, J. W. (1968a), "An analysis of energetic space radiation and dose rates", Marshall S.F.C., NASA TN D-4404, February.

3. Burrell, M. O. (1968b), Private communication, November.

4. Curtis, S. B. and Wilkinson, M. C. (1968), "Study of radiation hazards to man on extended missions", Boeing Co., NASA CR-1037.

5. Hildebrand, R. I. and Renkel, H. E. (1966), "The Lewis proton shielding code", Lewis Research Center, NASA TM X-52166.

6. Lahti, G. P.; Karp, I. M.; and Rosenbaum, B. M. (1968), "MCFLARE, a Monte-Carlo code to simulate solar flare events and estimate probable doses encountered on interplanetary missions", Lewis Research Center, NASA TN D-4311.

7. Norman, J. E. (1967), "Estimation of radiation hazard probabilities due to solar proton events during the maximum solar cycle phase", Summary Prog., Rep. SSL-27458 Brown Eng. Co.

8. Wilson, J. H. and Karcher, R. H. (1966), "Shielding effectiveness of soils against initial radiation", Holmes and Narver Inc. Rept. No. HN-186 (prepared for Oak Ridge National Laboratories).

Meteoroids

9. Bjork, R. L. (1963), "Review of physical processes in hypervelocity impact and penetration", Proc. 6th Symp. on Hypervelocity Impact.

10. Bjork, R. L.; Kreyenhagen, K. N.; and Wagner, M. H. (1967), "Analytical study of impact effects as applied to the meteoroid hazard", Shocks Hydrodynamics, Inc., NASA CR-757.

11. Burbank, P. B.; Cour-Palais, B. G.; and McAllum, W. E. (1965), "A meteoroid environment for near-earth, cislunar, and near-lunar explorations", Manned S.F.C., Houston, NASA TN D-2747.

12. Corp, E. L., et al. (1967), "Support for underground lunar shelter", in U.S. Bureau of Mines Annual Report on NASA Contract R 09-040-001, and private communication.

13. Cosby, W. A. and Lyle, R. G. (1965), "The meteoroid environment and its effects on materials and equipment", NASA SP-78.

14. Dohanyi, J. S. (1966), Bellcomm, Inc., TR 66-340-1.

15. Dohanyi, J. S. (1967), "Collision model meteoroids", Bellcomm, Inc., TR 67-340-3.

16. Fields, S. A.; Weathers, H. M.; Cox, R. M.; and Shotts, R. Q. (1967), "Problems and techniques of lunar surface mining", NASA TM X-53560, Marshall S.F.C.

17. Fish, R. H. (1968), "The penetration of porous projectiles in aluminum and plastic targets", Ames Research Center, NASA TN D-4504.

18. Gault, D. E.; Shoemaker, E. M.; and Moore, H. J. (1963), "Spray ejected from the lunar surface by meteoroid impact", Ames Research Center, NASA TN D-1767.

19. McMillan, A. R. (1968), "Experimental investigation of simulated meteoroid damage to various spacecraft structures", General Motors Co., NASA CR-915.

20. Moore, H. J. (1967), "The use of secondary impact craters as penetrometers of the lunar surface", Appendix A Langley Working Paper, Orbiter III LWP-407.

21. Naumann, R. J. (1966), "The near earth meteoroid environment", Marshall S.F.C. NASA TN D-3717.

22. Quaide, W. L. and Oberbeck, V. R. (1968), "Thickness determinations of lunar surface layer from lunar impact craters", Jrnl. of Geophys. Res., Vol. 73, n. 16.

23. Quigley, D. W. and Mitchell, J. K. (1968), "Development of low velocity soil penetration equations for determining the probable nature of lunar surface materials", (prepared for Marshall S.F.C. on NASA Contract NSR 05-003-189) Department of Civil Engineering, University of California, Berkeley.

24. Ross, H. P. (1968), "A simplified mathematical model for lunar crater erosion", Jrnl. of Geophys. Res., Vol. 73, n. 4, February.

25. Smith, R. E. (1965), "Space environment criteria guidelines for use in space vehicles development", Marshall S.F.C., NASA TM X-53273, May.

Temperature

26. A. D. Little, Inc. (1967), "Heat flow in the lunar surface layer", in Design Definition of Heat Flow Probe, Appendices, Vol. II, Contract No. SC-0205 for Bendix Systems Division.

27. Anonymous (1966), "Study of lunar geophysical surface and subsurface probes for Apollo Application Program", Final Report Vol. 2 (prepared for Marshall S.F.C. on Contract NAS 8-20243), Telemetry Div., Schlumberger Co.

28. Anonymous (1966), "Corporate IR and D study of lunar heat flow measurement", Final Rept., Bendix Systems Div., BSR-4577.

29. Bernett, E. C., et al. (1963), "Properties of simulated lunar materials in air and in vacuum", AIAA Journal, Vol. 1, n. 1402.

30. Buettner, K. J. (1963), "The moon's first decimeter", Planetary Space Science, Vol. 11, n. 135.

31. Carslaw, H. S. and Jaeger, J. C. (1959), Conduction of heat in solids, Oxford University Press, 2nd Ed., p. 68.

32. Clayton, J. F. (1966), "Heat flow experiment conceptual design study", ATR-15 Part 1, Technical Rept., Bendix Systems Division.

33. Dulnev, G. R., et al. (1967), "Possible structure of the lunar surface layer", NASA TT F-11.071.

34. Halajian, J. D., et al. (1967), "Correlation of mechanical and thermal properties of extraterrestrial materials", Grumann RE-280 (on Contract NAS 8-20084).

35. Harrison, J. K., et al. (1968), "Lunar thermal environmental criteria", Working Paper, Space Sciences Laboratory, Marshall Space Flight Center.

36. Jones, B. P. (1967), "Diurnal lunar temperature", AIAA Paper No. 67-259.

37. Linsky, J. L. (1966), "Models of the lunar surface including temperature dependent thermal properties", Harvard College Observatory Scient. Rept. No. 8, January.

38. Lucas, J. W.; et al. (1966), "Lunar surface temperature and thermal characteristics", Surveyor I Mission Report, J.P.L. Tech. Rept. 32-1023.

39. Lucas, J. W.; et al. (1967a), "Lunar surface temperature and thermal characteristics", Surveyor III Mission Report, J.P.L. Tech. Rept. 32-1177.

40. Lucas, J. W.; et al. (1967b), "Lunar surface temperature and thermal characteristics", Surveyor V Mission Report, J.P.L. Tech. Rept. 32-1246.

41. Lucas, J. W.; et al. (1968), "Lunar surface temperature and thermal characteristics", Surveyor VI Mission Report, J.P.L. Tech. Rept. 32-1262.

42. Watson, K. (1964), "Thermal conductivity measurements of selected silicate powders in vacuum at 150° - 350° K", California Inst. of Technology.

43. Wechsler, A. E. and Glaser, P. E. (1965), "Pressure effects on postulated lunar materials", Icarus, Vol. 4, n. 335.

LIST OF SYMBOLS

Radiation

d_{max}	maximum allowable dose/day (rads)
D_{max}	maximum allowable dose/mission (rads)
p	desired probability of no over-exposure (%)
t_{Al}	dimensionless shield thickness based on results for aluminum shields (g/cm^2)
t_d	dimensionless shield thickness for any material (g/cm^2)
t	soil shield thickness (cm)
γ	soil density (g/cm^3)

Meteoroids

A	shield area (m^2)
d_{max}	depth of largest crater (produced by largest primary impact of mass M_{max}) (cm)
k_1, k_2	constants of the mass flux model
m	meteoroid mass (g)
m_{max}	maximum meteoroid mass against which shield is designed (usually $m_{max} = M_{max}$) (g)
m_{ej}	mass of largest ejected fragment upon primary impact (g)
$(m_{ej})_1$	mass ejected by a primary impact = $\alpha \cdot m$ (g)
$(M_{ej})_1$	total mass ejected by primary impacts ($g/m^2/sec$)
$(M_{ej})_2$	total mass ejected by secondary impacts ($g/m^2/sec$)
$(M_{ej})_{max}$	$\alpha \cdot M_{max}$
$(M_{ej})_{mission}$	total mass ejected from shield by all impacts
M_{ej}	$(M_{ej})_1 + (M_{ej})_2$
M_{max}	maximum mass expected to impact on the shield over mission length with a probability p (g)

M_{tot}	total mass flux expected to impact on the shield with a probability p (g)
M_{shield}	total mass of the shield as designed (g)
N	total number of impacts above mass m (no./m^2/sec)
N*	total number of impacts of mass m (no./m^2/sec)
p	$(1 - 10^{-n})$% confidence level adopted for shield design with respect to perforation and erosion constraints. Applies to M_{max}
P	probability of impact above a given m_{max} for given A and T (%)
t	soil shield thickness
T	mission length on the lunar surface making use of shield (sec)
v	meteoroid velocity (km/sec)
v_{ej}	ejection velocity of primary ejecta taken as impact speed of secondary impacts (km/sec)
v_{max}	velocity of largest primary impact (km/sec)
V_{max}	volume ejected by largest primary impact = volume of largest expected crater in shield (cm^3)
α	$(m_{ej})_1/m$ = ratio of mass ejected by meteoroid to meteoroid's mass
β	ratio of primary impact crater diameter to depth
γ	bulk density of lunar soil (g/cm^3)
Δ	t/d_{max} (thick target)
ε	$(M_{ej})_{mission}/M_{shield}$ characterizes erosion

Temperature

c	specific heat (joule/g °K)
k	thermal conductivity (watt/cm, °K)
t	depth in lunar soil shield (cm)
T	temperature (°K)

$(\Delta T)_{max}$	maximum dirunal temperature fluctuation (°K)
$(\Delta T)_{allow}$	maximum allowable temperature fluctuation at depth (°K)
γ	lunar soil density (g/cm^3)
Γ	thermal inertia ($cm^2 \cdot sec^{1/2} \cdot °K/joule$)
δ	thermal diffusivity (cm^2/sec)
ξ	$(n\ \omega/2\delta)^{1/2}$ factor of exponential damping with depth
θ	time

NOTE: Some symbols differ from standard notations (e.g. Γ, θ,...) so that some recurring parameters (e.g. γ, t,...) can be kept the same throughout.